Currents mediated by non-NMDA glutamate receptors in rat magnocellular basal forebrain neurones in primary culture

A thesis submitted to the University of London
for the degree of Doctor of Philosophy
1997

by David Jack Waters

Department of Pharmacology
University College London
Gower Street
London WC1E 6BT

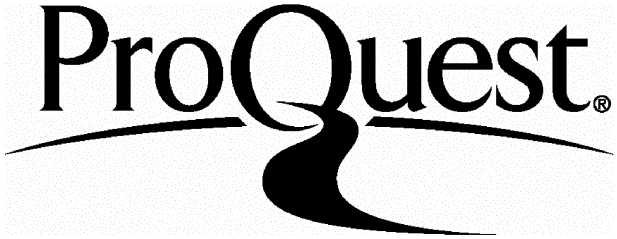

Abstract

Patch-clamp techniques were used to record glutamate receptor-mediated responses from magnocellular rat basal forebrain neurones maintained in dissociated culture. Both NMDA and non-NMDA receptor-mediated responses were observed and could be distinguished pharmacologically.

AMPA and kainate elicited inward currents. Responses to AMPA but not to kainate showed rapid desensitization. EC_{50}s for steady-state responses to AMPA and kainate were 2.7 and 138μM respectively. Responses were potentiated by cyclothiazide but not by Concanavalin A and were inhibited by GYKI 53655. These data indicate that non-NMDA receptor-mediated responses result predominantly from activation of an AMPA receptor. In the presence of GYKI 53655 small inward currents were observed upon kainate application. Responses decreased in amplitude during prolonged application, were insensitive to cyclothiazide and potentiated by Concanavalin A. These responses probably reflect kainate receptor activation.

Steady-state current-voltage relationships were examined in nucleated patches. With 30μM spermine in the pipette mildly outwardly rectifying through linear to strongly doubly-rectifying relationships were observed, suggesting a range of calcium permeabilities. AMPA receptor calcium permeabilities were quantitated using constant field theory to interpret the effects of solution exchanges on reversal potentials in acutely dissociated neurones. Relative calcium:sodium permeability ranged from 0.26 to 3.6, median 1.27. Extracellular calcium ions also reduced current amplitude, an effect mimicked by cadmium and by cobalt ions. The effect of cadmium was dose-dependent (EC_{50} 44μM) and voltage-sensitive.

Kainate application to acutely dissociated neurones resulted in calcium current inhibition. GYKI 53655 sensitivity indicated that the probable mechanism is calcium-dependent inactivation of calcium channels following calcium influx through AMPA receptors.

These data may explain the sensitivity of magnocellular cholinergic basal forebrain neurones to non-NMDA receptor agonists *in vivo* and are consistent with the suggestion that glutamate-induced calcium influx may contribute to selective loss of cholinergic neurones in dementia.

Contents

List of figures and tables

General Introduction

1.1 Anatomy of the rat basal forebrain (after Wainer & Mesulam, 1990) In the rat the basal forebrain consists of a number of diffuse nuclei distributed within the medial septum (MS), vertical and horizontal limbs of the diagonal band of Broca (VDBB and HDBB) and the nucleus basalis (NB), the latter falling within the boundaries of the substantia innominata (SI) and corresponding to the nucleus basalis of Meynert in primates. These nuclei are composed of heterogeneous collections of cells, among which the projecting neurones are magnocellular with somatic dimensions (in the rat) of approximately 15-20μm (minor axis) by 20-35μm (major axis). A large proportion of these projecting neurones are cholinergic, the remainder mostly GABAergic.

In view of inconsistencies in the use of this anatomical nomenclature by different authors and because these regions do not necessarily map onto functionally distinct cholinergic cell groups, Mesulam has proposed a classification based on the sites to which each subgroup projects. Hence projecting cholinergic cells of the medial septum have been designated Ch1, those of the vertical and horizontal limbs of the diagonal band Ch2 and Ch3 respectively and those of the nucleus basalis Ch4. These projections are illustrated schematically in figure 1.1.

Projections from the basal forebrain provide the principle source of cholinergic afferents to the cortex, hippocampus, olfactory bulb and amygdala and are thought to be important in a variety of processes including learning, arousal and memory. Projections from the nucleus basalis innervate every region and layer of the cerebral cortex. The axonal density of these projections is very high, causing Mesulam (1995) to state that 'its magnitude alone indicates that this pathway is likely to constitute the single most substantial regulatory afferent system of the cerebral cortex.'

The percentages of cells staining positive for choline acetyltransferase (ChAT) and acetylcholinesterase (AChE) and their principal projections are as follows:

Figure 1.1 - Schematic sagittal section through the rat brain

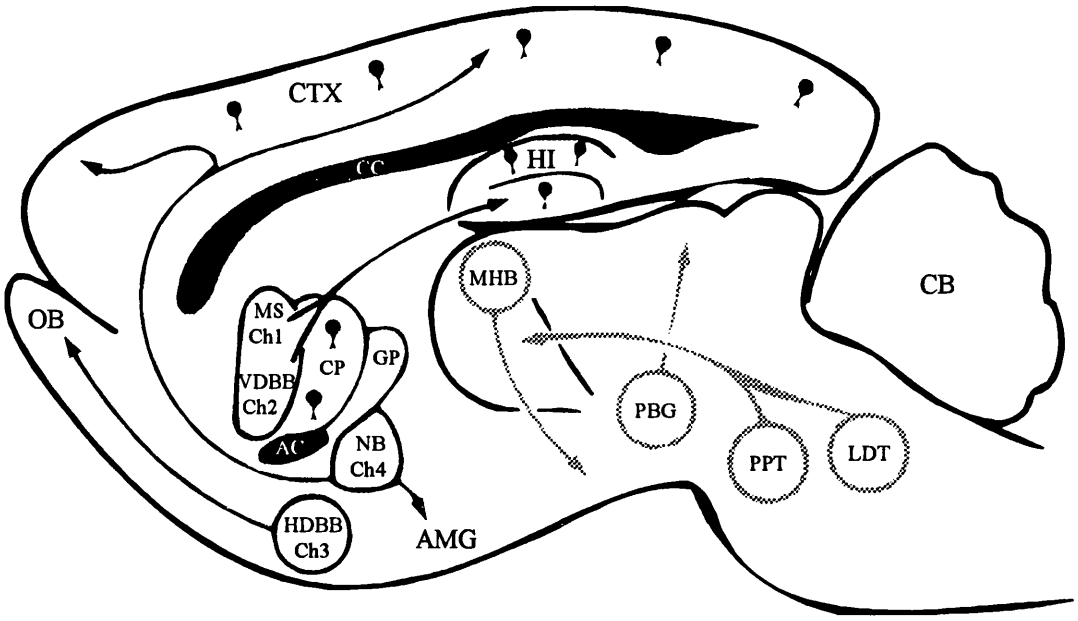

Basal forebrain regions:

MS	medial septum
VDBB	vertical limb of the diagonal band of Broca
HDBB	horizontal limb of the diagonal band of Broca
NB	nucleus basalis

Other regions containing projecting cholinergic neurones:

MHB	medial habenular nucleus
PBG	parabigeminal nucleus
PPT	pedunculopontine tegmental nucleus
LDT	lateral dorsal tegmental nucleus

Regions receiving cholinergic projections from the basal forebrain:

OB	olfactory bulb
CTX	cortex
HI	hippocampus
CB	cerebellum
AMG	amygdala

Other areas:

CC	corpus callosum
AC	anterior commissure
CP	caudate-putamen
GP	globus pallidus

indicates presence of cholinergic interneurones

Region	approximate proportion of cells cholinergic	principal projections
MS	30-50%	hippocampus
VDBB	50-75%	hippocampus neocortex
HDBB	<50-75%	olfactory bulb
NB	Not stated	cortex amygdala

1.2 Basal forebrain neurones and SDAT

Alzheimer's disease (and related conditions, collectively referred to as senile dementia of the Alzheimer-type, SDAT) is a progressive condition characterised by the loss of various mental functions, particularly memory. At the ultrastructural level degeneration is observed as regions of cellular damage, cell loss and fibrous deposits, termed neuritic plaques. Deposits consist largely of anomalously processed and/or phosphorylated proteins which accumulate both in neurites within neuritic plaques and in neuronal cell bodies, the latter being referred to as neurofibrillary tangles. These ultrastructural features are situated predominantly in the olfactory bulb, neocortex, motor cortex and hippocampus (see reviews by Price, 1986; Saper, 1988; Selkoe, 1991; Selkoe, 1994).

Various authors have suggested that loss of cortical cholinergic input may be an important factor in SDAT, the so-called cholinergic hypothesis of geriatric memory dysfunction. This hypothesis results from a wealth of studies concerning pronounced loss of cholinergic input into cortical regions during SDAT (see reviews by Bartus, Dean, Beer & Lippa, 1982 and by Mann, 1988).

Of particular significance was the discovery by Davies & Maloney (1976) that ChAT activity was reduced in cortical regions of SDAT patients relative to controls. This reduction was greatest in regions containing high densities of neurofibrillary tangles. In contrast, the activities of various marker enzymes for

GABAergic and for monoaminergic neurones were not significantly different between controls and patients with SDAT.

A similar approach was taken by Perry, Tomlinson, Blessed, Bergmann, Gibson & Perry (1978) who correlated loss of cortical ChAT activity with the cortical plaque count. Importantly these authors also linked cholinergic degeneration with mnemonic deficit, reporting a correlation between loss of post-mortem cortical ChAT activity with patients' mental test scores. Whilst a reduction of the GABAergic marker glutamic acid decarboxylase (GAD) was also observed for patients with SDAT, this reduction showed no relationship with plaque counts or mental test scores.

Loss of magnocellular basal forebrain neurones has also been documented, again by comparison of post-mortem tissue from controls and patients with SDAT. Whitehouse, Price, Struble, Clark, Coyle & DeLong (1982) noted a 73% reduction in density and a 79% reduction of total number of magnocellular neurones in the nucleus basalis of Meynert of SDAT patients.

In summary, these data suggest that marked loss of cholinergic magnocellular basal forebrain neurones occurs during SDAT and that this loss may be intrinsically associated with some of the symptoms of SDAT.

1.3 Excitotoxic injury in Alzheimer's Disease?

The mechanism of cell death in SDAT is unknown. One possibility is that unusually high concentrations of or unusually prolonged exposure to glutamate results in excessive calcium influx. This process is termed excitotoxicity and is known to be cytotoxic (Choi, 1987; Choi, 1988).

Excitotoxicity is thought to be a major cause of cell death in several forms of acute CNS injury (including epilepsy, hypoxia, ischaemia, hypoglycaemia and mechanical trauma) and also several chronic conditions (including sulphite oxidase deficiency, olivopontocerebellar atrophy, Guam amyotropic lateral sclerosis/ Parkinsonism-dementia (ALS/PD), lathyrism and Huntingdon's Disease). Of these conditions, ALS/PD stands out since several of the clinical and pathological features of this condition are common to SDAT, including the presence of paired helical filaments (a component of neurofibrillary tangles) in post-mortem tissue

(Choi, 1988). It is therefore clear that excessive glutamate exposure can generate some of the diagnostic features of SDAT under appropriate conditions.

Evidence for a role of excitotoxicity in hypoxia/ischaemia is now very strong (Choi, 1995). Under ischaemic conditions glutamate may be released not only as a direct consequence of neuronal depolarization, but also through reversal of glutamate uptake. Thus glutamate may be present in the extracellular space at extremely high concentrations: some authors estimate that glutamate concentrations are sustained at 100μM, such concentrations being neurotoxic (Szatkowski & Attwell, 1994). This is important firstly since it illustrates that neurotoxic extracellular concentrations of glutamate are obtained under certain conditions and secondly because it has been suggested that hypoxia and/or hypoglycaemia may contribute to cytotoxicity in SDAT (Yankner, 1996).

Exposure to β-amyloid peptides (thought to be a significant factor in SDAT) increases the sensitivities of cortical neurones to excitotoxicity *in vitro* (Koh, Yang & Cotman, 1990; Mattson, Cheng, Davis, Bryant, Lieberburg & Rydel, 1992). Cytotoxicity of K^+-induced calcium influx is also increased by β-amyloid peptides (Hartmann, Eckert & Müller, 1993) suggesting that the increased excitotoxicity probably results from loss of Ca^{2+}-homeostasis (Mattson, Barger, Cheng, Lieberburg, Smith-Swintosky & Rydel, 1993) rather than a specific effect of glutamate. Glutamate-induced calcium influx also causes expression by hippocampal (Mattson, 1990) and cortical neurones (Sautière, Sindou, Couratier, Hugon, Wattez & Delacourte, 1992) of antigenic epitopes characteristic of SDAT and *in vitro* causes selective loss of a subset of cortical and hippocampal neurones which are prone to degeneration in Alzheimer's disease (Burke, Yin & Weiss, 1995).

In summary, the role of overexposure to glutamate in neurodegenerative diseases is firmly established and *in vitro* studies have demonstrated that excitotoxicity is capable of producing Alzheimer-like characteristics. These data suggest that overexposure to glutamate is one route by which Alzheimer-like degeneration might be induced *in vivo*.

1.4 Glutamate receptors

The excitatory effects of glutamate on the CNS were first reported by Hayashi (1954) who injected sodium glutamate into the brains of several species of vertebrate (including humans) and observed convulsions, motor effects and effects on reflexes and conditioning.

Effects at the single cell level were first described by Curtis, Phillis & Watkins (1959) who recorded the activities of single spinal neurones in the anaesthetized cat using intracellular microelectrodes and applied glutamate by iontophoresis. Following this 'preliminary report' in Nature, these authors published a more extensive study in 1960, concluding that a variety of acidic amino acids each caused chemical excitation of interneurones, Renshaw cells and motoneurones, but that these effects were 'non-specific' and that it was 'unlikely ... that either glutamic, aspartic or cysteic acids are excitatory transmitters,' (Curtis, Phyllis & Watkins, 1960).

This conclusion has proved erroneous, glutamatergic transmission being the most abundant excitatory synaptic mechanism in the vertebrate CNS.

1.4.1 Glutamate receptor subtypes

Glutamate receptors fall into two distinct classes: those with an integral ion channel (ionotropic receptors) and those coupled to G-proteins (metabotropic receptors).

In common with all G-protein-coupled receptors, metabotropic glutamate receptors (mGluRs) contain 7 transmembrane domains. 8 mGluR genes have been identified, each encoding a functional receptor. These have been grouped into 3 classes based on sequence identity, class I consisting of mGluRs 1 & 5, class II of mGluRs 2 & 3 and class III of mGluRs 4,6,7 & 8. Class I receptors are coupled to phosphoinositide metabolism and classes II and III to cyclic nucleotide metabolism. Class-selective agonists are available, (1S,3R)-1-aminocyclopentane-1,3-dicarboxylic acid (trans-ACPD) acting at receptors of classes I and II and L(+)-2-amino-4-phosphonobutyric acid (L-AP4) at class III receptors (Pin & Duvoisin, 1995).

Ionotropic glutamate receptors can be sub-divided into NMDA and non-

NMDA receptors on pharmacological grounds. NMDA receptors are stimulated by N-methyl-D-aspartate (NMDA) and are sensitive to the competitive antagonist D(-)-2-amino-5-phosphonopentanoic acid (AP5). Non-NMDA receptors are insensitive to AP5, but are sensitive to quinoxalinediones (Honoré, Davies, Drejer, Fletcher, Jacobsen, Lodge & Nielsen, 1988; Watkins, Krogsgaard-Larsen & Honoré, 1990; Wilding & Huettner, 1996).

Several non-NMDA receptor agonists are in common use, including (S)-α-amino-3-hydroxy-5-methyl-4-isoxazolepropionic acid (AMPA), kainate, domoate and quisqualate. The potencies of these agonists and the kinetics of the elicited responses differ between preparations. This gave rise to some controversy regarding whether these agonists acted at a single or at multiple receptors (Jahr & Stevens, 1987; Cull-Candy & Usowicz, 1987).

1.4.2 Cloned receptors - classification

The cloning of ionotropic glutamate receptors was a major watershed in the field, categorically settling the single/multiple receptor issue and clearly defining the pharmacological differences between receptor subtypes. Thus NMDA and non-NMDA receptors are distinct molecular entities and, further, two classes of non-NMDA receptor exist, termed AMPA and kainate receptors in view of their preferential activation by these two agonists.

5 NMDA receptor genes have been cloned. Only the ~100kD NMDAR1 (NR1) subunit forms functional channels upon homomeric expression, NMDARs 2A-2D (NRs 2A-2D; each ~130-160kD) displaying no functional activity when homomerically expressed but influencing the properties of NMDAR1 upon co-expression (Hollmann & Heinemann, 1994).

9 non-NMDA receptor genes, all of ~100kD, have been identified and named GluRs 1-7, KA1 and KA2. These can be grouped into 3 classes according to both degrees of sequence identity and functional properties: (i) the AMPA receptor subunits GluR1-GluR4, (ii) the kainate receptor subunits GluR5-GluR7, which correspond to low-affinity kainate binding sites observed in rat brain membranes, and (iii) the KA1 and KA2 subunits, which correspond to high-affinity kainate binding sites observed in rat brain (Hollmann & Heinemann, 1994; Bettler

& Mulle, 1995). Upon homomeric expression, all subunits possess significant binding affinities for agonists. In addition, GluRs 1-6 all form functional channels, yielding electrophysiologically detectable currents upon agonist application. In contrast, no detectable current results from homomeric expression of GluR7, KA1 or KA2 (Hollmann & Heinemann, 1994).

The stoichiometry in which the non-NMDA receptor subunits combine to produce native receptors is unknown, but heteromeric channels are formed upon co-expression. Heteromeric expression has revealed that AMPA receptor subunits will interact upon co-expression with each other. Likewise, all kainate receptor subunits are capable of interaction with each other. In contrast, combination of AMPA with kainate receptor subunits does not occur, co-expression of AMPA and kainate receptor subunits producing two independent populations of channels with functional properties as observed following homomeric expression (see for example Partin, Patneau, Winters, Mayer & Buonanno, 1993).

1.4.3 Cloned non-NMDA receptors - structure

The generic model of ionotropic receptor structure consists of a length of polypeptide containing four hydrophobic α-helical segments which are thought to span the membrane (transmembrane domains). Thus both amino- and carboxy-termini of the polypeptide are extracellular and only the 2 loops of polypeptide between transmembrane domains (TMDs) I & II and III & IV are intracellular. Following hydropathy analysis this membrane topology was initially assigned to both NMDA and non-NMDA ionotropic glutamate receptors (Hollmann & Heinemann, 1994; McBain & Mayer, 1994).

Glycosylation and phosphorylation sites have subsequently been identified in what were thought to be intracellularly and extracellularly located regions of ionotropic glutamate receptor peptides, respectively. These data strongly suggest an alternative topology, giving rise to several proposed models. In one model TMDII does not traverse the membrane, but forms an intramembrane loop. This is the favoured model at present since removal of the TMD II region does not displace glycosylation sites C-terminal to TMD II to the intracellular side of the membrane (Wo & Oswald, 1994). Thus the carboxy-terminus and the 2 loops of

Figure 1.4 - Putative general structure of non-NMDA receptors

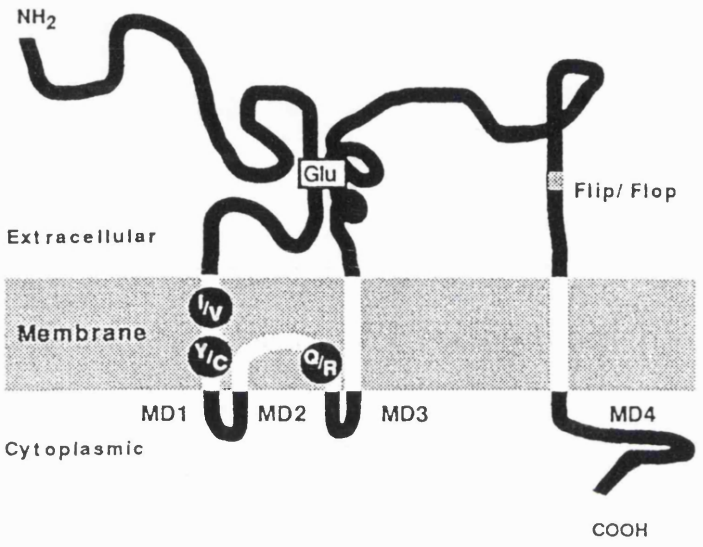

Glu glutamate binding site

black circles sites of RNA editing

transmembrane domains are shown in white and labelled MD1-4

(Modified from Bettler & Mulle, 1995)

peptide between TMDs I & II and II & III are thought to be intracellular (Seeburg, 1993; McBain & Mayer, 1994; Bettler & Mulle, 1995). That the membrane topology of ionotropic glutamate receptors should differ from the 'conventional' structure of ligand-gated ion channels is not surprising in view of the low sequence identity, GluRs 1-4 showing approximately 20% identity with other ligand-gated receptors (Hollmann & Heinemann, 1994).

Receptor diversity is expanded by differential and by alternative splicing. Differential splicing has been reported at the C-terminus of GluR4. Alternative splicing occurs at both N- and C-termini of GluR5. The functional consequences of splicing at these sites are unclear. In contrast, alternative splicing of a site between TMDs III and IV of GluRs 1-4 strongly influences functional properties (Sommer, Keinänen, Verdoorn, Wisden, Burnashev, Herb, Köhler, Takagi, Sakmann & Seeburg, 1990). This so-called flip/flop site consists of 115 base-pairs and strongly influences desensitization; both rates of desensitization and sensitivities to agents which modulate desensitization (Hollmann & Heinemann, 1994; Mosbacher, Schoepfer, Monyer, Burnashev, Seeburg & Ruppersberg, 1994; Partin, Patneau & Mayer, 1994; Partin, Bowie & Mayer, 1995).

Diversity is further increased by RNA editing, an extremely unusual mechanism in which a single base is replaced at the RNA level (Sommer, Köhler, Sprengel & Seeburg, 1991). This form of post-translational modification is observed at three sites in ionotropic glutamate receptors, all of which influence rectification and ion selectivity. The first site to be identified was the Q/R/N site in TMD II. Genes for all 9 non-NMDA subunits encode a glutamine (Q) residue at this site, but GluR2 peptides invariably contain an arginine (R) at this site as a result of RNA editing. GluRs 1,3,4 & 7 and KA1 & 2 are always found in the unedited (Q-containing) form, whereas edited (R-containing) and unedited forms of GluR5 and GluR6 may co-exist. (The NMDAR genes all encode an asparagine (N) residue at this site.) Two more sites have been found in TMD II of GluRs 5 and 6. GluR5 subunits are invariably edited at these sites, whereas editing of GluR6 is incomplete resulting in the co-existence of several receptor isoforms (Hollmann & Heinemann, 1994; Bettler & Mulle, 1995).

Comparison with bacterial amino acid binding proteins has led to the

suggestion that the agonist binding site of non-NMDA receptors may be formed by residues from both the N-terminal domain and the extracellular loop between TMDs III and IV (Bettler & Mulle, 1995).

Numerous glycosylation and phosphorylation consensus sequences have been identified on non-NMDA receptors. GluRs 1-4 contain 5-6 potential N-glycosylation sites in their extracellular loops and are both N- and O-glycosylated. Less is known about glycosylation of GluRs 5-7, KA1 and KA2, but GluR6 appears to be glycosylated in the loop between TMDs III & IV (Hollmann & Heinemann, 1994). Protein kinase A (PKA), protein kinase C (PKC) and calcium/calmodulin kinase II have all been reported to phosphorylate non-NMDA receptors (Roche, Tingley & Huganir, 1994). The sites of PKA and PKC phosphorylation both appear to be in the C-terminal domain. Phosphorylation by PKA at a C-terminal site increases current amplitude (Roche, O'Brien, Mammen, Bernhardt & Huganir, 1996).

1.4.4 Cloned non-NMDA receptors - pharmacology & kinetics

Cloning permitted clear division of non-NMDA receptors into AMPA and kainate receptors on pharmacological grounds. No selective agonists or antagonists are readily available for either AMPA or kainate receptors hence these receptors are generally distinguished using agonist potencies and kinetics/desensitization properties.

Agonist potencies for AMPA subunits follow the sequence: AMPA $\approx$ domoate $>$ glutamate $>$ kainate, with approximate EC_{50}s (for steady-state currents) of 1-10, 5-30 and 30-130μM respectively (Hollmann & Heinemann, 1994). Hill slopes for these agonists are typically $\sim$1.2-1.4 and it has been suggested that the binding of two molecules of agonist may be required for channel opening (see for example Stein, Cox, Seeburg & Verdoorn, 1992).

Glutamate elicits rapidly rising and desensitizing responses (Edmonds, Gibb & Colquhoun, 1995). Desensitization time constants for responses to 1mM glutamate are approximately 1-6ms for homomerically expressed subunits with flip receptors generally displaying slightly slower desensitization than the corresponding flop splice variants (Mosbacher, Schoepfer, Monyer, Burnashev,

Seeburg & Ruppersberg, 1994). Desensitization of AMPA receptors to glutamate is almost complete, steady state current amplitudes being less than 10% (often 1-2%) of peak current amplitude (Partin, Patneau & Mayer, 1994; Mosbacher, Schoepfer, Monyer, Burnashev, Seeburg & Ruppersberg, 1994). In addition to influencing the rates of desensitization, the flip/flop module influences the extent of desensitization, flop receptors displaying greater desensitization than flip receptors (Sommer, Keinänen, Verdoorn, Wisden, Burnashev, Herb, Köhler, Takagi, Sakmann, & Seeburg, 1990; Partin, Patneau & Mayer, 1994).

AMPA elicits similar responses to glutamate at AMPA receptors, whereas kainate and domoate both produce non-desensitizing responses. Maximal concentrations of glutamate and of AMPA often appear to produce smaller responses than kainate or domoate, leading to glutamate and AMPA being labelled partial agonists by some authors. This may be anomalous since the extremely rapid desensitization of responses to glutamate and AMPA will result in underestimation of the peak current amplitudes to these two agonists upon any but the fastest of applications.

Kainate receptors display a different agonist potency profile: domoate > kainate > glutamate > AMPA, AMPA producing no response at GluR6. Respective steady-state EC_{50}s are approximately 0.1-1, 1-30, 30-300 and 3000μM (Hollmann & Heinemann, 1994). All these agonists produce desensitization. Whilst kainate and domoate elicit similar maximum peak current amplitudes at GluR5, kainate produces slightly more ($\sim$90%) desensitization than domoate ($\sim$85%). Desensitization is generally biphasic, with time constants of approximately 10-15 & 50-150ms for glutamate (1mM) and 30-50 & 400-700ms for kainate (0.5-1mM). The faster time constant accounts for the majority of current decay for both agonists (Huettner, 1990; Wong & Mayer, 1993; Hollmann & Heinemann, 1994). Time constants for desensitization of GluR6 receptors to domoate were much slower ($\sim$2s for 50μM domoate) whereas desensitization to kainate was similar to that at GluR5. Responses of GluR6 to glutamate are similar to those of GluR5, showing complete desensitization following a biexponential timecourse with time constants of $\sim$10 & $\sim$70ms for 1mM glutamate (Sommer, Burnashev, Verdoorn, Keinänen, Sakmann & Seeburg, 1992).

AMPA and kainate receptors also differ with regard to their sensitivities to agents which inhibit desensitization. Desensitization of AMPA receptors is selectively inhibited by aniracetam and by benzothiadiazides, such as cyclothiazide. The degree to which these compounds inhibit desensitization is strongly influenced by the flip/flop module. Aniracetam displays stronger inhibition of desensitization at flop receptors than at flip receptors (Partin, Fleck & Mayer, 1996). Cyclothiazide would appear to operate via a different mechanism since it decreases the rate of desensitization of flop receptors, but has been found capable of almost completely eliminating desensitization at flip receptors (Partin, Patneau & Mayer, 1994; Partin, Bowie & Mayer, 1995; Partin, Fleck & Mayer, 1996).

Cyclothiazide also shifts agonist dose-response curves for flip receptors to the left, reducing the EC_{50} for the agonist without changing the Hill slope (Patneau, Vyklicky & Mayer, 1993; Partin, Patneau & Mayer, 1994). The rate of relief of these effects upon wash-out of cyclothiazide is faster for flop than for flip receptors (Partin, Patneau & Mayer, 1994).

A single amino acid residue within the flip/flop region is responsible for these differences, identified as residue 750 in GluR1 (Partin, Bowie & Mayer, 1995). Mutations at this position also modulate deactivation (Partin, Fleck & Mayer, 1996). Heteromeric expression has revealed that flip subunits exert a stronger influence than flop subunits on the cyclothiazide sensitivities of receptors composed of a mixture of flip and flop subunits (Partin, Patneau & Mayer, 1994).

Cyclothiazide also acts as a channel blocker (Patneau, Vyklicky & Mayer, 1993; Partin, Patneau & Mayer, 1994). Such channel block occurs at both AMPA and kainate receptors and is voltage-independent (Patneau, Vyklicky & Mayer, 1993). Thus cyclothiazide does not alter peak or steady-state current-voltage relationships at AMPA (or kainate) receptors. An apparent effect of cyclothiazide on the I-V relationship of the peak response may be observed where agonist application is insufficiently rapid to resolve the true peak response (Patneau, Vyklicky & Mayer, 1993) since peak and steady-state relationships are slighly different due to a gating mechanism which is not only time- but also voltage-dependent (Jonas & Sakmann, 1992).

In addition to inhibiting the desensitization of AMPA receptors to glutamate

and to AMPA, cyclothiazide increases the amplitude of current evoked by kainate. The mechanism by which cyclothiazide produces this effect is unclear, but it has been suggested that kainate may induce very rapid desensitization of AMPA receptors, such that the desensitizing component is observed only with extraordinarily rapid agonist applications (Patneau, Vycklicky & Mayer, 1993). No such desensitization has ever been observed in cells expressing only AMPA receptors, even upon very fast stepper-application of kainate to outside-out patches (see for example Jonas & Sakmann, 1992). Thus it seems likely that cyclothiazide influences AMPA receptor-mediated responses by additional mechanism(s). Cyclothiazide has also been shown to have pre-synaptic actions, presumably independent of its effects at AMPA receptors (Diamond & Jahr, 1995).

Cyclothiazide does not inhibit desensitization of kainate receptors (Partin, Patneau, Winters, Mayer & Buonanno, 1993; Wong & Mayer, 1993) but several lectins have been found to inhibit desensitization of both AMPA and kainate receptors (Zorumski & Thio, 1992). The lectin Concanavalin A (ConA) is frequently used for this purpose and has been shown to exert greater effects at kainate than at AMPA receptors (Mayer & Vyklicky, 1989; Partin, Patneau, Winters, Mayer & Buonanno, 1993; Wong & Mayer, 1993).

ConA has been shown to alter the Hill slope for the action of kainate at kainate receptors. This was interpreted as indicating that the binding of two agonist molecules was required for channel opening prior to exposure to ConA (Huettner, 1990). However, comparison of dose-response relationships in the absence and presence of ConA is complicated by possible desensitization.

1.4.5 Cloned non-NMDA receptors - ion permeability

Since the first ionotropic glutamate receptor subunit was cloned by Hollmann, O'Shea-Greenfield, Rogers & Heinemann (1989) numerous publications have appeared describing the properties of the various clones. Of particular interest are molecular determinants of divalent cation permeability.

Prior to cloning studies it was generally accepted that non-NMDA receptors were appreciably permeable only to monovalent cations. Significant calcium-permeability of non-NMDA receptors had been demonstrated only in hippocampal

neurones (Iino, Ozawa & Tsuzuki, 1990; Ozawa, Iino & Tsuzuki, 1991) and in retinal bipolar cells (Gilbertson, Scobey & Wilson, 1991).

Studies of cloned receptors have demonstrated that homomerically expressed AMPA receptor subunits are all calcium permeable except the GluR2 subunit (Hollmann, Hartley & Heinemann, 1991; Burnashev, Monyer, Seeburg & Sakmann, 1992). As GluR2 is dominant in heteromeric expression systems (Burnashev, Monyer, Seeburg & Sakmann, 1992) its widespread distribution may account for the low divalent cation permeabilities of many native AMPA receptors (see Hollmann & Heinemann, 1994). GluR2 is also the only AMPA receptor subunit with a doubly rectifying I-V relationship and dominates rectification in heteromeric expression systems (Hume, Dingledine & Heinemann, 1991; Verdoorn, Burnashev, Monyer, Seeburg & Sakmann, 1991).

Divalent cation permeability and double rectification are closely linked in that both are largely determined by the residue occupying the Q/R site (Hume, Dingledine & Heinemann, 1991; Burnashev, Monyer, Seeburg & Sakmann, 1992). The presence of a glutamine residue (Q; unedited) confers high divalent cation permeability whereas an arginine residue (R; edited) confers low divalent cation permeability (Burnashev, Monyer, Seeburg & Sakmann, 1992). The genes for all four AMPA receptor subunits encode a glutamine in this position but in native GluR2 subunits the corresponding location is invariably occupied by an arginine residue (Sommer, Köhler, Sprengel & Seeburg, 1991). This apparent anomaly results from constitutive RNA editing in which the codon for this particular glutamine is altered to an arginine codon prior to translation (Sommer, Köhler, Sprengel & Seeburg, 1991). Since all GluR2 mRNAs are edited in this way all native GluR2 subunits have low divalent cation permeabilities. In contrast, native GluR1, GluR3 and GluR4 receptors are not edited and so express a glutamine residue at the Q/R site (Sommer, Köhler, Sprengel & Seeburg, 1991).

Site directed mutagenesis studies have confirmed the importance of this site for both divalent cation permeability and rectification properties, but have also revealed that these two phenomena can be separated: certain amino acid substitutions can result in a receptor with high divalent permeability and a linear I-V relationship or *vice versa* (see Hollmann & Heinemann, 1994). Properties

more akin to the NMDA receptor are observed with an asparagine residue at this site, asparagine being the naturally occurring amino acid at the corresponding site of the NMDA receptor (Burnashev, Schoepfer, Monyer, Ruppersberg, Günther, Seeburg & Sakmann, 1992). The Q/R site is therefore also known as the N/Q/R site.

In addition to the Q/R site a number of other sites are known to influence divalent cation permeability. For example divalent cation permeability can be greatly increased by substitution of a tryptophan for lysine 577 of GluR1 (Ferrer-Montiel, Sun & Montal, 1996).

With regard to native AMPA receptors, the relationship between rectification and divalent cation permeability was initially unclear since these two features seemed correlated in only some preparations. For instance, retinal bipolar cells (Gilbertson, Scobey & Wilson, 1991) neocortical neurones (Jonas, Racca, Sakmann, Seeburg & Monyer, 1994) and avian auditory neurones (Otis, Raman & Trussell, 1995) were all reported to express calcium-permeable non-NMDA receptors with linear or outwardly rectifying I-V relationships.

This discrepancy was resolved with the discovery that intracellular spermine was responsible for the double rectification of divalent cation permeable non-NMDA receptors. Loss of rectification with time could thus be observed under certain conditions. This loss probably results from dialysis of the cell/patch since it is not observed when recordings are obtained using the permeabilized patch method and does not occur during whole cell recording if spermine is included in the intracellular solution. In addition spermine affects rectification in a dose-dependent manner (Bowie & Mayer, 1995; Donevan & Rogawski, 1995; Isa, Iino, Itazawa & Ozawa, 1995; Kamboj, Swanson & Cull-Candy, 1995; Koh, Burnashev & Jonas, 1995).

The genes for kainate receptor subunits (GluR5-7 & KA-1 & -2) also encode a glutamine at the Q/R site. Of these genes only GluR5 and GluR6 are edited at the Q/R site. Unlike GluR2, editing is only partial in that some copies remain unedited. Thus edited and unedited GluR5 and GluR6 subunits may coexist. Rectification properties are determined by the Q/R site, as for AMPA receptors. In contrast, the Q/R site does not dominate divalent cation permeability of kainate

receptors, permeability being influenced by several sites. These sites include the Q/R site and RNA editing sites in TMD I (see Hollmann & Heinemann, 1994).

1.5 Glutamatergic projections to the basal forebrain

The basal forebrain receives a plethora of inputs which terminate therein. There is also the possibility that some proportion of the fibres traversing the basal forebrain may release transmitters *en passant*. Thus the basal forebrain may receive input from any of numerous regions. These include various cortical areas, striatum, hippocampus, amygdala, hypothalamus, thalamus, subthalamic regions, tegmental regions, substantia nigra, locus coeruleus, raphe nuclei and the reticular formation. Transmitters released onto magnocellular cholinergic neurones include GABA, glutamate, substance P, neuropeptide Y, noradrenaline, dopamine and possibly acetylcholine (Záborski, Cullinan & Braun, 1991).

Carnes, Fuller & Price (1990) investigated glutamatergic/aspartatergic input into rat basal forebrain by retrograde labelling, injecting [^{3}H]-D-aspartate into the medial septum, diagonal band and nucleus basalis. The result was retrograde labelling of numerous regions, including cortical regions, hippocampus, amygdala, thalamus, hypothalamus, lateral septum, habenula, caudate/putamen, olfactory tubercle, nucleus accumbens, tegmental regions, raphe nuclei and locus coeruleus. The authors quantitated their data by estimating the density of retrograde labelling which resulted from injections into each region of the basal forebrain. Accordingly, major projections were as follows:

to medial septum and VDBB	thalamus, hypothalamus, lateral septum
to HDBB	olfactory cortex, thalamus, lateral septum
to anterior nucleus basalis	olfactory cortex, thalamus
to posterior nucleus basalis	thalamus, caudate/putamen

1.6 Glutamate receptors expressed in the rat basal forebrain

Given these glutamatergic projections to the basal forebrain, one might expect basal forebrain neurones to express glutamate receptors. However, little literature is available regarding the expression of glutamate receptors by cells within the basal forebrain. Only two studies have localized glutamate receptors to

magnocellular cholinergic neurones, both of these being concerned with AMPA receptor subunits. Further publications consider the presence of kainate, NMDA and metabotropic receptors within the basal forebrain, but provide no information as to which cells within the basal forebrain express these subunits.

The expression of AMPA receptor subunits by magnocellular cholinergic basal forebrain neurones was first investigated by Martin, Blackstone, Levey, Huganir & Price (1993) who used antibodies of three idiotypes; one raised against GluR1, one against GluR4 and one against an epitope common to GluR2, GluR3 and GluR4c. Immunocytochemistry was combined with staining for ChAT, for GAD, and for parvalbumin (a marker for GABAergic neurones within the basal forebrain). In rat, GluR1 was found to be expressed on the somata and dendrites of large neurones throughout the basal forebrain. GluR1 immunoreactivity was observed for the majority of GAD- and parvalbumin-positive neurones, but whilst some GAD- and parvalbumin-negative neurones expressed GluR1 no colocalization of GluR1 immunoreactivity and ChAT staining was observed. GluR2/3/4c was less abundant than GluR1 and GluR4 was expressed at still lower levels than GluR2/3/4c. No attempt was made to colocalize GluR2/3/4c or GluR4 immunoreactivities with markers for cholinergic or GABAergic neurones.

Page & Everitt (1995) investigated AMPA receptor expression in rat basal forebrain using antibodies with three idiotypes; one against GluR1, one against GluR2 and GluR3 and one against GluR4. Colocalization with antibodies against nerve growth factor receptor (NGFr) was also quantified. Their results largely concurred with those of Martin, Blackstone, Levey, Huganir & Price (1993), Page and Everitt finding that GluR1 levels were high throughout the basal forebrain, that GluR4 immunoreactivity was widely distributed and that GluR2/3 immunoreactivity was relatively scarce, being present at low levels in the nucleus basalis. GluR4 immunoreactivity colocalized with NGFr immunoreactivity such that approximately 60% of NGFr-positive neurones were also GluR4-positive. In contrast, only approximately 10% of NGFr-positive neurones were GluR1 positive and approximately 10% GluR2/3-positive.

Whilst no studies have examined the locations within basal forebrain of other glutamate receptor subunits, a number of subunits have been detected.

Petralia, Wang & Wenthold (1994a) raised antibodies of two idiotypes; one against KA2 and a second against GluR6/7. Using these antibodies, low to moderate expression of both epitopes was observed in the diagonal band.

Both NMDAR1 and NMDAR2 subunits are also present in the rat basal forebrain. Petralia, Yokotani & Wenthold (1994) reported moderate levels of NMDAR1 in both horizontal and vertical limbs of the diagonal band of Broca. Unfortunately their polyclonal antibody, raised against C-terminal peptide, bound only four of the seven splice variants of the NMDAR1 subunit. In a second study, the same group found that NMDAR2 expression was distributed similarly to NMDAR1 (Petralia, Wang & Wenthold, 1994b). Again, polyclonal antibodies were raised, this time to C-terminus peptide of NMDAR2A, which were found to possess high affinity for NMDAR2A and NMDAR2B subunits and only much lower affinity for NMDAR2C and NMDAR2D subunits.

Shigemoto, Nakanishi & Mizuno (1992) used *in situ* hybridization histochemistry to locate mGluR1 RNA and reported moderate to high expression in the nuclei of the diagonal band. They also noted 'intensely labelled large neurons...scattered' in the horizontal limb of the diagonal band of Broca and substantia innominata. Similar approaches were taken to investigate expression of mGluR2 (Ohishi, Shigemoto, Nakanishi & Mizuno, 1993a) and of mGluR3 (Ohishi, Shigemoto, Nakanishi & Mizuno, 1993b). Low levels of mGluR2 were expressed in both medial septum and nuclei of the diagonal band. Low levels of mGluR3 were detected in the nuclei of the diagonal band, but none was present in the medial septum.

In summary, numerous glutamate receptor subunits are known to be expressed by cells within the basal forebrain, but only GluR4, and to a lesser degree GluRs 1-3, have been localized to magnocellular cholinergic neurones.

1.7 Electrophysiology of the rat basal forebrain

1.7.1 Voltage-gated currents

Several authors have investigated the electrophysiological properties of rat cholinergic magnocellular basal forebrain neurones using voltage-clamp techniques. In addition to the sodium current (Nakajima, Nakajima, Obata, Carlson &

Yamaguchi, 1985) both low and high voltage-activated calcium currents have been recorded (see section 5.1.2). Several potassium currents have been observed, namely delayed rectifier, A-current and inward rectifier (Stanfield, Nakajima & Yamaguchi, 1985; Nakajima, Nakajima, Obata, Carlson & Yamaguchi, 1985; Yamaguchi, Nakajima, Nakajima & Stanfield, 1990; Takano, Stanfield, Nakajima & Nakajima, 1995; Waters, Sim & Allen, unpublished observations). Some authors have also observed an apamin-sensitive calcium-activated potassium conductance giving rise to a slow afterhyperpolarization (Markram & Segal, 1990; Gorelova & Reiner, 1996).

1.7.2 Ligand-gated currents

Few publications are available regarding ligand-gated currents in basal forebrain neurones. Kumamoto & Murata (1995b, 1996) have investigated γ-aminobutyric acid receptor type A ($GABA_AR$) -mediated responses and strychnine-sensitive glycine receptor-mediated responses.

These authors have also characterised ionotropic glutamate receptor-mediated responses from foetal rat septal neurones in dissociated culture (Kumamoto & Murata, 1995a). Glutamate, AMPA, quisqualate, kainate and NMDA all produced inward currents in a dose-dependent manner. Responses to all but kainate showed some desensitization when applied using a flow tube or by pressure-application. NMDA receptor-mediated currents were sensitive to glycine, AP5, MK-801, magnesium and zinc ions. In contrast, non-NMDA receptor-mediated currents were sensitive to CNQX, with a dissociation constant of 0.27μM for the responses to kainate. Current-voltage relationships for non-NMDA receptor-mediated responses, recorded without spermine in the intracellular solution, were outwardly rectifying and were influenced very little by changes in extracellular calcium concentration, suggesting that divalent ion permeabilities of the non-NMDA receptors expressed by these neurones were low.

Schneggenburger, Zhou, Konnerth & Neher (1993) and Schneggenburger, Tempia & Konnerth (1993) combined electrophysiological and optical methods to quantitate the contribution of calcium to glutamate receptor-mediated currents in septal neurones. With an extracellular calcium concentration of 1.6mM, these

authors found that calcium carried 1.2-1.4% of AMPA- or kainate-induced current. Optical methods were also employed by Bleakman, Roback, Wainer, Miller & Harrison (1993) who found that 10μM glutamate, AMPA and kainate each produced a rise in intracellular free calcium concentration of several hundred nanomolar. That these agonists were acting at non-NMDA receptors was verified using CNQX and DNQX.

1.8 Aims of the present work

(1) To establish which classes of glutamate receptor are expressed by basal forebrain neurones.

(2) To investigate the unusual features of non-NMDA receptors expressed by basal forebrain neurones, including calcium permeability and block by divalent ions.

(3) To investigate the possibility that glutamate application may inhibit voltage-gated calcium channel activity, through metabotropic glutamate receptors and/or through non-NMDA receptors.

Methods

Glutamate receptors expressed by basal forebrain neurones were studied using two preparations: (i) dissociated cultures typically maintained for 2-4 weeks *in vitro* prior to recording, and (ii) acutely dissociated neurones.

Much of the data presented below concern neurones in culture. The production and maintenance of dissociated cultures proved extremely difficult; culture problems undoubtedly provided the greatest impediment to the present work. In addition, cultured neurones possessed extensive processes leading to concern regarding space-clamp errors and some uncertainty exists regarding phenotypic changes in culture. Acutely dissociated neurones were found to be preferable for many experiments (chronologically, the later experiments) avoiding these culture-related problems.

2.1 Culture methods

Cholinergic magnocellular basal forebrain neurones were grown in dissociated culture with other basal forebrain cell types using the method of Allen, Sim & Brown (1993).

2.1.1 Dissociation procedure

Post-natal day 11-14 Sprague-Dawley rat pups were killed by decapitation (no anaesthesia). The brain was rapidly removed and placed in ice-cold Gey's balanced salt solution supplemented with 0.6% (w/v) D-glucose (total 0.7%) and 8mM $MgCl_2$ (total 8.28mM) hereafter referred to as GBSS. After hemisection in GBSS, 400μm coronal slices were cut using a McIlwain tissue chopper and the slices returned to GBSS. Regions of the basal forebrain nuclei within the slices were visually identified using a light microscope (transillumination, approx. x20 total magnification).

Using the classification of Mesulam *et al* as recounted by Wainer & Mesulam (1990), regions corresponding to Ch3 (nucleus of the horizontal limb of the diagonal band of Broca) and Ch4 (substantia innominata/nucleus basalis of Meynert) were dissected from the slices. The tissue fragments were washed

twice in Ca^{2+}-, Mg^{2+}-free Hanks' balanced salt solution containing 10mM HEPES (HEPES/HBSS) then once in a similar solution containing 0.125% (w/v) trypsin. The tissue fragments were then resuspended in trypsin-containing HEPES/HBSS and incubated for 1 hour at 37°C in an humidifed atmosphere of 5% CO_2 in air, with one change into fresh trypsin-containing medium after 30 minutes.

After enzyme treatment, tissue fragments were washed repeatedly in Ca^{2+}-, Mg^{2+}-free Hanks' balance salt solution supplemented with 8mM $MgCl_2$, 10% (v/v) heat-inactivated foetal calf serum and 10μg/ml deoxyribonuclease I. The tissue was then transferred to a similar solution containing 20μg/ml deoxyribonuclease I and mechanically dissociated by trituration through a flame-polished pasteur pipette.

The resulting cell suspension was centrifuged at 27g for 10 minutes and the pellet resuspended in approximately 1ml of growth medium of the following composition:

40% (v/v)	Dulbecco's modified Eagle's medium
40% (v/v)	Leibovitz's L-15 medium
10% (v/v)	foetal calf serum
25ng/ml	Nerve Growth Factor 7S
0.29mg/ml	L-Glutamine
6% (w/v)	D-Glucose
0.15-0.3%	Sodium hydrogencarbonate

Cells were plated onto prepared 35mm polystyrene cell culture dishes which had been coated with 50μg/ml poly-D-lysine, washed thoroughly and allowed to dry. The cultures were placed in an humidified atmosphere of 5% CO_2 in air at 37°C. Growth medium was replaced after approximately 3 hours.

2.1.2 Maintenance in culture

Medium was replaced approximately 24 hours after plating and thereafter as required; generally every 3-7 days. Where required a cocktail of anti-mitotics was added after a minimum of several days in culture, to give final

concentrations of approximately 0.6μM each of cytosine-β-D-arabinofuranoside, 5-fluoro-2'-deoxyuridine and uridine (all supplied by Sigma). Cells were maintained in culture for 1-8 weeks prior to use, though were generally used after 2-4 weeks in culture.

Cultures are illustrated in figure 2.1. (Age of cultures: 14 DIV)

2.1.3 Acutely dissociated neurones

The above dissociation procedure was also used to obtain neurones for acute use. Cells were plated onto alcian blue-coated borosilicate glass coverslips rather than polylysine-coated plates. Coverslips were dipped into 96% ethanol, flamed and allowed to cool. A few minutes prior to plating, coverslips were covered with 0.1% alcian blue (in dH_2O). After 1-2 minutes coverslips were dipped into distilled water to remove excess alcian blue, and then into growth medium. Cells were plated whilst the coverslips were still wet. Cells were used between 1 and 10 hours after plating.

Figure 2.1 Phase contrast micrographs of basal forebrain neurones in dissociated culture. A, Typical culture under low magnification. Several magnocellular neurones are clearly visible (labelled). B, Type II neurone under high magnification. C (overleaf), Type I neurone. D (overleaf), Type IV neurone.

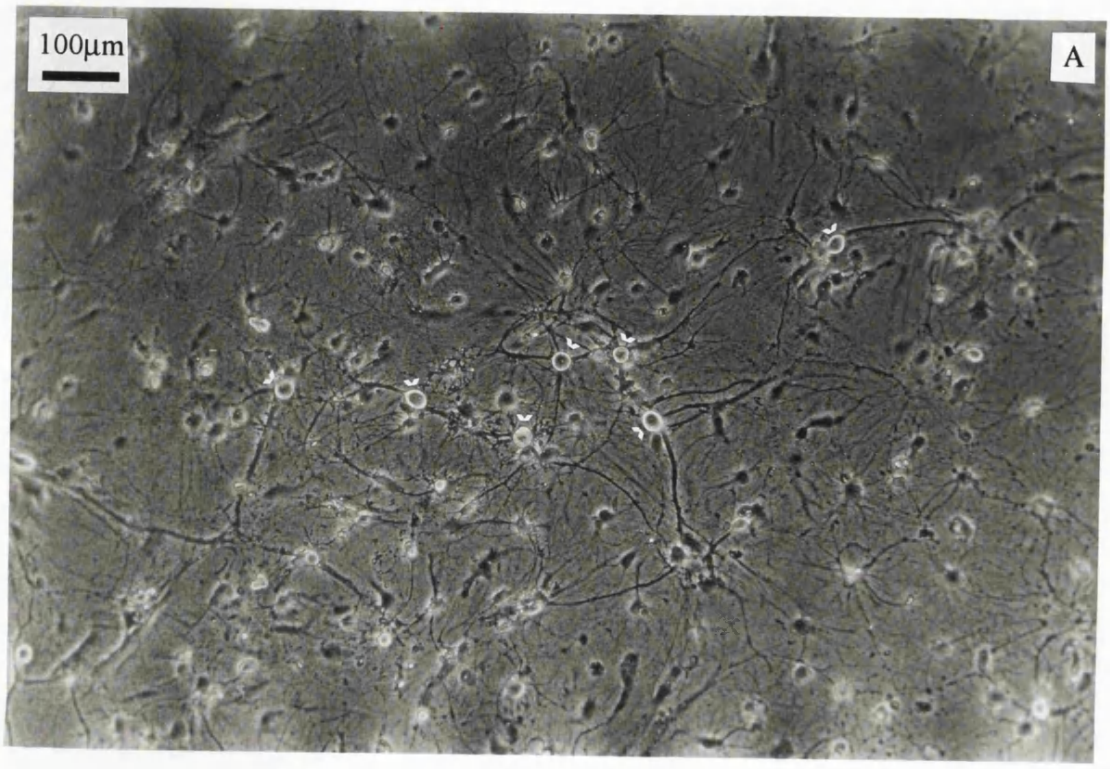
100μm
A

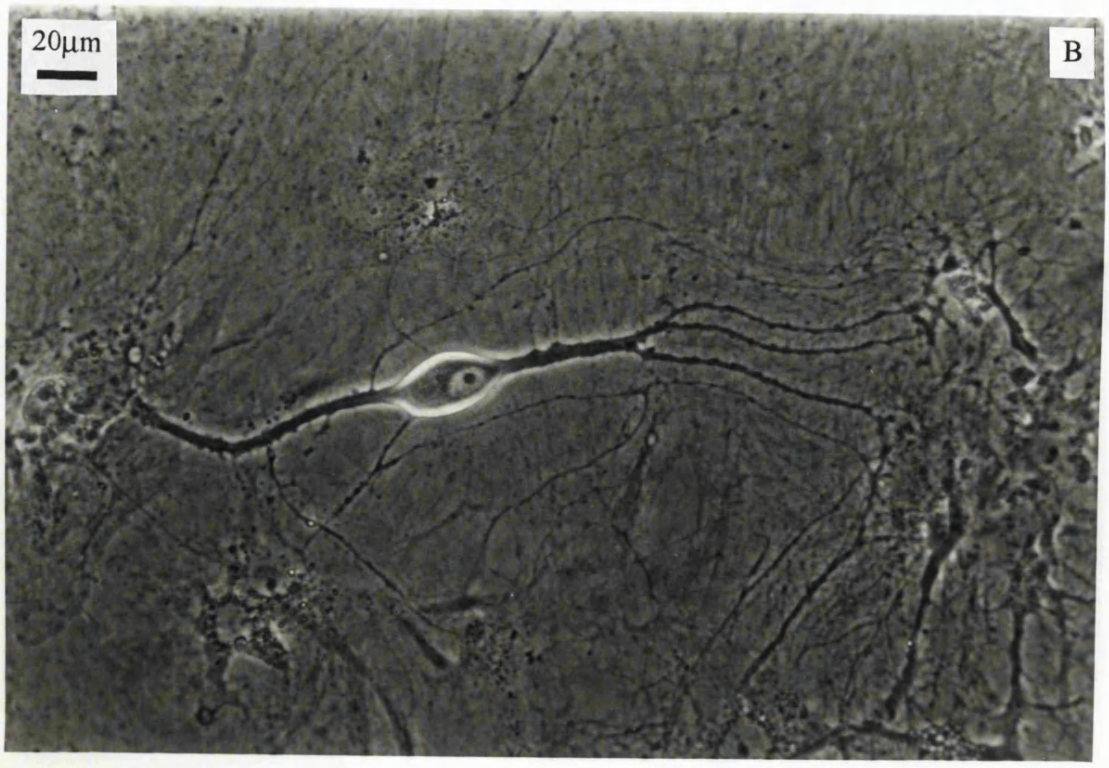
20μm
B

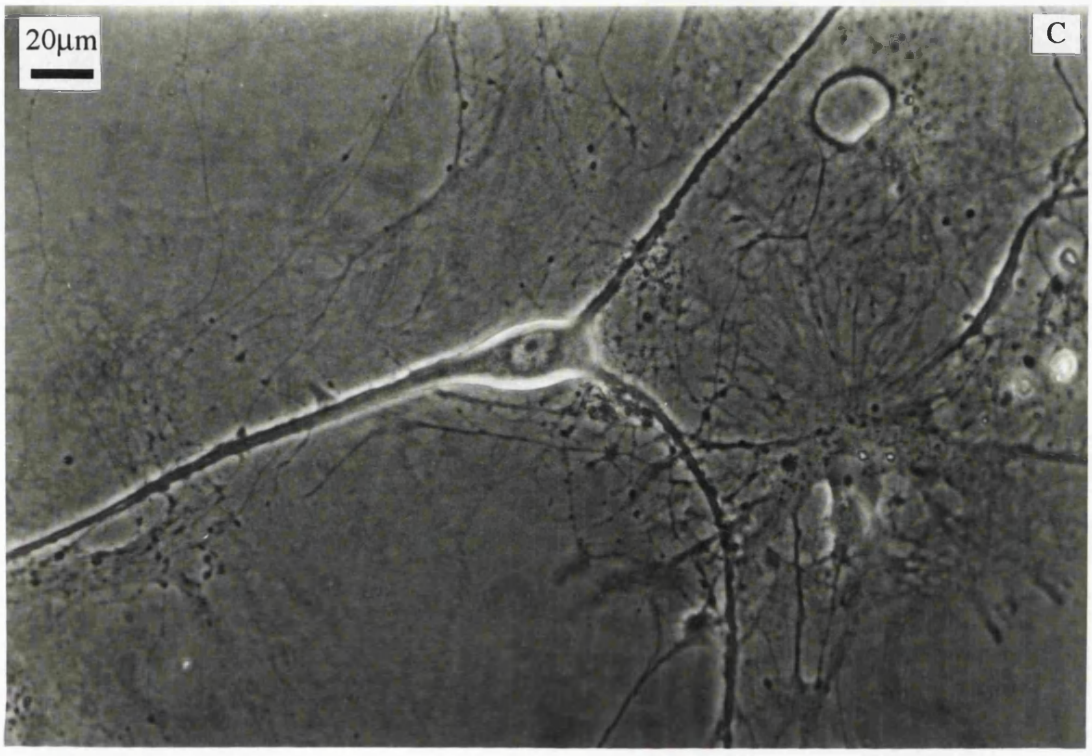
20μm
C

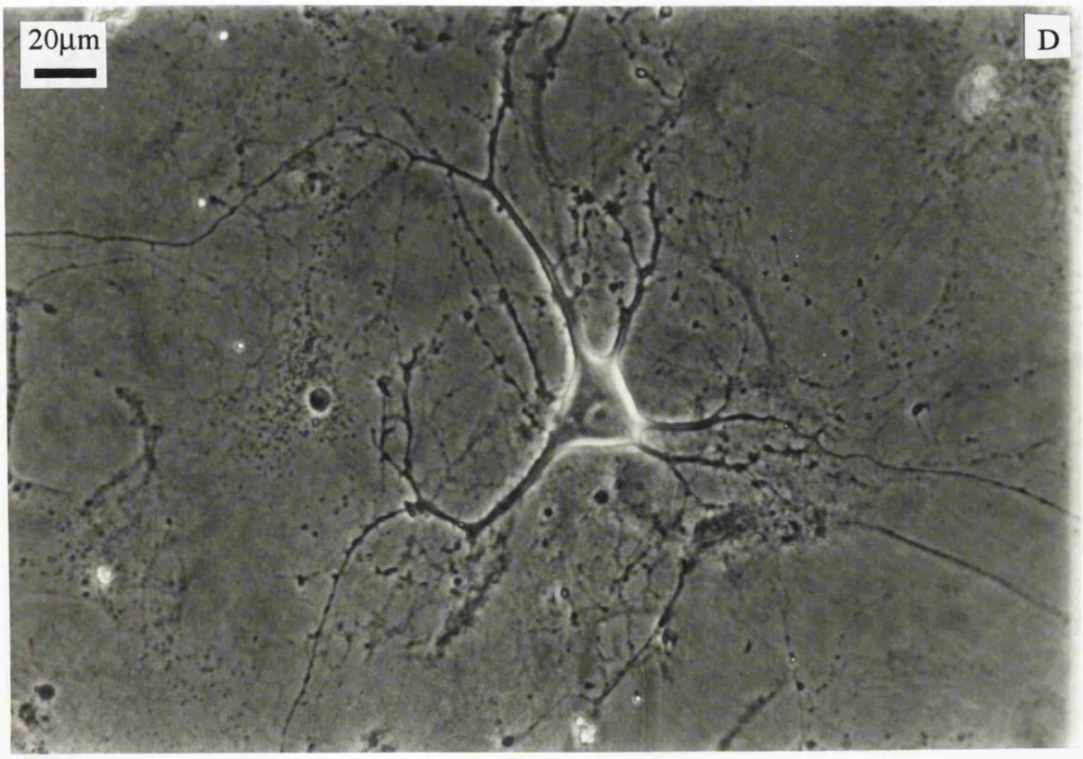
20μm
D

2.2 Recording setup

2.2.1 General

The microscope was placed on an air table for vibrational isolation and surrounded by a Faraday cage for electrical isolation. Recordings were obtained using various configurations of the patch-clamp technique (Hamill, Marty, Neher, Sakmann, & Sigworth, 1981).

Current- and voltage-clamps were imposed using a patch-clamp or a switch-clamp amplifier as appropriate. Voltage-clamp was established and monitored with the aid of two oscilloscopes. Current and voltage commands were generated using either a timer unit or the computer, the latter (connected to the amplifier by the DMA board) using the pClamp suite of software. Amplifier output was lowpass filtered using the amplifier's integral filter (4-pole Bessel) and an external filter unit (8-pole Bessel) where appropriate. The signal was recorded using a pen recorder, DAT tape-recorder and/or personal computer. Output to the computer was recorded using pClamp or axotape software after pre-amplification of the signal where appropriate.

Recordings were obtained from cells only if the seal in the cell-attached configuration was in excess of 1GΩ and resting membrane potential was at least -60mV. Immediately following recording the electrode was removed from the cell and the junction potential noted. Cells were generally held at -70mV.

2.2.2 Electrodes

Pipettes were fabricated from borosilicate glass capillaries on a vertical electrode puller. For recording electrodes, pipettes were coated in Sylgard silicone elastomer. The Sylgard was cured using a heating coil (constructed in-house). Prior to recording, the electrodes were fire-polished using a microforge. Electrode, holder and headstage were positioned using a micromanipulator. Electrode resistance was typically 4-8MΩ when filled with the intracellular solution given in section 2.2.4 (below).

2.2.3 Bath ground and electrode connections

A bath ground electrode containing 0.9% (w/v) NaCl and 2-3% agarose

contained within a length of borosilicate glass capilary tube connected the bath solution to a 3M KCl solution contained in a separate reservoir. This KCl solution contacted the AgCl terminal of a Ag/AgCl half-cell, which was connected by a length of wire to the earth point of the headstage.

The headstage was in turn connected to the intracellular solution filling the electrode by a length of silver wire with a AgCl-coated surface, thus forming a second Ag/AgCl half-cell. The silver wire was coated with AgCl by electrolysis; the silver wire to be coated was placed in 0.9% (w/v) NaCl and formed the anode. A second silver wire formed the cathode and AgCl coating was acheived by the passage of approximately 8μA of current for approximately 1 minute. The recording set-up is schematically illustrated in figure 2.2.

2.2.4 Recording solutions

Intracellular solution:

K acetate	108mM
KCl	15.6mM
HEPES	40mM
NaOH	10-12mM (pH 7.3)
EGTA	3mM
$CaCl_2$	0.822mM*
$MgCl_2$	1mM
Mg.ATP	4mM
Na_2.GTP	0.1mM

*free calcium concentration 30nM

Approx. 260mOsM

Accompaying 'modified Krebs' extracellular solution:

NaCl	123mM
KCl	3mM
$CaCl_2$	2.5mM
$MgCl_2$	1.2mM
HEPES	5mM (pH7.4)
$NaHCO_3$	25mM
Glucose	11mM

0.5μM tetrodotoxin where necessary

Approx. 285mOsM

The extracellular solution was continuously gassed with 95%O_2/5%CO_2.

Figure 2.2 - Recording bath setup

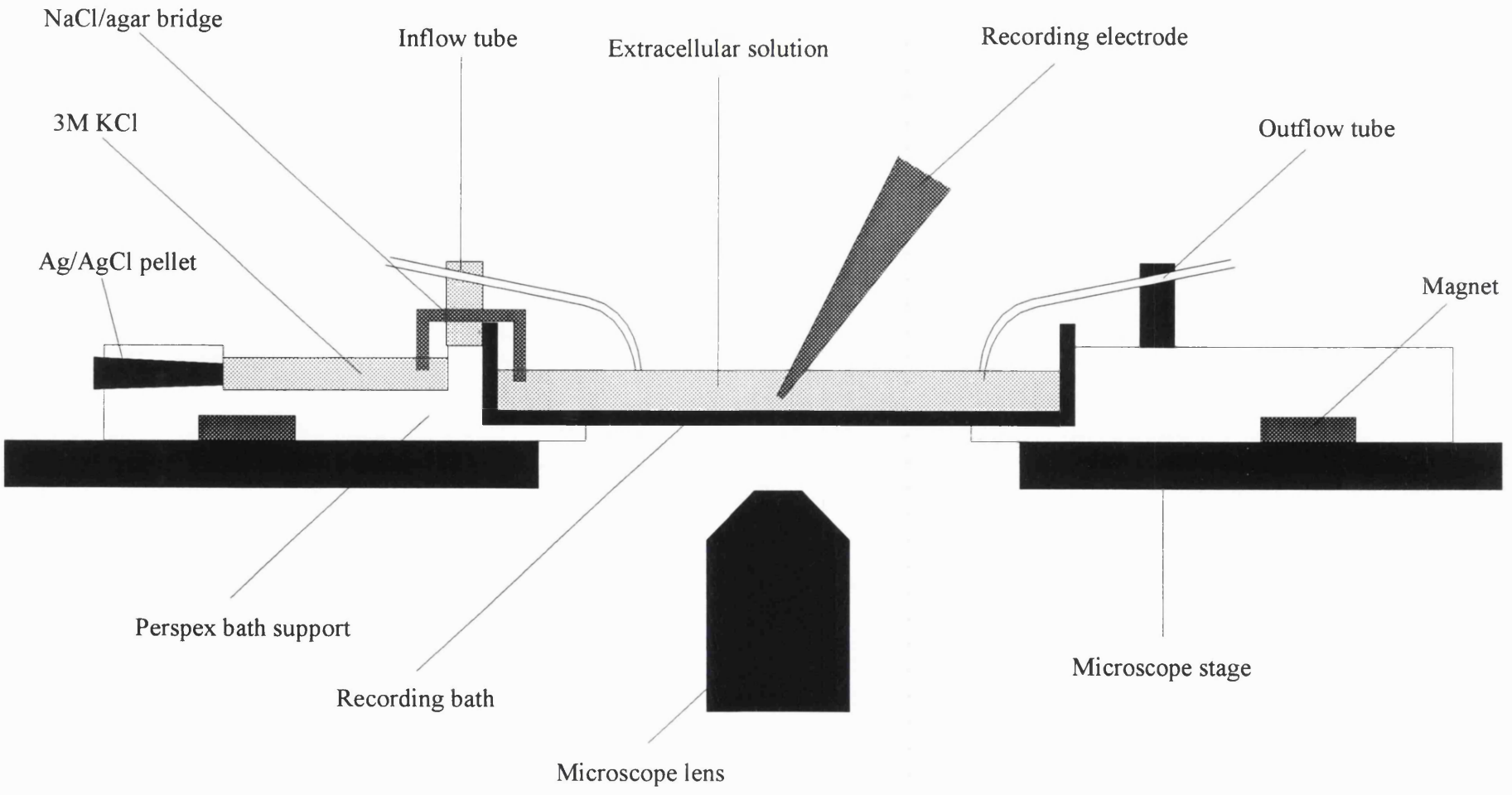

2.3 Capacitance Measurements

Few authors have published capacitance values for basal forebrain cells either in slices or dissociated culture. Castellano & López-Barneo (1991) gave a value of 8 $\pm$ 3 pF for acutely dissociated medial septal neurones from adult guinea pig. Murchison & Griffith (1995, 1996) gave mean values of 15-18pF (depending on age of animal) for acutely dissociated medial septum/diagonal band neurones from adult rat. These values are surpisingly low, corresponding to cells of diameter 7-8μm and 11-12μm for the two publications respectively (assuming a specific membrane capacitance of 1μF/cm^2 and spherical cell). Presumably neither paper concerns magnocellular neurones. In contrast, Griffith, Taylor and Davis (1994) used acutely dissociated neurones from adult guinea pig medial septum/diagonal band and reported capacitances of 10-60pF. The upper limit corresponds to a cell of diameter 44μm. This range therefore includes magnocellular neurones.

In order to express the magnitude of the glutamate receptor-mediated currents from basal forebrain neurones as current densities, it was necessary to measure cell capacitance. Capacitance was measured under voltage-clamp conditions. Cells were clamped to -70mV using an axopatch-200A amplifier and 5mV hyperpolarizing voltage steps were applied. Records were leak-subtracted using the axopatch circuitry. The current trace was filtered at 10kHz and digitized at 40kHz. Current responses to ten steps, delivered at 1Hz, were recorded, adjusted for any slight shift in holding current and averaged prior to analysis.

A typical resulting trace is illustrated in fig 2.3.1. The capacitative transient decayed to baseline in approximately 10-15ms. Decay of the transient was generally best fit by a second order exponential (example given in inset) though transients from some cells were best fit by first order exponential decays.

Capacitative charge transfer was measured as the integral of the transient upon hyperpolarization, from the beginning of the rising phase of the transient to a point where decay of the transient was complete (marked on fig. 2.3.1 as 1

Figure 2.3.1 Capacitance measurements - method

Current trace showing capacitance transients resulting from 5mV hyperpolarization (duration 30ms) used to measure cell capacitance. Capacitative charge transfer was calculated by integration of the transient. Lines 1 and 2 define the limits between which capacitance was calculated by integration.

Figure 2.3.1

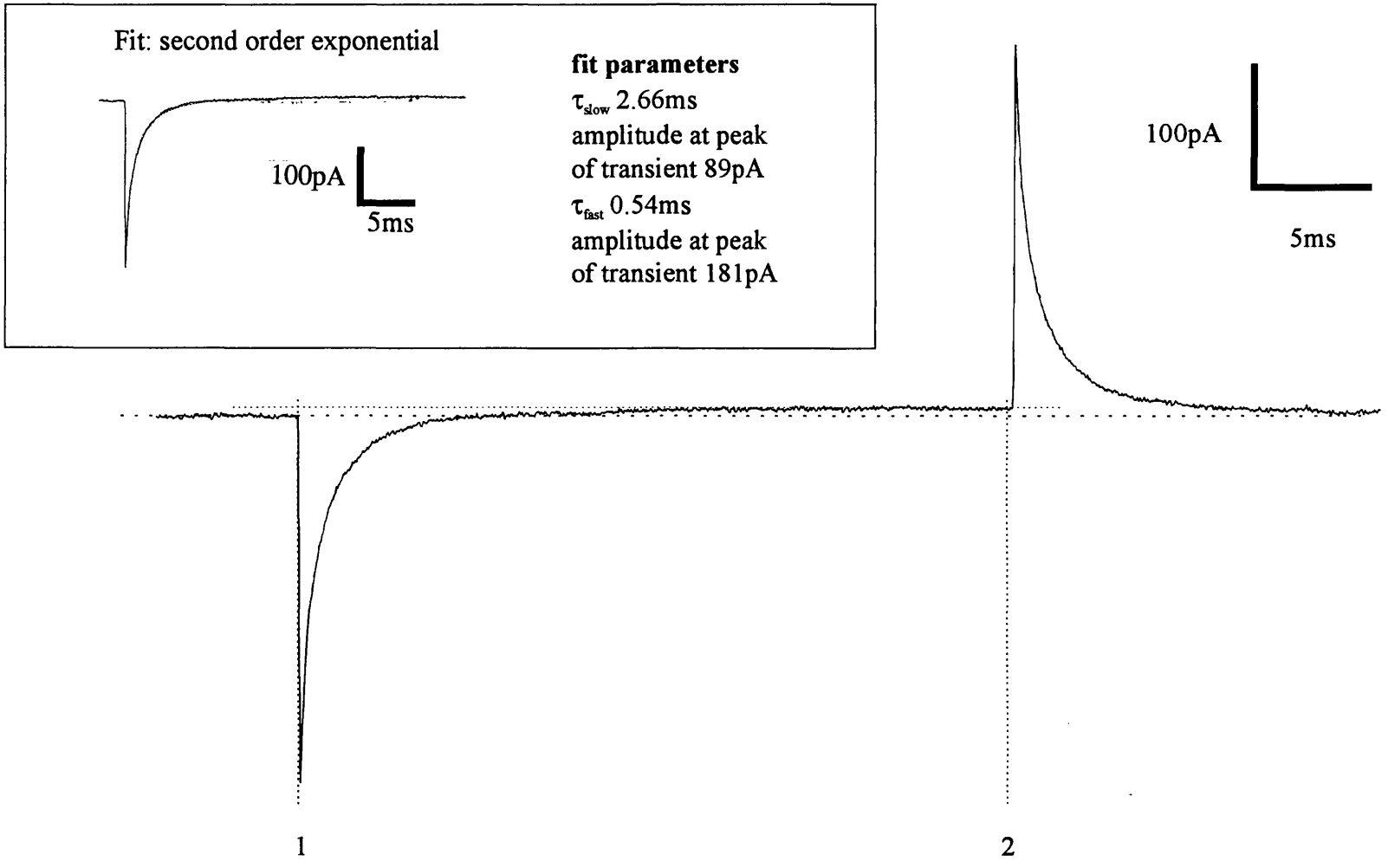
Fit: second order exponential
100pA
5ms
fit parameters
τ_{slow} 2.66ms
amplitude at peak
of transient 89pA
τ_{fast} 0.54ms
amplitude at peak
of transient 181pA
100pA
5ms
1
2

and 2 respectively). As a result of slight inaccuracy in adjustment of the leak subtraction circuitry, the baseline at -75mV was generally slightly shifted from that at -70mV. These two baselines are illustrated in fig. 2.3.1 as dashed and dotted horizontal lines respectively. The -75mV baseline was used when calculating capacitative charge transfer. The cell capacitance was calculated from the measured charge transfer by dividing charge transfer (expressed in Coulombs) by the amplitude of the voltage step (5×10^{-3} volts).

This also permitted calculation of access resistance, by dividing the time constant of the decay by the cell capacitance. Input resistance was estimated from the setting of the leak subtraction circuitry.

Capacitance values were calculated in this manner for 106 cells of 8 to 31 days in culture and are plotted in fig. 2.3.2 (upper panel). It is clear that mean capacitance does not change after 10 days in culture. The capacitance histogram shown in fig. 2.3.3 (upper panel) was generated from cells which had been in culture for at least 10 days and shows that capacitance was approximately normally distributed. Mean capacitance was 61 ± 1.6pF ($n=102$). Assuming a membrane capacitance of $1\mu F/cm^2$, this corresponds to a surface area of a sphere of diameter $44\mu m$. This is greater than the somatic diameter of the majority of magnocellular basal forebrain neurones and probably indicates that proximal processes contribute to the capacitance measured at the soma (consistent biexponential decay of the transient). An alternative explanation is that the specific membrane capacitance of basal forebrain neurones is greater than $1\mu F/cm^2$.

Of 106 cells, 28 had input resistances of less than 100MΩ (the lower limit of the axopatch leak subtraction circuitry). The histogram shown in fig. 2.3.3 (lower panel) shows input resistances for the remaining 78 cells. The distribution of input resistances is not clearly normal. The median value (of all 106 cells) was 110MΩ.

Cell capacitance was also plotted against cell morphological type revealing no correlation (figure 2.3.2, lower panel). Cells were classified according to the nomenclature of Sim (1994) who distinguished four cell types on the grounds of somatic shape and dendritic structure. By this nomenclature,

a type I neurone is tripolar with an approximately pyramidal soma, type II is bipolar with two principal dendrites projecting from an approximately oval soma, type III is bipolar with twoprincipaldendrites one of which bifurcates within approximately 10μm of the soma and type IV is multipolar. Sim found that morphology in dissociated culture was indistinguishable from that in slice preparations.

Figure 2.3.2
Plots of cell capacitance (ordinate) against duration for which neurones were maintained in culture prior to recording (abscissa, upper panel) and cell morphology (abscissa, lower panel). Cell capacitance was measured as stated in the text and stabilized at 61 ± 1.6pF after 10 days *in vitro* regardless of cell morphology.

Figure 2.3.2

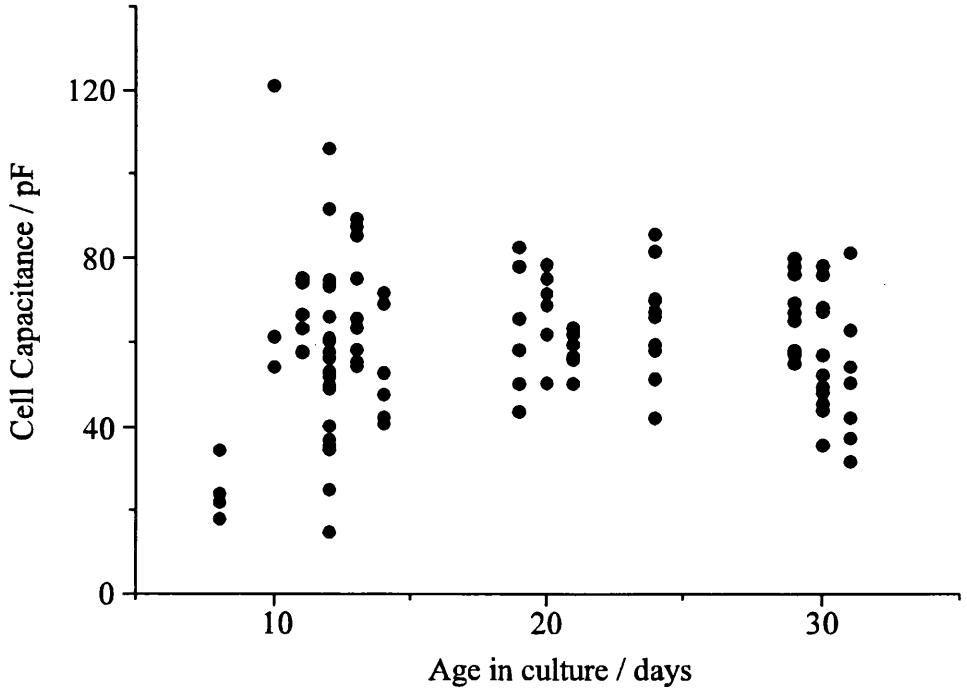
Cell Capacitance / pF
120
80
40
0
10
20
30
Age in culture / days

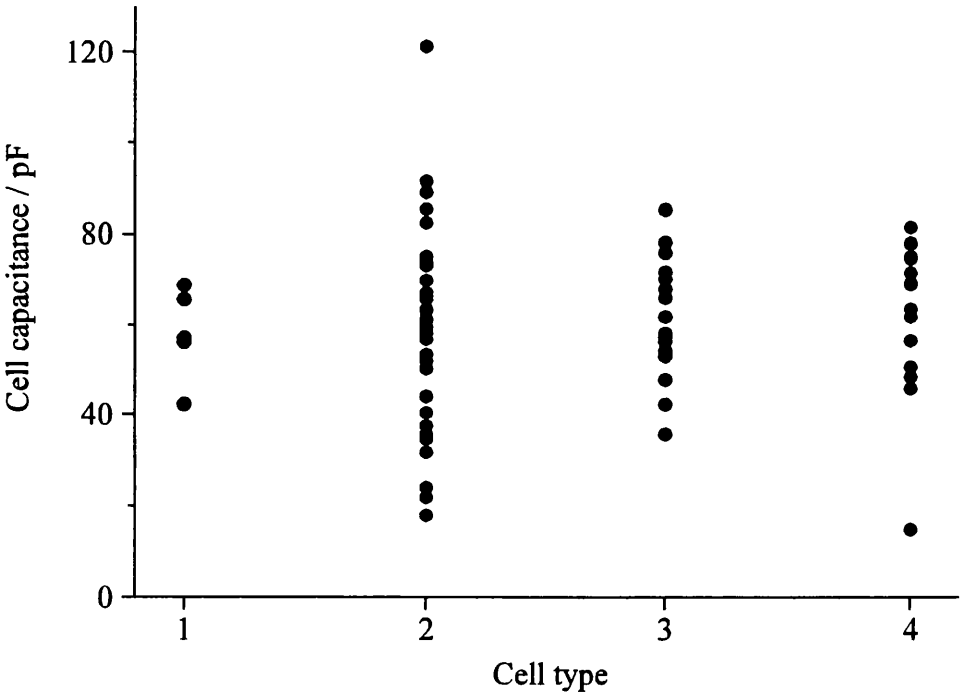
Cell capacitance / pF
120
80
40
0
1
2
3
4
Cell type

Figure 2.3.3
Histograms of cell capacitance (data from cells after a minimum of 10 days *in vitro*, upper panel) and input resistance (lower panel). Cell capacitance was approximately normally distributed with mean ± SEM of 61 ± 1.6pF (n=102). The distribution of input resistances appears to be skewed, possibly because 28 neurones had input resistances of less than 110MΩ. Median input resistance was 110MΩ.

Figure 2.3.3

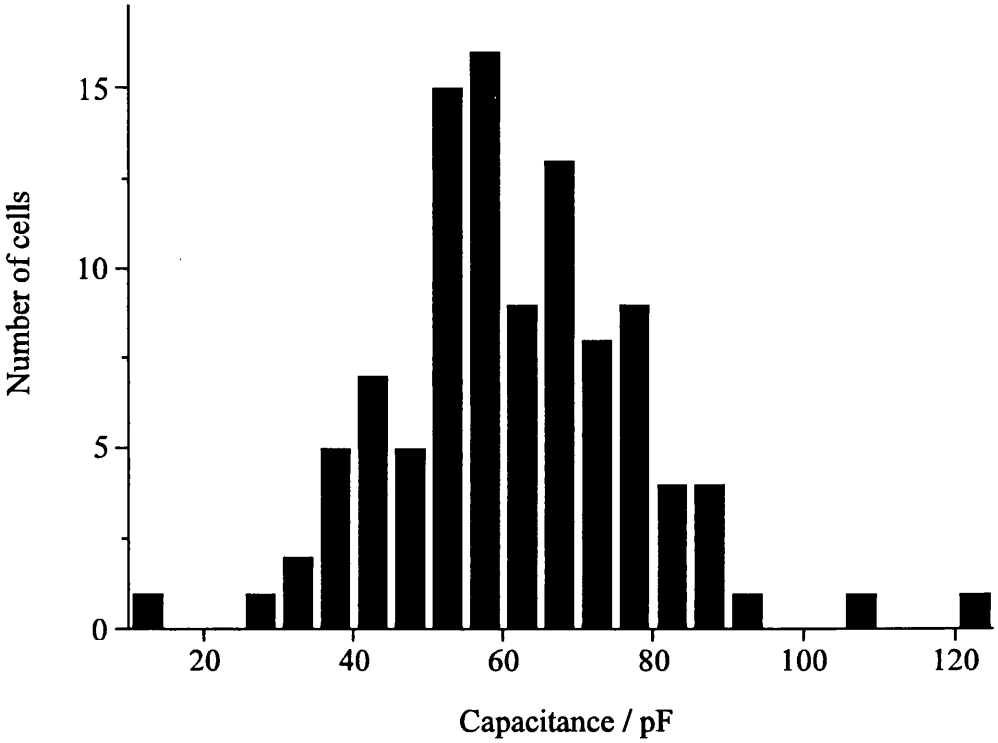
Number of cells
15
10
5
0
20
40
60
80
100
120
Capacitance / pF

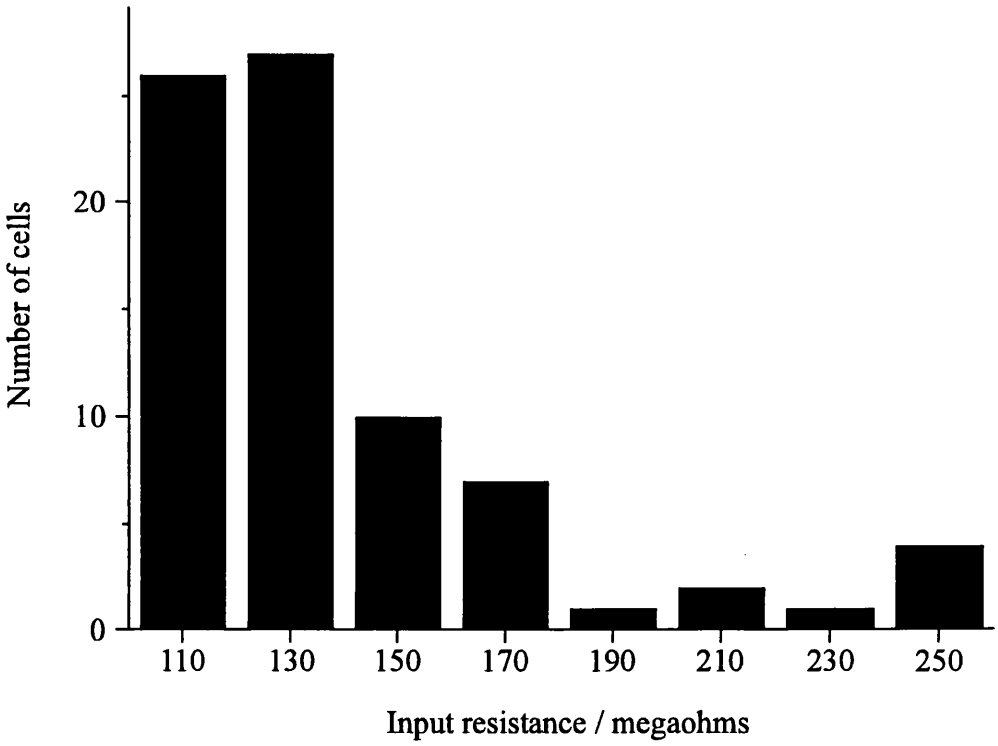
Number of cells
20
10
0
110
130
150
170
190
210
230
250
Input resistance / megaohms

2.4 Perfusion systems

2.4.1 Superfusion system

All electrophysiological recordings were made from cells grown in 35mm culture dishes. For recording, the lid of the dish was discarded, the base constituting the recording 'bath'. The bath was placed into a hole in a 12mm deep perspex plate, designed to hold the bath, and this in turn was mounted on the microscope stage. Magnets inset into the base of the perspex plate immobilised the bath relative to the microscope stage. Fitted to the perspex plate on either side of the bath were small clamps which held and permitted the positioning of two stainless steel tubes. Through these tubes flowed the incoming and outgoing solutions by which the bath was perfused.

An array of 50ml reservoirs was mounted approximately 60cm above the level of the recording bath. These contained the modified Krebs extracellular solution into which any compounds which were to be 'bath-applied' were dissolved. Solutions from these reservoirs fed via a short length polyethylene or nylon tubing into a multi-way tap from which a single outflow permitted the passage of solution under gravity down a length of flexible polyethylene or nylon tubing to one end of one of the stainless steel tubes (inflow), the other end of which was placed in the 35mm dish. The second steel tube (outflow) was connected by a length of silicone elastomer tubing to a peristaltic pump which removed solution from the bath. The output of the peristaltic pump was passed into another length of polyethylene or nylon tubing which either fed to waste or returned solution to one of the perfusion reservoirs, as appropriate. This set-up resulted in a bath volume of a few ml and a total volume for the perfusion system (excluding the reservoirs) of approximately 10ml. Bath solution could be exchanged in approximately 30 seconds with a flow rate of approximately 10 ml per minute.

2.4.2 Drug application methods

Drugs were applied to cells using three methods; bath-application, pressure-application and stepper-application. Bath-perfusion consisted of simply adding the drug to the reservoir from which the bath was superfused. This resulted in application of a known concentration of drug to the cell surface, but only produced very slow changes in drug concentration (maximum concentration achieved after approximately 20 seconds).

For pressure-application a glass pipette was filled with extracellular solution into which was dissolved the drug to be applied (referred to as the test solution). The pipette tip was generally placed within 10μm of the cell soma and pressure applied to the rear of the pipette. Pipette tip diameters were typically as used for recording electrodes. The application of pressure was controlled by pressure-application apparatus (constructed in-house). Application was initiated and terminated either manually (by means of a switch) or automatically (using a TTL input from a timer or the computer). Pressure was supplied by compressed gas cylinder (either a nitrogen or air). The pressure applied to the rear of the pipette was typically 4-6lb/in^2. Whilst this method offered a faster method of drug application, it also carried a number of disadvantages:

(i) Diffusion from the tip of the pipette may cause some tonic stimulation or desensitization of receptors.

(ii) Pressure-application inevitably results in the delayed application of the drug to relatively remote part of the cell. When studying a fast response, such as that resulting from stimulation of ionotropic glutamate receptors, this can severely complicate the kinetics of the response.

(iii) Mixing of the pressure-ejected solution with the bulk superfusing solution leads to uncertainty as to the precise concentration of drug at the cell surface.

(iv) Only one solution can be applied from a pipette since there is no method of exchange of solution in the pipette. Hence if two solutions are to be applied, then this requires either the use of two application systems or the exchange of one application pipette for another during recording.

These problems can be overcome with the use of a fast stepper or step-translator device. Such devices have been widely used with excised patches for the 'concentration-clamp' technique, the faster devices offering complete solution exchange within a few hundred micro-seconds. Test solution flows continually from an application tube or pipette and is rapidly applied to the patch or cell by lateral translation of the tube or pipette.

Continual flow of drug-containing solution into the bath obviously presents the problem of tonic application of drug to the patch/cell. In the context of application to excised patches this is generally overcome by perfusing both control and test solutions simultaneously through the two halves of a borosilicate pipette with a central division (theta glass). The patch is then placed in the stream of control solution and the distance of the lateral step movement is then adjusted such that translation results in rapid transfer of the patch from control to test solution. Thus test solution contaminates the bath solution, but this is unimportant since the patch is bathed in control or test solution from the stepper device rather than the bath solution. This is illustrated in figure 2.4(a).

The use of theta glass is not practicable for perfusion of a whole cell, since mixing of the two streams of solution with each other and with the bath solution is significant within the distance required to perfuse a whole cell. Mixing is also exacerbated by deflection from the bottom of the culture dish. Therefore an alternative application system was devised as follows. Test solution flowed continually through a single application pipette of tip diameter 50-150μm. This was positioned using a micromanipulator such that the tip of the pipette was approximately 50-100μm from the soma when applying test solution. The tip of the application pipette was step translated 0.5-1mm to/from the cell. A second pipette of similar tip diameter was mounted on a micromanipulator and oriented toward the cell soma with its tip placed

approximately 200μm from the soma. From this second pipette continually flowed control (or 'wash') solution.

These two pipettes were positioned such that the position of the step-application pipette determined which of the two flows was dominant. That the cell was not exposed to drug when the application pipette was 'stepped away' from the cell was verified by interrupting the flow of test solution. The cell was not considered exposed to drug if the holding current did not change upon cessation or restoration of the flow of test solution. Similarly, that the cell was exposed to the full test concentration of drug was verified by suspension of 'wash' solution flow during test solution application.

The application pipette was gravity-fed from 2-5ml reservoirs. The translation distance was set manually and the timing and duration of application was determined either manually or automatically (using TTL pulses from a timer or the computer).

The advantages are simply that the test solution is rapidly applied to the whole cell at a known concentration without exposure of the cell to drug between applications. In addition, the test solution can be changed during recording by switching to a different test solution between applications.

There are a number of practical problems with this method. These include the frequent blockage of the two pipettes by debris and air bubbles. In addition, this technique necessarily uses larger quantities of drug than pressure-application.

This technique is illustrated schematically in figure 2.4.

Figure 2.4 - Stepper application system

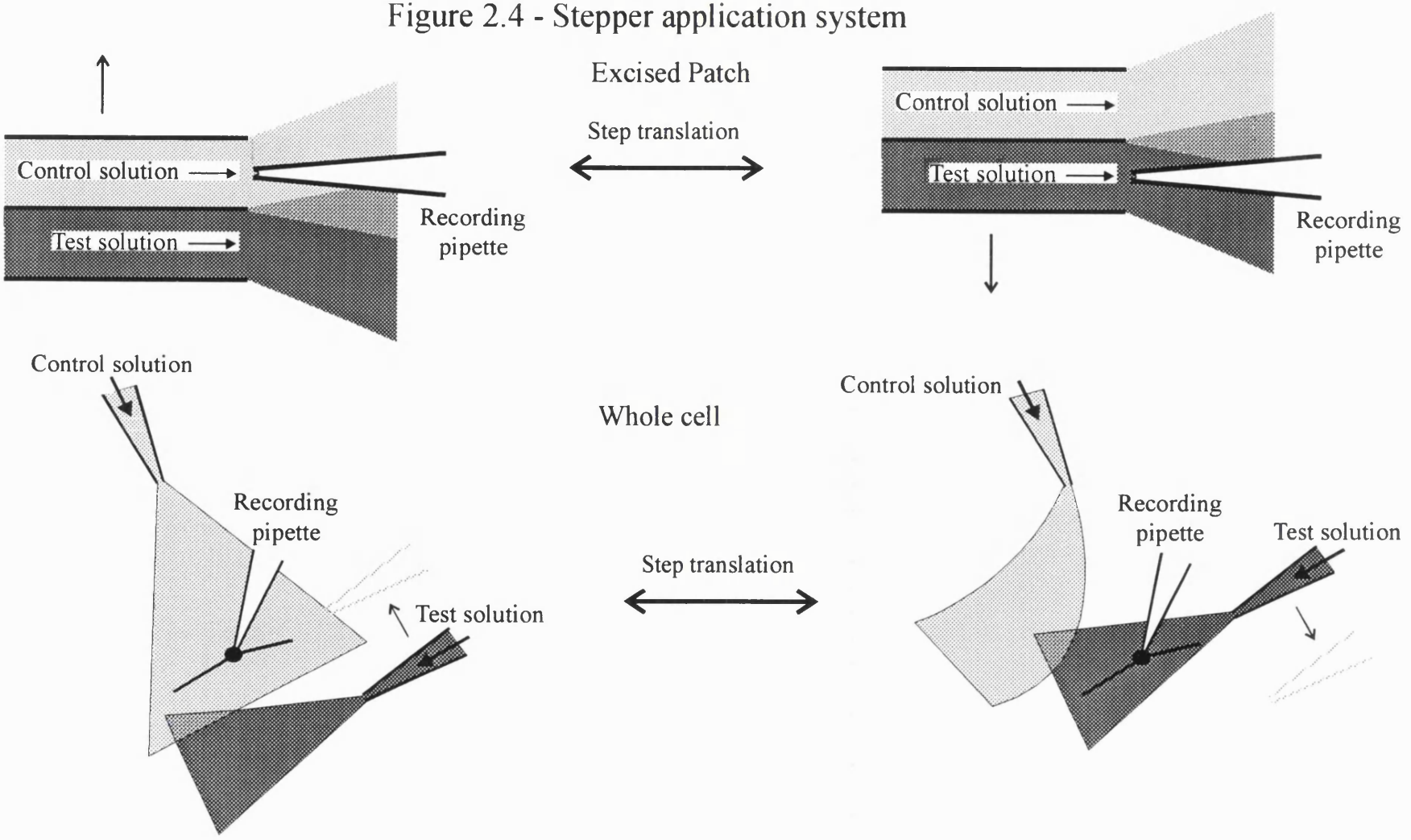

2.5 Nucleated patches & I-V relationships

2.5.1 Difficulties

Attempts to record current-voltage (I-V) relationships for glutamate receptor-mediated currents encountered a number of problems, summarised as follows:

(i) In order to gain control of membrane potential positive to -40 to -30mV it was necessary to inhibit the very large potassium currents (A-current and delayed rectifier) found in these cells using tetraethyl ammonium (TEA) or a caesium-based (rather than the more normal potassium-based) intracellular solution. Unfortunately this is prone to cause space-clamp problems with cells with large processes. This is because the membrane potentials of poorly clamped processes are under strong influence of potassium conductances. Inhibition of potassium conductances relieves this stabilising influence by increasing the input resistance of the membrane. The result is that depolarization of the soma can result in membrane potential disturbances in the processes, such as calcium 'action-potentials', which can propagate back to the soma, causing a loss of somatic voltage-clamp or 'escape'. The answer to this problem is generally to generate ramp I-Vs, ramping the voltage rapidly to complete the ramp before the escape current appears.

(ii) Basal forebrain neurones also express a high density of calcium channels (Allen, Sim & Brown, 1993). These can be readily blocked using cadmium, but this was unfortunately also found to block glutamate receptor-mediated currents.

(iii) An obvious solution to these space-clamp problems was to record from outside-out patches, but these proved very difficult to pull and the extreme voltage excursions required for I-V relationships invariably resulted in breakdown of the pipette-membrane seal.

2.5.2 *Nucleated patch technique*

A solution to these problems was found in the nucleated patch method (Sather, Dieudonné, MacDonald & Ascher, 1992). This is essentially an outside-out macropatch in which the nucleus (and some cytoplasmic structures) are contained within the patch. The formation of the nucleated patch is summarised in figure 2.5. After achieving the whole-cell configuration, negative pressure was applied to the pipette resulting in migration of the nucleus across the cell towards the tip of the pipette. Under continued negative pressure the pipette was slowly withdrawn from the cell, yielding an excised outside-out patch of plasma membrane enveloping and mechanically supported by the nucleus.

Nucleated patches were pulled using similar electrodes and the same extracellular solution as for whole-cell recording. Capacitative current transients recorded from nucleated patches (see section 2.1) decayed with a single exponential timecourse. Patches generally had capacitances of around 3pF, access resistances of 20-40MΩ and input resistances of 500MΩ-1GΩ (estimated from axopatch leak subtraction circuitry).

Current-voltage relationships were recorded from nucleated patches using either the 'normal' intracellular solution (given above) and partial replacement of extracellular sodium with 25mM TEA.Cl (extracellular sodium reduced to 98mM) or using a caesium-based intracellular solution. In both instances, ATP and GTP were excluded from the intracellular solution and 30μM spermine was added. Intracellular spermine has been shown to prevent loss of rectification of calcium-permeable non-NMDA receptors but binds to nucleotides (Watanabe, Kusama-Eguchi, Kobayashi & Igarashi, 1991).

Series resistance errors were generally reduced using series resistance compensation of 80-95%. Currents were filtered at 10kHz (12-pole Bessel filter) and acquired at 40kHz.

Nucleated patch capacitance values measured from neurones after 30-31 days *in vitro* (DIV) ranged from 2.6 to 4.4 pF with a median value of 3.2pF (n=15).

Figure 2.5 Nucleated patch technique

Schematic illustration of the method employed to pull a nucleated patch. After achieving the whole-cell recording configuration, negative pressure was applied to the recording pipette and maintained resulting in migration of the nucleus across the cell body towards the tip of the pipette. Slow withdrawl of the recording pipette, whilst maintaining negative pressure, produced a nucleated patch.

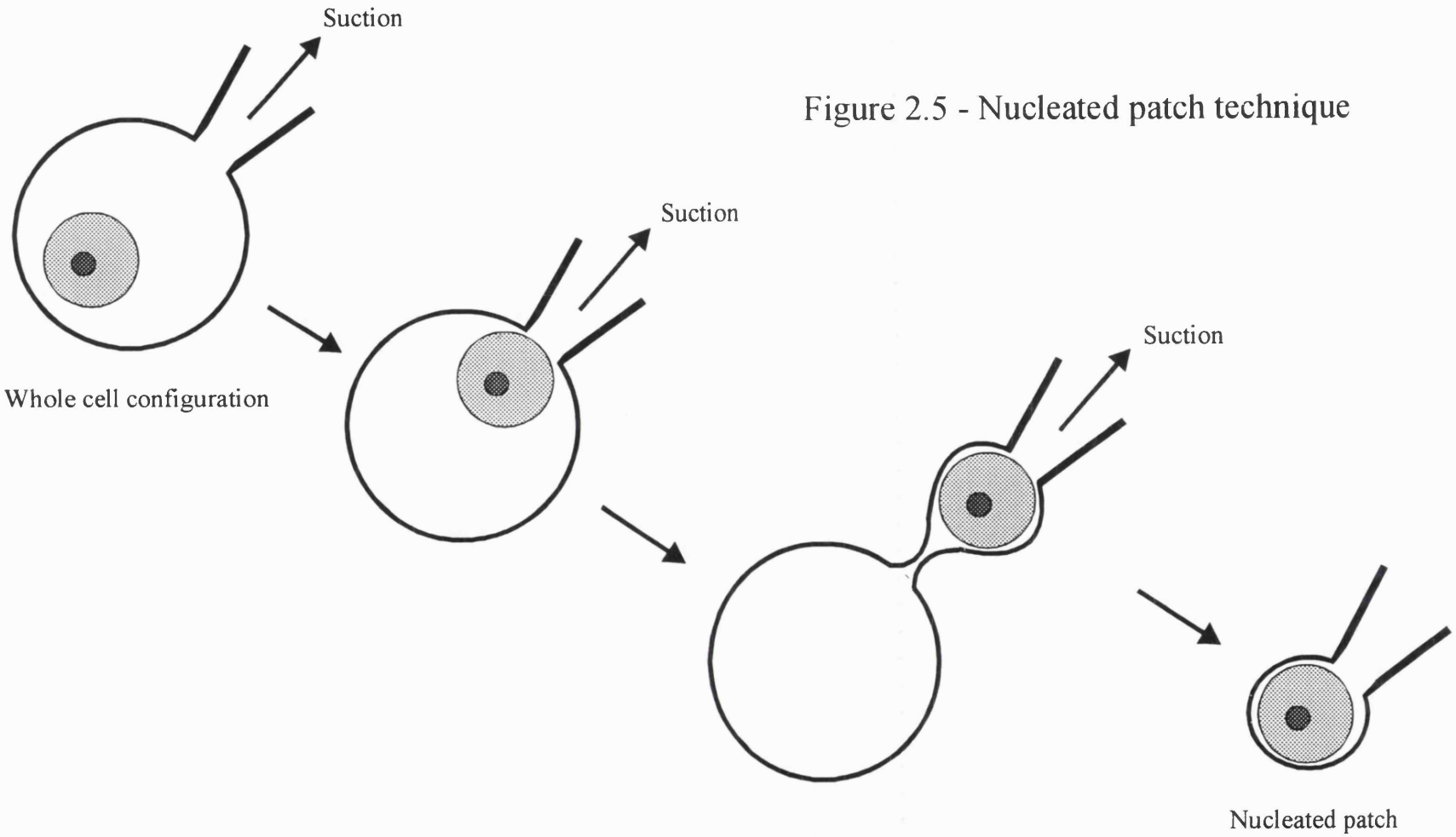

Figure 2.5 - Nucleated patch technique

2.5.3 Recording solutions

Intracellular solution:		Accompanying extracellular solution:	
Cs Acetate	102.4mM		
CsCl	10.6mM	NaCl	110mM
HEPES	40mM	KCl	3mM
NaCl	10-12mM (pH 7.3)	$CaCl_2$	2.5mM
EGTA	3mM	$MgCl_2$	1.6mM
$CaCl_2$	0.822mM*	HEPES	5mM (pH7.4)
$MgCl_2$	1.2mM	$NaHCO_3$	25mM
Mg.ATP	4mM	Glucose	11mM
Na_2.GTP	0.1mM		
Spermine	30μM	0.5μM tetrodotoxin where necessary	

*free calcium concentration 30nM

The extracellular solution was continuously gassed with 95%O_2/5%CO_2.

2.5.4 Voltage protocol and analysis

Nucleated patches were held at -70mV and the following protocol was applied to the patch: (i) a step to -120mV, (ii) a ramp from -120 to +120mV, (iii) a brief period holding at +120mV, (iv) a ramp from +120 to -120mV, (v) a brief period at -120mV, (vi) a step to -70mV. This is illustrated in figure 4.3.1 (uppermost panel).

This protocol was repeated every 10-30 seconds. Once the current amplitude was stable, several (generally ten) episodes were acquired. 1mM kainate was then bath-applied and another ten episodes acquired. A further ten episodes were acquired after removal of kainate from the bath. Sequential episodes were inspected during aquisition to ensure that under each condition there was no change in the I-V characteristics with time. Each run of ten episodes was averaged off-line to yield the net current-time relationship for

each condition.

Current before and after kainate were compared and the data accepted for further analysis only if the difference was negligible. Each I-V relationship was then generated by subtraction of the control trace from that in the presence of kainate using Clampfit (pClamp) software. The resulting leak-subtracted trace and a waveform copy was exported into Origin software where the two were plotted to yield the I-V relationship for kainate action at AMPA receptors.

2.6 Reversal potential shifts

Relative permeability coefficients for caesium, sodium and calcium ions permeating non-NMDA receptors were estimated using constant field theory (see appendix 7.4).

Acutely dissociated cells were voltage-clamped using the whole-cell variant of the patch-clamp technique and a discontinuous single-electrode voltage-clamp amplifier. The intracellular solution was as follows:

30mM	CsF
65mM	CsOH
40mM	HEPES
30mM	BAPTA
30μM	spermine

This solution had a pH of 7.3 and an osmolarity of 307mOsM. 30mM CsF was used to inhibit voltage-gated calcium currents and 30mM BAPTA to prevent intracellular calcium accumulation (see section 4.4.1, below).

Cells were bathed in an extracellular solution identical to that given in section 2.2.4 (above) except for the addition of 20mM mannitol to increase the osmolarity to that of the intracellular solution. After obtaining the whole cell recording condition the extracellular solution was exchanged (see below).

Current-voltage relationships were generated by imposing voltage ramps from -100 to +100 and back to -100mV. Relationships generated under control conditions were subtracted from relationships generated in the presence of 1mM

kainate as follows: several (generally five) consecutive traces (filtered at 1kHz) were averaged for each condition (+/- kainate). These manipulations were performed using pClamp software on both current and acquired voltage traces. Averaged traces were exported (in ASCII format), were imported into Origin software and current was plotted against acquired voltage. An I-V relationship for a kainate-induced current could then be calculated by subtraction of the control I-V relationship from the I-V relationship in the presence of kainate. Note that Origin software is capable of allowing for the non-linear nature of the voltage error when making this calculation.

I-V relationships for the kainate-sensitive current were generated in three extracellular solutions:

(i) Ca^{2+}-extracellular:		(ii) Na^+/Ca^{2+}-extracellular:		(iii) Na^+-extracellular:	
$CaCl_2$	100mM	NaCl	50mM	NaCl	100mM
$Ca(OH)_2$	2.27mM	NaOH	4mM	NaOH	4mM
HEPES	10mM	$CaCl_2$	50mM	$CaCl_2$	1mM
D-mannitol	60mM	HEPES	10mM	HEPES	10mM
		D-mannitol	80mM	D-mannitol	110mM

Each of these solutions was at pH 7.3 and had an osmolarity of 300-310mOsM. The concentrations of kainate added to these solutions were adjusted to account for binding to calcium (Gu & Huang, 1991) so that a free kainate concentration of 1mM was achieved by the addition of 1mM, 1.347mM and 1.7mM kainate to Na^+-, Na^+/Ca^+- and Ca^{2+}-extracellular solutions respectively.

Reversal potentials for the kainate-sensitive currents in each of these solutions were measured from plotted I-V relationships. Reversal potentials were corrected for a junction potential of -3mV in each of these solutions. From these reversal potential measurements, relative permeabilities for the caesium, sodium and calcium ions permeating non-NMDA receptors were calculated using the extended constant field equation:

$$E_{rev} = (RT/F) \ln \{[-b + \sqrt{(b^2-4ac)}]/2a\}$$

where E_{rev} is the reversal potential,

R, T and F are the gas and Faraday constants and the absolute temperature respectively,

$a = [Cs^+]_i$

$b = [Cs^+]_i - [Na^+]_o.(P_{Na}/P_{Cs})$

$c = -[Na^+]_o.(P_{Na}/P_{Cs}) - 4[Ca^{2+}]_o.(P_{Ca}/P_{Cs})$

$[\alpha]$ denotes the ion activity, not concentration, of ion α. Subscripts i and o refer to intracellular and extracellular activites respectively. P_i represents the permeability coefficient for ion i through the non-NMDA receptor.

Further explanation of these calculations and of the constant field equations is given in appendix 7.4.

Activity coefficients for metal ion salts were calculated according to Pitzer & Mayorga (1973). Ion activities were calculated from these values by assuming that (i) the activities of caesium and of sodium ions in these solutions were equal to the activities of the corresponding salts, and (ii) the activity coefficient of the calcium ion was equal to the square of the activity coefficient of the corresponding salt (Guggenheim convention). These calculations are detailed in appendix 7.3.

Calculated ion activites were as follows:

$[Cs^+]_i$	75.57mM
$[Na^+]_o$	37.09 and 80.19 in Na^+/Ca^{2+}- and Na^+-extracellulars respectively
$[Ca^{2+}]_o$	27.26, 13.64 and 0.29 in Ca^{2+}-, Na^{2+}/Ca^{2+}- and Na^{2+}-extracellulars respectively.

2.7 Calcium current recording

Calcium currents were recorded using published methods (Allen, Sim & Brown, 1993; Allen & Brown, 1993). Currents were studied using both acutely dissociated cells and cells which had been maintained in culture for one day.

Potassium currents were inhibited using an intracellular solution containing caesium ions, 4-aminopyridine (4-AP) and TEA and by including TEA.Cl in the extracellular solution.

The composition of the intracellular solution was as follows:

CsCl	10.6mM	$CaCl_2$	0.822mM*
CsAc	102.4mM	$MgCl_2$	1.2mM
TEA.Cl	5mM	Mg.ATP	4mM
4-AP	5mM	Na_2.GTP	0.1mM
HEPES	40mM		
NaOH	10-12mM (pH 7.3)	* free calcium	
EGTA	3mM	concentration 30nM	

The initial extracellular solution was identical to that given in section 2.2.4 (above). Currents were recorded using the whole-cell variant of the patch-clamp technique. Cells were held at -80mV using discontinuous single-electrode voltage-clamp. Acutely dissociated cells and cells after 1 DIV possess very small or no processes, hence cells will have been very well space-clamped.

Having established voltage-clamp, the extracellular solution was exchanged for one of the following composition:

NaCl	90mM	$NaHCO_3$	25mM
TEA.Cl	30mM	Glucose	11mM
KCl	3mM	TTX	0.5μM
$CaCl_2$	2.5mM		
$MgCl_2$	1.6mM	This solution was continuously	
HEPES	5mM (pH7.4)	gassed with 95%O_2/5%CO_2.	

Currents were elicited by voltage steps to 0mV.

Ionotropic Glutamate Receptor Subtypes

3.1 Introduction

Whilst both ionotropic and metabotropic glutamate receptors are expressed within the rat basal forebrain, little functional data are available. The presence of both NMDA and non-NMDA receptors has been established and basic agonist and antagonist pharmacologies have been investigated (Jasek & Griffith, 1995; Kumamoto & Murata, 1995a). Whether non-NMDA receptor-mediated responses resulted from AMPA or kainate receptor stimulation was not investigated in either study. It was therefore important to determine which glutamate receptor types are functionally expressed by basal forebrain neurones prior to investigating the properties of these receptors.

Pharmacological tools are readily available to characterise functional NMDA, non-NMDA and metabotropic receptors (see reviews by Mayer & Westbrook, 1987b; Collingridge & Lester, 1989; Monaghan, Bridges & Cotman, 1989; Bettler & Mulle, 1995). Further classification of native non-NMDA receptors into AMPA and kainate subtypes is more difficult, there being a lack of pharmacological tools for this purpose. The functional differences between AMPA and kainate receptors have only really become clear with the advent of molecular biological techniques.

Molecular biological approaches have produced a number of glutamate receptor subunit clones and receptor subunit composition has been shown to influence the functional properties of receptors. Unfortunately these functional differences are generally too subtle to permit the subunit composition of native receptors to be determined from their kinetic and pharmacological properties alone. Distinguishing between responses mediated by native AMPA and kainate receptors requires the use of several different approaches, each individually less than definitive.

Firstly, agonist kinetics and pharmacology are characteristic of the receptor subtype underlying the response. Secondly, several substances such as the benzothiadiazide cyclothiazide and the lectin ConA have been found to inhibit desensitization of mammalian non-NMDA receptors (Yamada & Tang,

1993; Mayer & Vyklicky, 1989). Both show some selectivity between AMPA and kainate receptors making them useful tools with which to distinguish between responses mediated by AMPA and by kainate receptors.

Cyclothiazide potentiates AMPA receptor-mediated responses. The mechanism of action is not entirely clear. Whilst cyclothiazide undoubtedly inhibits desensitization, thereby potentiating responses to those agonists which cause AMPA receptor desensitization, it also potentiates responses to kainate (acting at an AMPA receptor) suggesting that it may also cause potentiation *via* another route. It is clear that this is not attributable to an effect at a kainate receptor, since whilst cyclothiazide is a weak channel blocker at both AMPA and kainate receptors, cyclothiazide potentiates only responses mediated by AMPA receptors, not kainate receptors. This selectivity has been consistently observed for both native and recombinant receptors (Patneau, Vyklicky & Mayer, 1993; Yamada & Tang, 1993; Wong & Mayer, 1993; Partin, Patneau, Winters, Mayer & Buonanno, 1993; Partin, Patneau & Mayer, 1994).

In contrast ConA inhibits desensitization of kainate receptors. ConA is less selective than cyclothiazide in that it also inhibits desensitization at some AMPA receptors (native and recombinant) though kainate receptor-mediated responses are much more strongly potentiated. Interestingly, the degree of potentiation by ConA is much greater at recombinant than at native kainate receptors (Huettner, 1990; Wong & Mayer, 1993; Partin, Patneau, Winters, Mayer & Buonanno, 1993).

In addition, a number of selective agonists and antagonists are under development. The most promising are the 2,3-benzodiazepines. First synthesized as muscle relaxants, 2,3-benzodiazepines are also non-competitive antagonists at non-NMDA receptors (Tarnawa, Farkas, Berzsenyi, Pataki & Andrási, 1989; Ouardouz & Durand, 1991; Donevan & Rogawski, 1993; Zorumski, Yamada, Price & Olney, 1993; Desai, Burnett, Ornstein & Schoepp, 1995; Wilding & Huettner, 1995). Of these compounds GYKI 52466 (1-(4-aminophenyl)-4-methyl-7,8-methylenedioxy-5H-2,3-benzodiazepine) and GYKI 53655 (1-(4-aminophenyl)-3-methylcarbamyl-4-methyl-7,8-methylenedioxy-3,4-dihydro-5H-2,3-benzodiazepine, also known as LY 300168) have received

particular attention with regard to their actions at non-NMDA receptors. Both are more potent at AMPA receptors than at kainate receptors, GYKI 53655 particularly so (Paternain, Morales & Lerma, 1995; Wilding & Huettner, 1995).

Aims

To determine which classes of glutamate receptor are expressed by basal forebrain neurones. In particular, to determine whether both AMPA- and kainate-type non-NMDA receptors are present and, if so, to establish methods by which responses mediated by these two receptor classes can be distinguished. This requires a combination of approaches, considering agonist kinetics and pharmacology, the effects of cyclothiazide and concanavalin A and the use the selective antagonist GYKI 53655.

3.2 Results - basic pharmacology & kinetics

3.2.1 Glutamate increases excitability

Application of glutamate to basal forebrain neurones caused depolarization and firing. This is illustrated in figure 3.2.1. Brief pressure-application of 100μM glutamate to the soma of an unclamped neurone resulted in rapid depolarization and firing followed by slow (approx. 4s) recovery to baseline. Glutamate by pressure- or bath-application caused a dose-dependent depolarization (or inward current under voltage-clamp to -70mV) in all neurones studied.

More prolonged application of glutamate resulted in a sustained depolarization in the continued presence of glutamate. This depolarization was accompanied by a decrease in input resistance. Resting membrane potential was restored following removal of glutamate.

The observed decrease in input resistance did not result from the activation of other conductances upon depolarization rather than directly from ionotropic glutamate receptor activation since input resistance was not restored upon manual clamp of neurones to -70mV (not shown). The results were confirmed by voltage-clamp experiments (not shown).

Figure 3.2.1 Glutamate increases excitability

Upper panel (A): a voltage recording from a neurone with a resting membrane potential of -76mV (no current applied). Arrowheads mark applications of 100μM glutamate for 30ms by pressure application to the soma. The inset shows the first response on an expanded timescale. The amplitude of the action potential clearly decreases with time, presumably as a result of depolarization-induced sodium channel inactivation.

Lower panel (B): the effects of more prolonged application of 100μM glutamate. Glutamate was applied by bath perfusion, with the bath inflow positioned close to the cell. In this example, the membrane potential stabilizes in the presence of glutamate at approximately -30mV. 50pA hyperpolarizing current steps were applied, from which a decrease in input resistance is clearly visible. In this cell, input resistance was decreased from 225MΩ under resting conditions to 50MΩ in the presence of glutamate.

A

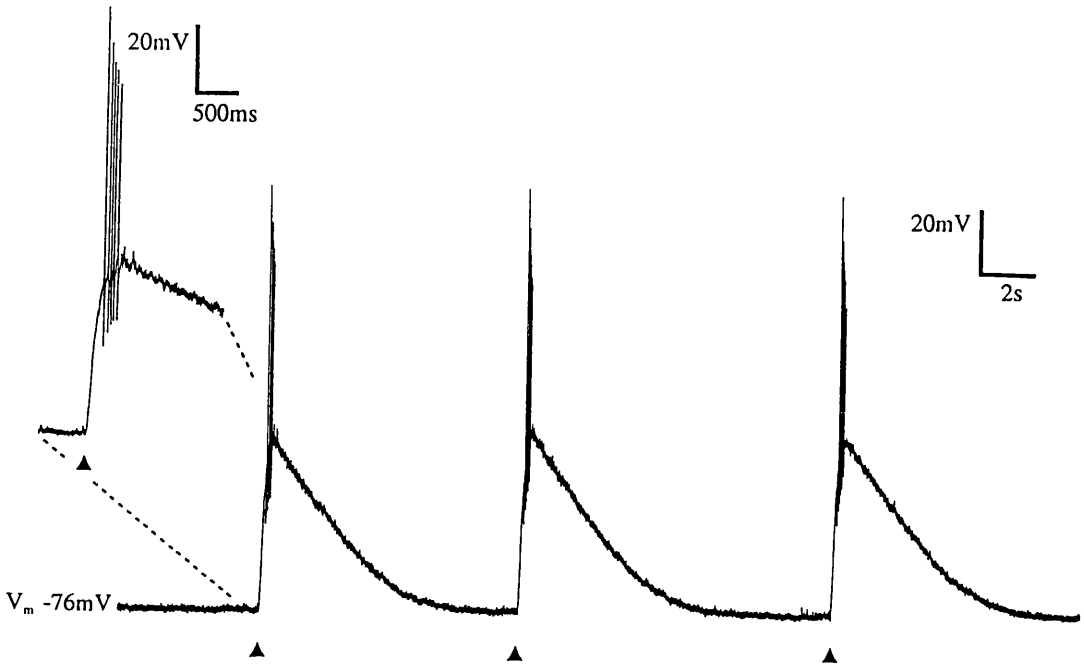

B

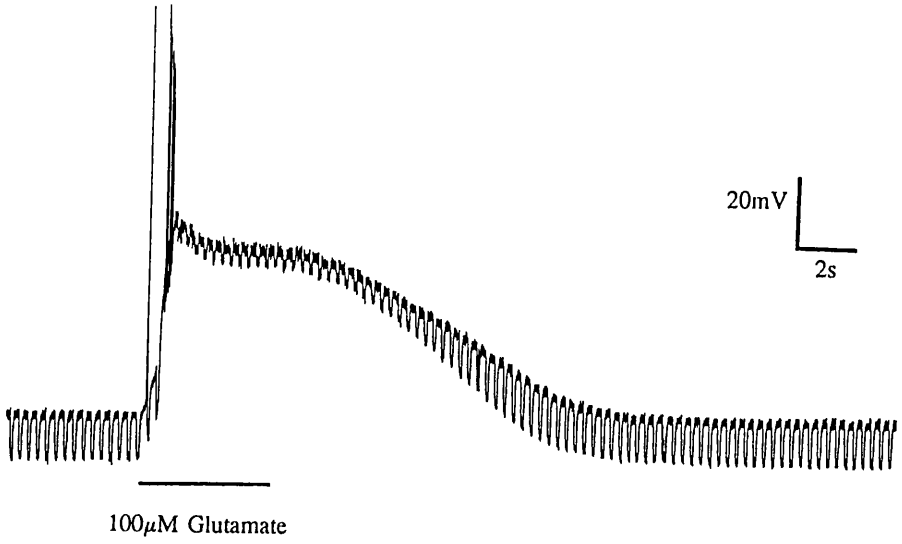

3.2.2 Basic receptor pharmacology

The presence of functional NMDA and non-NMDA receptors was readily demonstrated pharmacologically, as illustrated in figure 3.2.2. AMPA and kainate (both non-NMDA receptor agonists) and N-methyl-D-aspartate (NMDA) all elicited inward currents from basal forebrain neurones voltage-clamped to -70mV.

Responses to AMPA and to kainate were reversibly antagonized by the non-NMDA receptor antagonist 6-cyano-7-nitroquinoxaline-2,3-dione (CNQX) in a dose-dependent manner. Similarly, responses to NMDA (recorded in magnesium-free extracellular solution) were reversibly and dose-dependently antagonized by the NMDA receptor antagonist AP5 and by addition of 1mM magnesium chloride to the extracellular solution.

Examples of the effects of CNQX, AP5 and magnesium ions on AMPA-kainate- and NMDA-elicited responses are illustrated in figure 3.2.2.

Concentrations of up to 30μM CNQX did not inhibit responses to NMDA. Likewise, responses to AMPA and to kainate were not inhibited by AP5 or by extracellular magnesium ions (data not shown). Responses to glutamate, to AMPA, to kainate and to NMDA could all be inhibited by 10mM kynurenic acid (data not shown).

Addition of 10μM glycine to the extracellular solution approximately doubled the amplitude of responses to NMDA in approximately 50% of cells studied. No effect of glycine was observed in the remaining instances. This may reflect contamination of the water supply with glycine.

Metabotropic glutamate receptor agonists were also applied to basal forebrain neurones, but no effects were ever observed. (1S,3R)-1-aminocyclopentane-1,3-dicarboxylic acid (trans-ACPD) and L(+)-2-amino-4-phosphonobutyric acid (L-AP4) were each applied at 10 and 100μM by both bath- and pressure-applications, but elicited no currents. Each agonist was also tested for its effects on brief pressure-applications of glutamate, but again neither agonist had any effect. The lack of any effect may reflect a loss of intracellular messengers as a result of dialysis of the cell during whole-cell

Figure 3.2.2 Basic receptor pharmacology

Panels A, B & C show current traces from three neurones, each clamped to -70mV using discontinuous single-electrode voltage-clamp (dSEVC). Arrowheads mark 200ms pressure-applications of agonists. Applications were repeated at intervals of 30 seconds (panels A and B) or 20 seconds (panel C). Voltage errors at the peaks of agonist-induced currents were less than 1mV. (Voltage traces were excluded for clarity). Each panel shows three sequential responses to an ionotropic glutamate receptor agonist under various conditions.

Panels A and B show responses to 30μM AMPA and to 1mM kainate under control conditions, in the presence of 30μM CNQX in the superfusing solution (denoted by the application bar) and after washout of CNQX from the bath. Panel C shows responses to 100μM NMDA (recorded in the absence of extracellular magnesium and without added glycine) and illustrates the effects of AP5 and 1mM magnesium ions, each added to the extracellular solution.

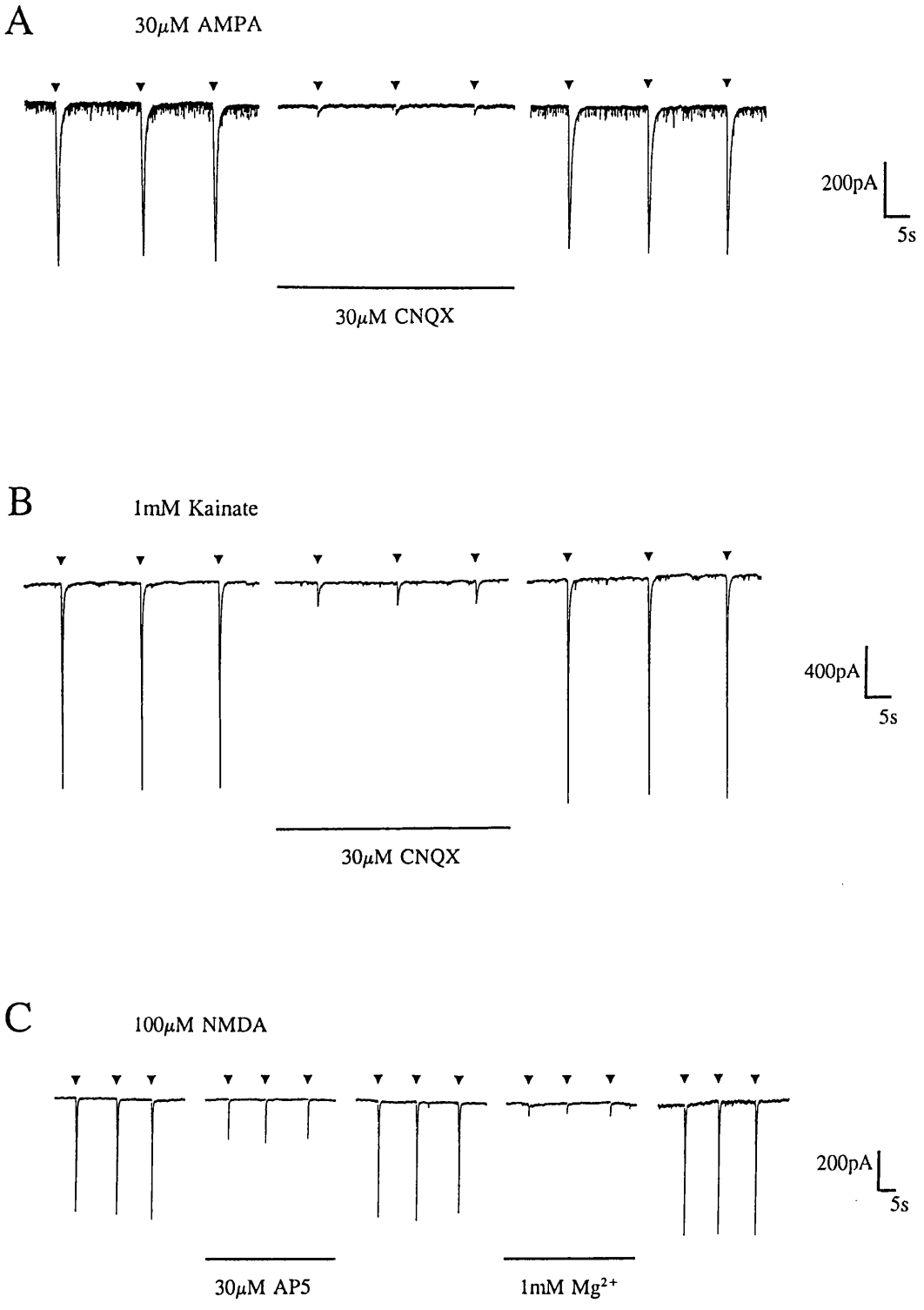
A
30μM AMPA
200pA
5s
30μM CNQX
B
1mM Kainate
400pA
5s
30μM CNQX
C
100μM NMDA
200pA
5s
30μM AP5
1mM Mg2+

recording or that metabotropic receptors are present only on dendrites. The former hypothesis could be tested using the perforated patch technique, which has been used to preserve metabotropic glutamate receptor-mediated responses in hippocampal neurones (Shirasaki, Harata & Akaike, 1994).

3.2.3 Agonist kinetics - glutamate and NMDA

Pressure- or stepper-application of glutamate produced a rapidly activating response, which displayed pronounced and rapid desensitization. In the example given in figure 3.2.3, the current to 100μM glutamate (applied using a stepper device and recorded in the presence of extracellular magnesium and AP5) displayed a 10-90% rise time of 16ms and a 10-90% decay time of 700ms (decay from peak to steady state current amplitude). In the example shown the current desensitized to a steady-state level of 40% of the peak current amplitude. Time constants for desensitization of recombinant AMPA receptors are typically around 1-6ms (Mosbacher, Schoepfer, Monyer, Burnashev, Seeburg & Ruppersberg, 1994). Hence 40% is likely to be an underestimate of the true extent of desensitization in basal forebrain neurones since the rate of glutamate application was probably too slow to resolve the true peak current amplitude.

In contrast, desensitization to NMDA followed a slower time-course and the degree of desensitization was less. An increase in current noise was also observed upon application of NMDA. These features are also illustrated in figure 3.2.3.

These pharmacological and kinetic data are consistent with the expression by basal forebrain neurones of both NMDA and non-NMDA glutamate receptors. They do not, however, indicate which subtype(s) of non-NMDA receptors are expressed by basal forebrain neurones.

3.2.4 Agonist kinetics - AMPA and kainate

Pressure-application of AMPA and of kainate to basal forebrain neurones produced responses with distinct kinetics, illustrated in figure 3.2.4. The kinetics of AMPA-application were similar to those of glutamate,

Figure 3.2.3 Agonist kinetics - glutamate and NMDA

An illustration of typical responses of basal forebrain neurones to glutamate and to NMDA. Neurones were voltage-clamped to -70mV by dSEVC; current traces are shown above the corresponding voltage traces.

Glutamate was applied to the whole cell by stepper-application with 1.2mM magnesium chloride and 10μM AP5 in the extracellular solution.

NMDA was pressure-applied to the soma in the absence of extracellular magnesium.

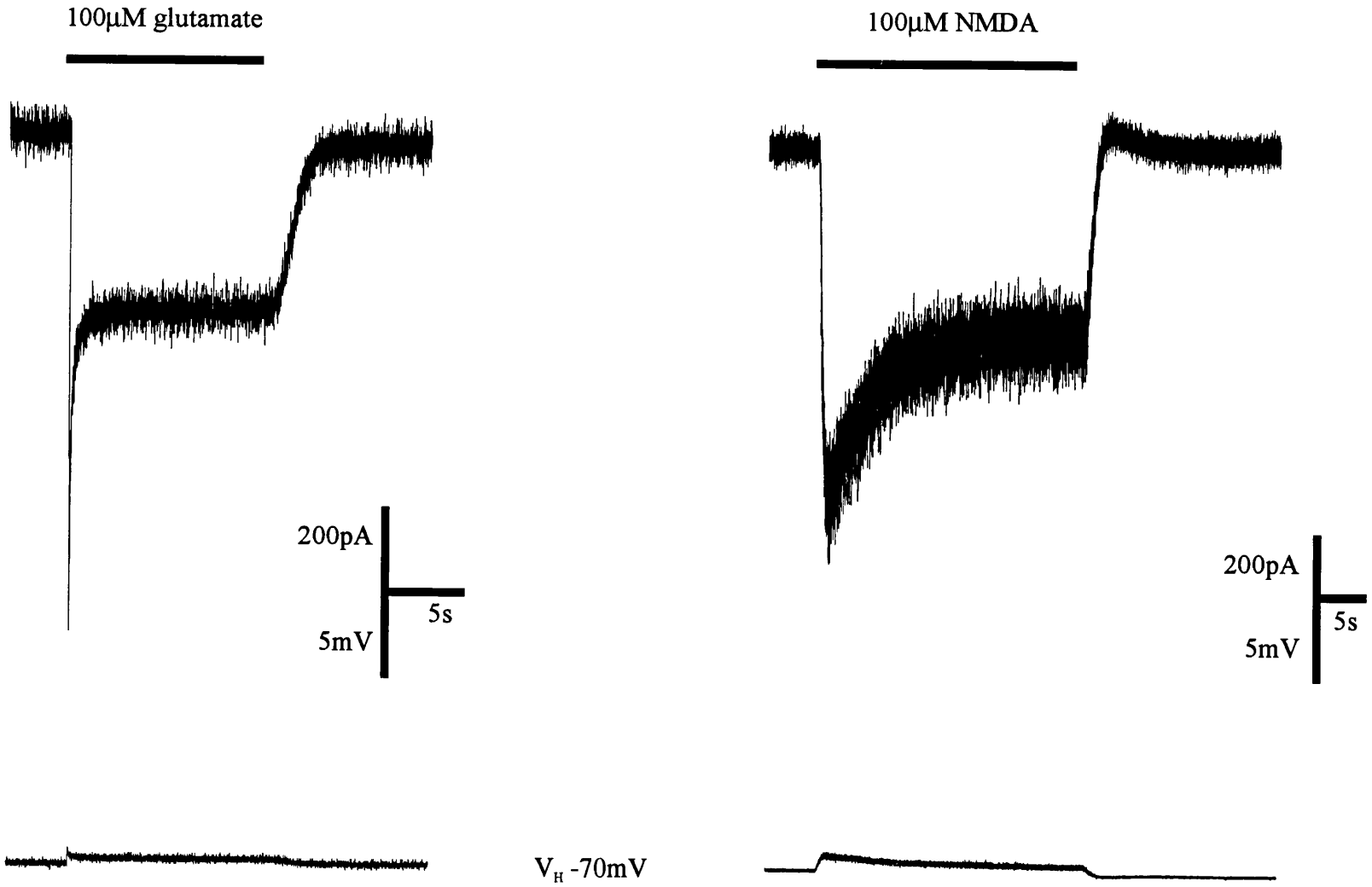
100μM glutamate
200pA
5s
5mV
100μM NMDA
200pA
5s
5mV
V_H -70mV

Figure 3.2.4 Agonist kinetics - AMPA and kainate

Currents to AMPA and to kainate are kinetically distinct. In the typical examples shown, neurones were voltage-clamped to -70mV using dSEVC; current traces are shown above the corresponding voltage traces. Agonists were pressure-applied. AMPA and kainate produced kinetically distinct responses which were accompanied by an increase in current noise.

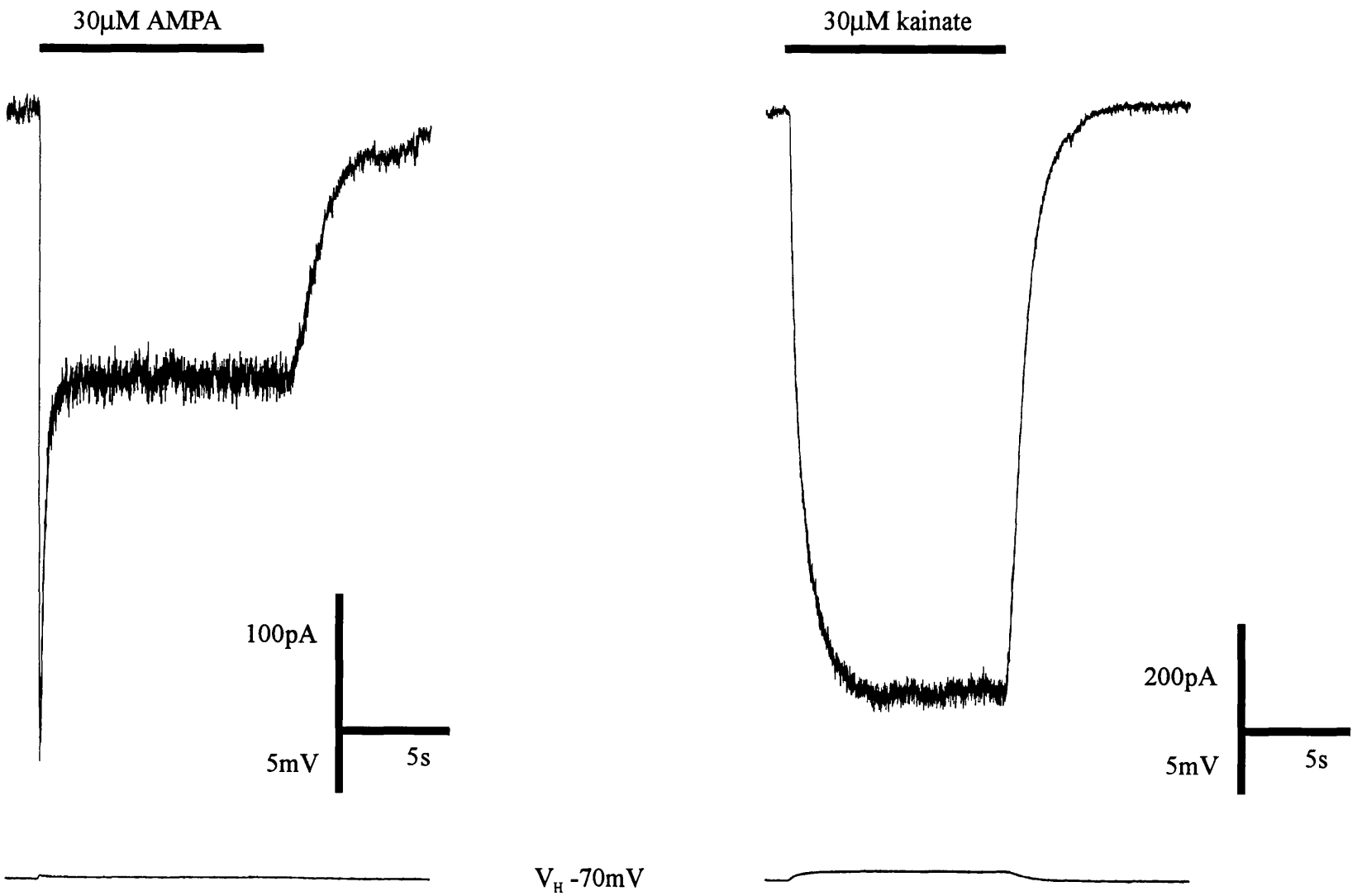
30μM AMPA
100pA
5mV
5s
30μM kainate
200pA
5mV
5s
V_H -70mV

consisting of rapid activation and desensitization to a steady-state level. In contrast, responses to kainate exhibited a slower rise and lacked desensitization. Such kinetics are characteristic of responses of AMPA receptors to these two agonists, moreover responses to kainate would be expected to exhibit a desensitizing component were kainate acting at a kainate receptor (see for instance Paternain, Morales & Lerma, 1995).

Pressure-application of quisqualate elicited responses with similar kinetics to those of glutamate and AMPA and domoate produced responses with kinetics similar to those of kainate.

No desensitization was observed to any of these agonists (glutamate, NMDA, AMPA, kainate, quisqualate and domoate) upon bath application, just a steady-state current. During bath-application of high concentrations of kainate some decline in current amplitude was observed. This decline exhibited very slow kinetics and was observed only when drawing very large currents. Therefore this decline probably results from ion redistribution rather than pharmacological desensitization.

3.2.5 AMPA and kainate dose-response data

Dose-response curves for steady-state currents to these two agonists are presented in figure 3.2.5. EC_{50} values are 2.7 $\pm$ 0.4μM (n=5) and 138 $\pm$ 25μM (n=10) for AMPA and kainate respectively. Corresponding Hill slopes are 1.35 $\pm$ 0.18 and 1.24 $\pm$ 0.09. These values, particularly the low micromolar EC_{50} value for AMPA, again suggest that these responses are mediated by AMPA rather than kainate receptors.

3.2.6 Maximum current amplitudes to kainate

High concentrations of AMPA and kainate elicited very large steady-state currents. Current amplitude was found to increase with time in culture. Maximum steady-state current amplitudes from the dose-response data for kainate are plotted against time *in vitro* in figure 3.2.6. Maximum current increased from approximately 2nA at day 5 to approximately 13nA at day 16 *in vitro* (V_H -70mV). No dose-response data are available outside this age bracket,

Figure 3.2.5 AMPA and kainate dose-response data

Steady-state dose-response relationships were generated by bath-application of AMPA and of kainate. Neurones were voltage-clamped to -70mV using dSEVC.

Data from individual cells were fit using an independent binding model of the form

$$y = y_{min} + ((y_{max}-y_{min})/(1+(10^{(logEC50-X)n})))$$

where n is the Hill coefficient

y_{min} and y_{max} are the fitted minimum and maximum currents respectively

An example of data from one cell fitted with this function is given in the upper panel. The maximum current amplitude calculated by the fitting routine is indicated by a horizontal dotted line. Similarly, maximum current amplitude for each cell was derived from the fitted sigmoid. The data were then normalized to these maxima and the means and standard errors for the normalized current values were calculated for each agonist concentration. These values are plotted in the lower panel. Mean EC_{50} and Hill slope values were calculated from the values for individual cells. The curves shown in the lower panel were constrained to these mean EC_{50} and Hill slope values and to minima and maxima of 0 and 1 respectively. Numbers of cells are given in parentheses.

The application of very high concentrations of kainate to cells clamped to -70mV typically resulted in large voltage errors. Current measurements were only accepted for analysis provided voltage error was less than 5mV with the result that dose-response relationships generated at -70mV lacked data points at high agonist concentrations. Therefore, dose-response relationships for kainate were also generated in two neurones clamped to -40mV. EC_{50} and Hill slope values from curves fitted to data from these two neurones were similar to those at -70mV, hence the kainate data represent pooled data from the two voltages.

Individual cell

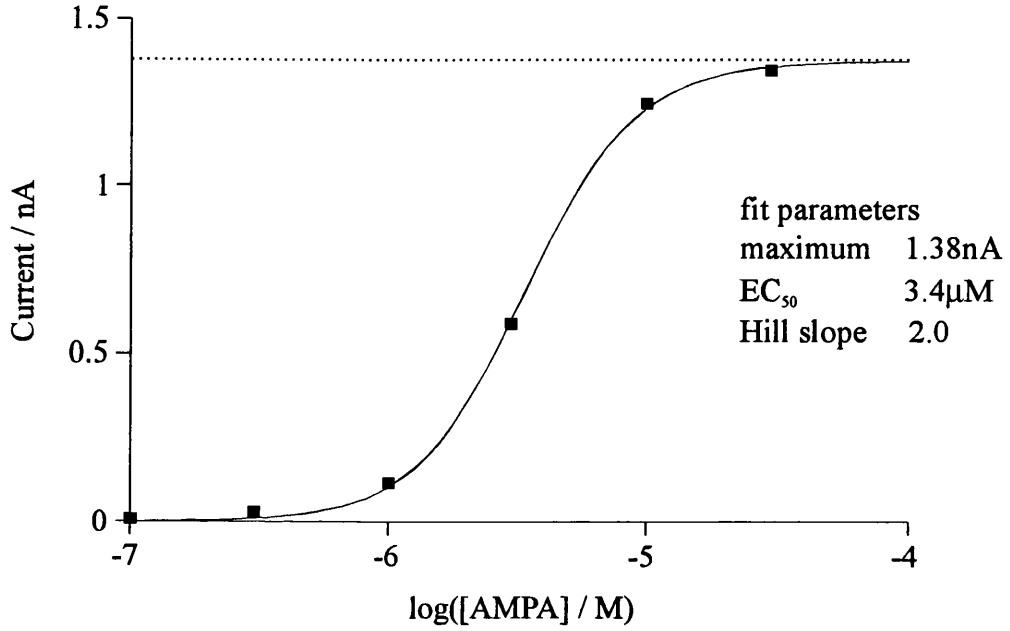

Mean dose-response curves

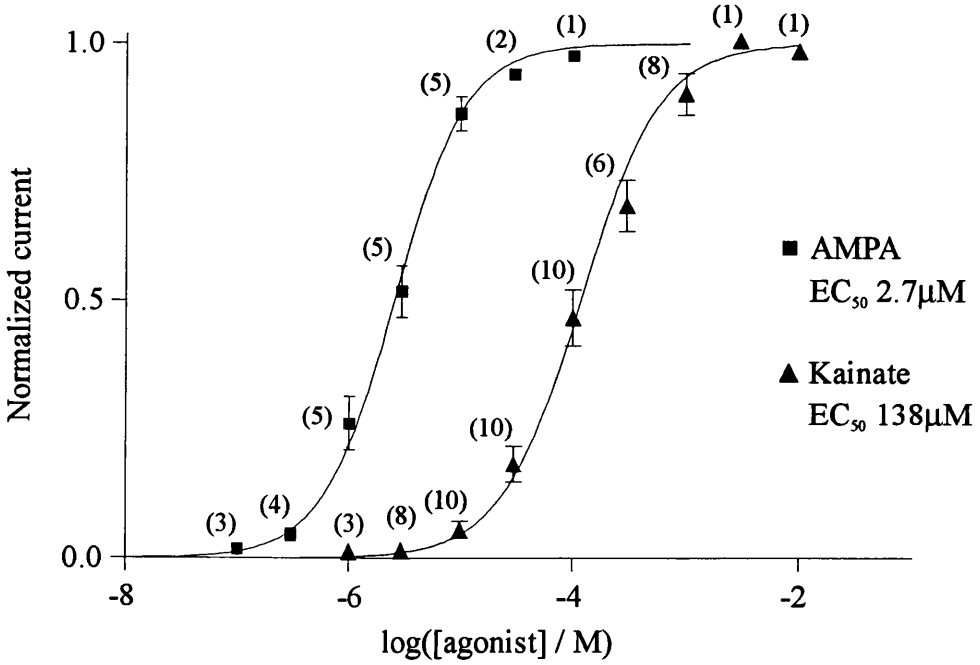

Figure 3.2.6 Maximum current amplitudes to kainate

Maximum kainate-induced current amplitudes were plotted against time *in vitro* revealing an increase in current amplitude with time in culture. Plotted maximum current amplitudes are extrapolated maxima from the dose-response data used to generate the mean kainate dose-response curve given in figure 3.2.5. Each point corresponds to the theoretical maximum current generated in one of the 8 cells held at -70mV (see figure 3.2.5).

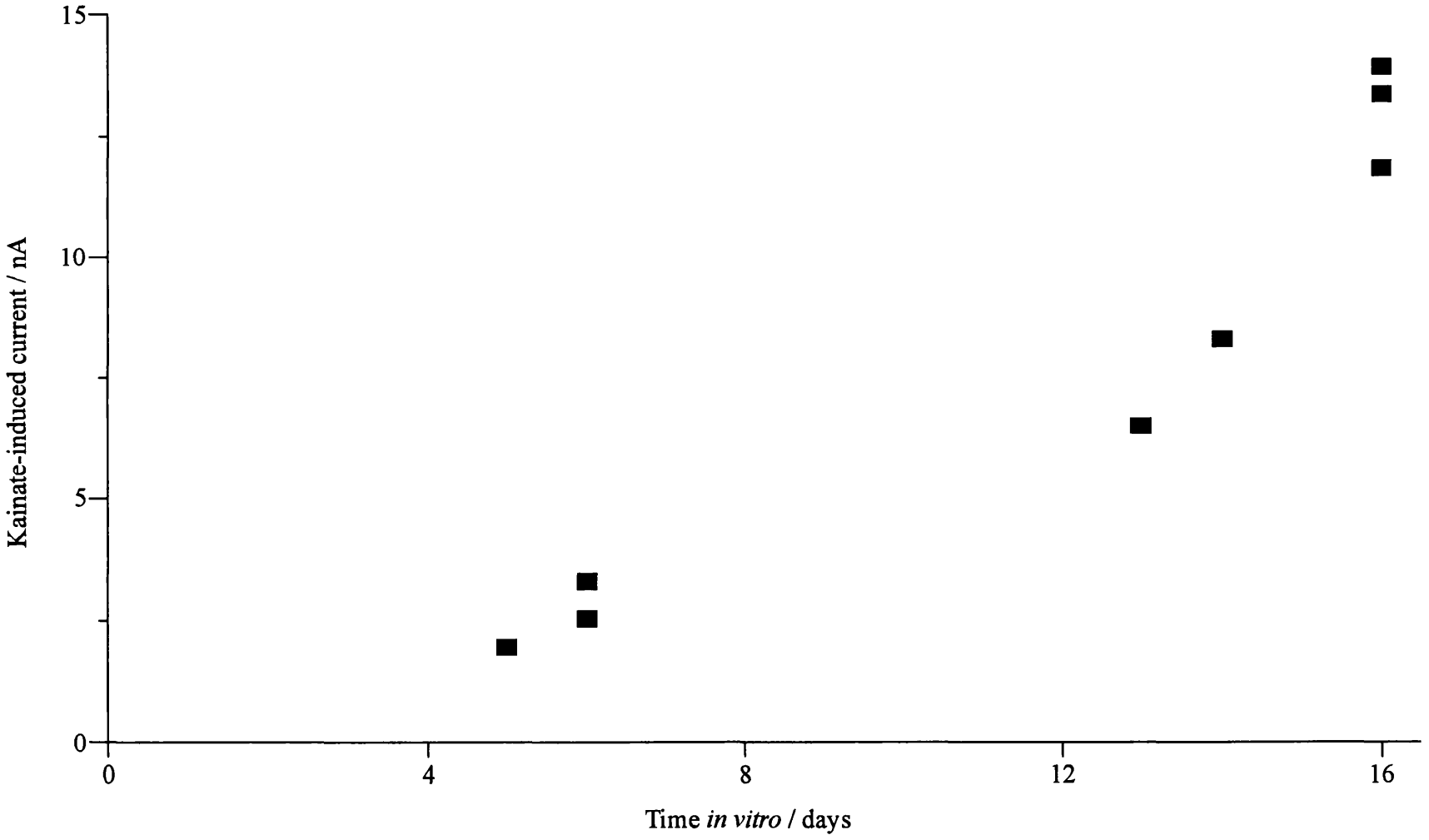
15
10
5
0
Kainate-induced current / nA
0
4
8
12
16
Time *in vitro* / days

since currents were too small or too large to permit the generation of dose-response data.

A current amplitude of 13nA corresponds to a current density of approximately 220pA/pF, assuming a cell capacitance of 60pF (see section 2.3). Current densities were not calculated for AMPA. Maximum steady-state current amplitudes were typically several nanoamperes, appreciably smaller than for kainate. The difference in current amplitudes to these two agonists is presumably the result of desensitization to AMPA but not to kainate.

3.3 Results - cyclothiazide & concanavalin A

3.3.1 Effects on responses to AMPA

Responses to AMPA were potentiated by cyclothiazide ($n>20$), but not ConA ($n=6$), even after 30 minutes of exposure. This is illustrated for a typical cell in figure 3.3.1.

In this example control responses to AMPA showed no desensitization, probably as a result of leakage of AMPA from the application pipette. In addition to increasing current amplitude, cyclothiazide also altered the kinetics of the response to AMPA. In the presence of cyclothiazide current amplitude upon application of AMPA rose rapidly then decreased in the continued presence of AMPA. The most likely explanation is that cyclothiazide reduced the rate of desensitization to AMPA, but did not entirely eliminate desensitization. These data reinforce the suggestion that responses to AMPA result from stimulation of an AMPA receptor with negligible contribution from a kainate receptor.

3.3.2 Effects on responses to kainate

The results of a similar protocol to investigate the effects of cyclothiazide and ConA on responses to kainate are shown in figure 3.3.2. Again, cyclothiazide increased current amplitude ($n=10$), suggesting the involvement of an AMPA receptor.

The effect of ConA was less clear; in the majority of cells ConA produced no discernible effect, but in the example given ConA appeared to

Figure 3.3.1 Cyclothiazide & ConA - effects on responses to AMPA
The upper panel illustrates the effects of cyclothiazide and ConA on responses to AMPA recorded from a single cell. 3μM AMPA was repeatedly applied by pressure-application with the cell clamped to -70mV by dSEVC. 100μM cyclothiazide and 0.3mg/ml ConA were bath-applied. Each data point represents peak current amplitude for a single agonist application.

Sample traces from which the curent amplitude measurements were made are presented in the lower panel. The displayed traces are those indicated by arrows in the upper panel. Voltage traces are shown below current traces.

To prevent dilution of cyclothiazide during prolonged pressure-application, the pressure-application pipette was replaced upon bath-application of cyclothiazide with a pipette containing both AMPA and cyclothiazide. The original pipette was replaced upon returning to control bathing solution; that the pipette could be replaced such that the response was not significantly different from the control was verified in separate experiments.

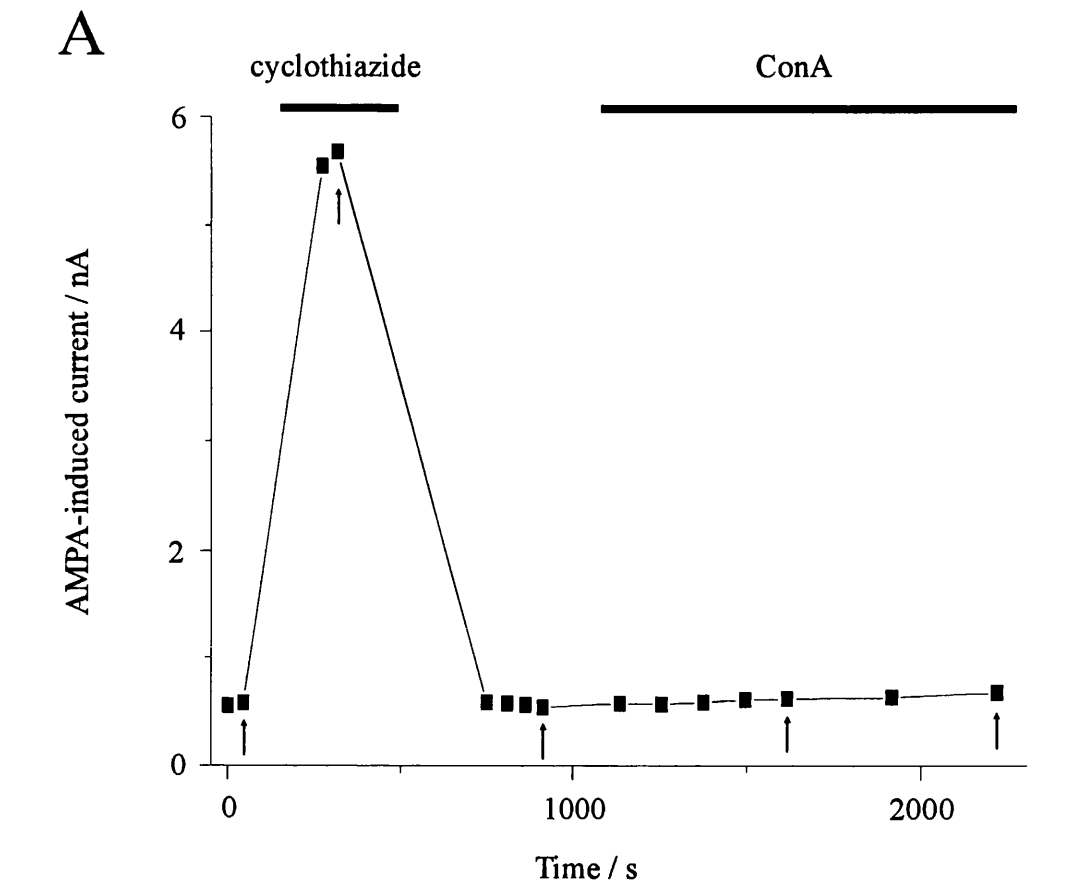
A
cyclothiazide
ConA
AMPA-induced current / nA
6
4
2
0
0
1000
2000
Time / s

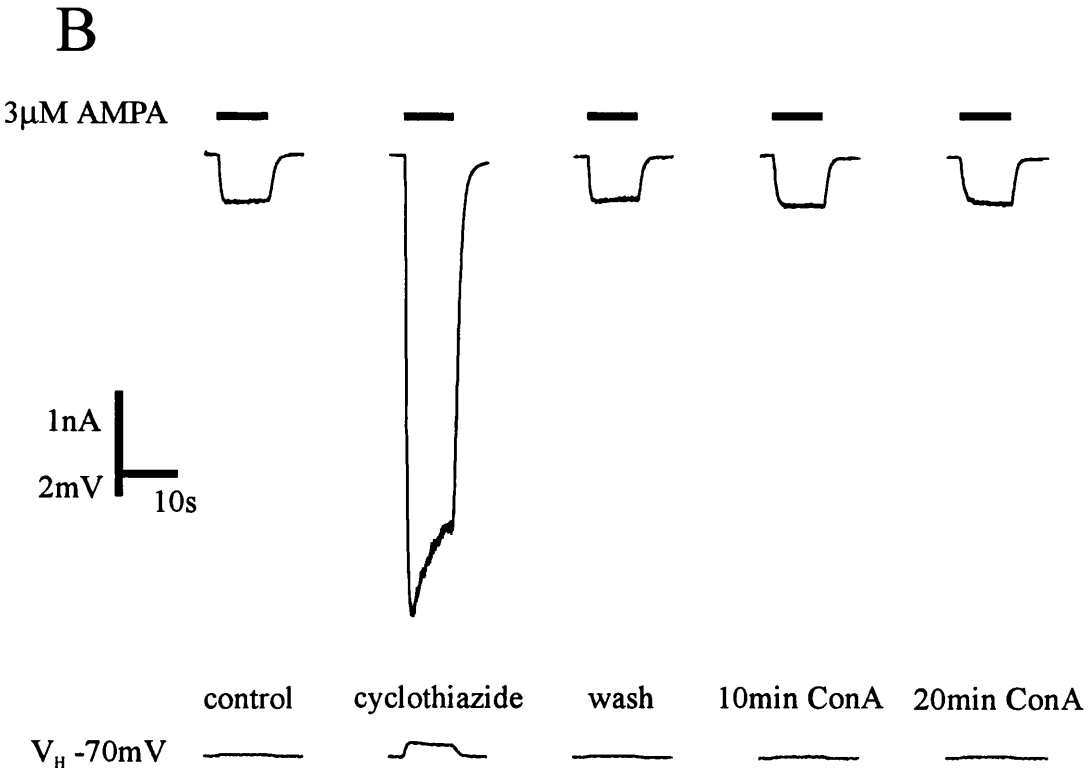
B
3μM AMPA
1nA
2mV
10s
control
cyclothiazide
wash
10min ConA
20min ConA
V_H -70mV

Figure 3.3.2 Cyclothiazide & ConA - effects on responses to kainate

Effects on current to kainate analogous to that shown for AMPA in figure 3.3.1. The neurone was clamped to -70mV using dSEVC and 10μM kainate was pressure-applied in the presence and absence of 100μM cyclothiazide and 0.3mg/ml ConA. Cyclothiazide was included in the pressure-application pipette used when cyclothiazide was in the bathing solution.

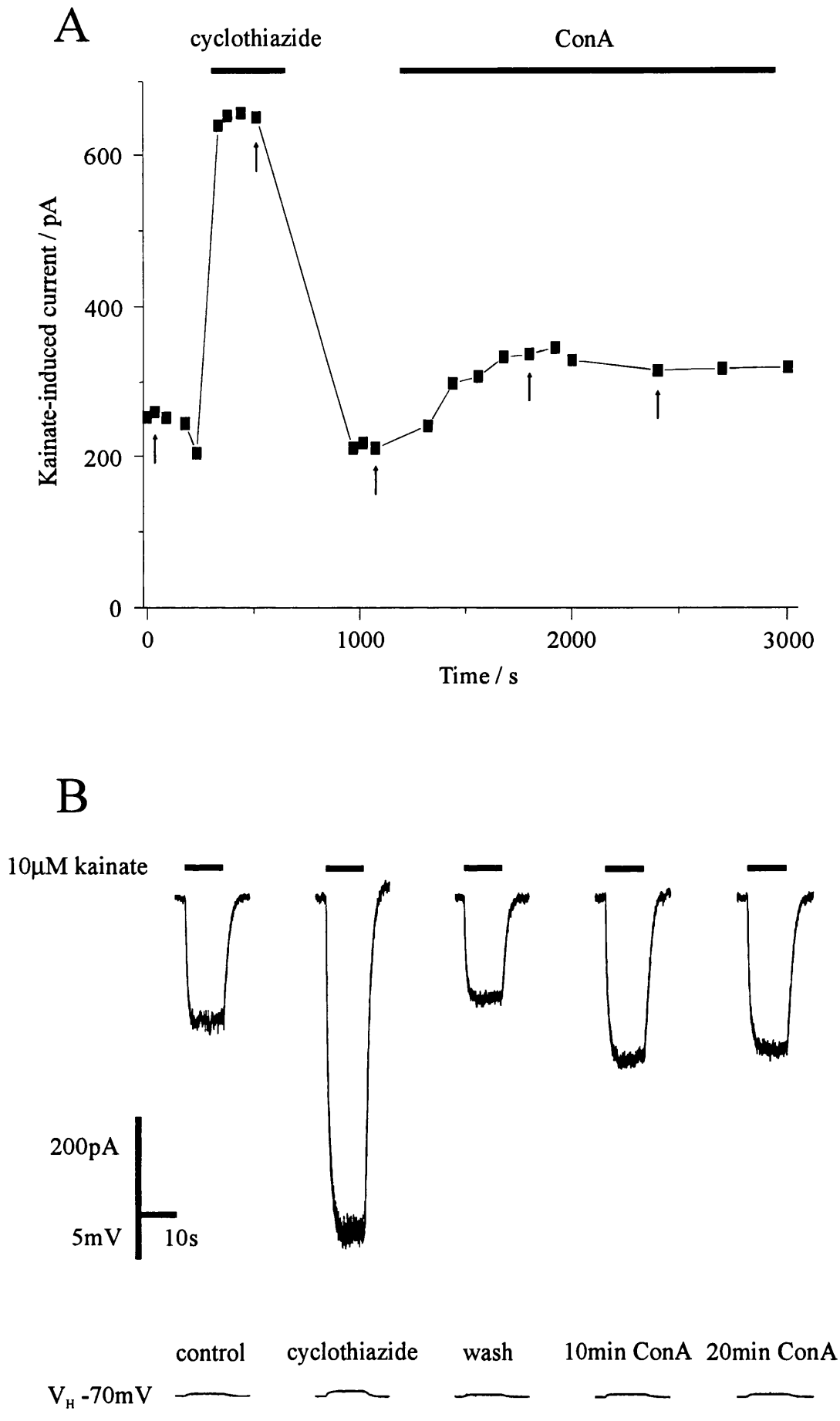
A
cyclothiazide
ConA
Kainate-induced current / pA
600
400
200
0
0
1000
2000
3000
Time / s
B
10μM kainate
200pA
5mV
10s
control
cyclothiazide
wash
10min ConA
20min ConA
V_H -70mV

potentiate responses to kainate by approximately 50%. The degree of potentiation is difficult to estimate since current amplitude was not stable. Whilst there was some suggestion that ConA may have potentiated responses from other cells, the degree of potentiation was similarly too small to be clearly resolved above the variation of the control responses (n=10). One conclusion can therefore be made, that the majority or all of the current observed under these conditions resulted from AMPA receptor activation.

3.3.3 Cyclothiazide dose-response data

Dose-response data for cyclothiazide were generated by examining the effect of bath-application of cyclothiazide on the amplitudes of responses to brief pressure-applications of AMPA. The resulting dose-response curve is illustrated in the upper panel of figure 3.3.3. The EC_{50} was 47μM, Hill slopes were within the range 2.4-3.5 and potentiation by cyclothiazide from 2.6 to 13.

These data were generated using 100ms pressure-applications of AMPA and bath-application of cyclothiazide. It was intended that bath-application would permit equilibrium binding of cyclothiazide whilst the brief applications of agonist would minimise unbinding of cyclothiazide over the timescale in which the current was recorded. For any given concentration of cyclothiazide responses to briefer applications of agonist were potentiated less, suggesting that the method of agonist application may have influenced the dose-response data (discussed below, see section 3.6.1).

In view of the uncertainty which resulted from the method of application of agonist, similar experiments were conducted using stepper-application of kainate. In this context, this approach proved very difficult in practice and was therefore discarded. However, one example of a dose-response relationship generated by this method is given in figure 3.3.3 (lower panel). The Hill slope of this relationship is shallower than those from pressure-applied AMPA and more consistent with published data. The EC_{50} value of 16μM is slightly lower than for pressure-applied AMPA, but of the same order of magnitude. Maximal effective concentrations of cyclothiazide potentiated responses by 2.85-fold, similar to published values.

Figure 3.3.3 Cyclothiazide dose-response data

The upper panel shows mean dose-response data for the effect of bath application of cyclothiazide on 100ms pressure-applications of 10μM AMPA.

Degree of potentiation by cyclothiazide was calculated as:

(current amplitude in cyclothiazide/current amplitude of control) - 1

Values ranged from 2.6 to 13. In order to generate a mean dose-response curve, data from each cell were normalized to the maximum potentiation given by the top of the fitted dose-response curve and the normalized values used to calculate the mean ($\pm$SEM) potentiations shown. The fitted curve was constrained to the mean EC_{50} and Hill slope values (calculated from the values for individual cells) and to a minimum and maximum of 0 and 1 respectively.

The lower panel gives dose-response data for a single neurone. Kainate was stepper-applied and cyclothiazide bath-applied. The fitted curve was constrained to a minimum of 0.

A

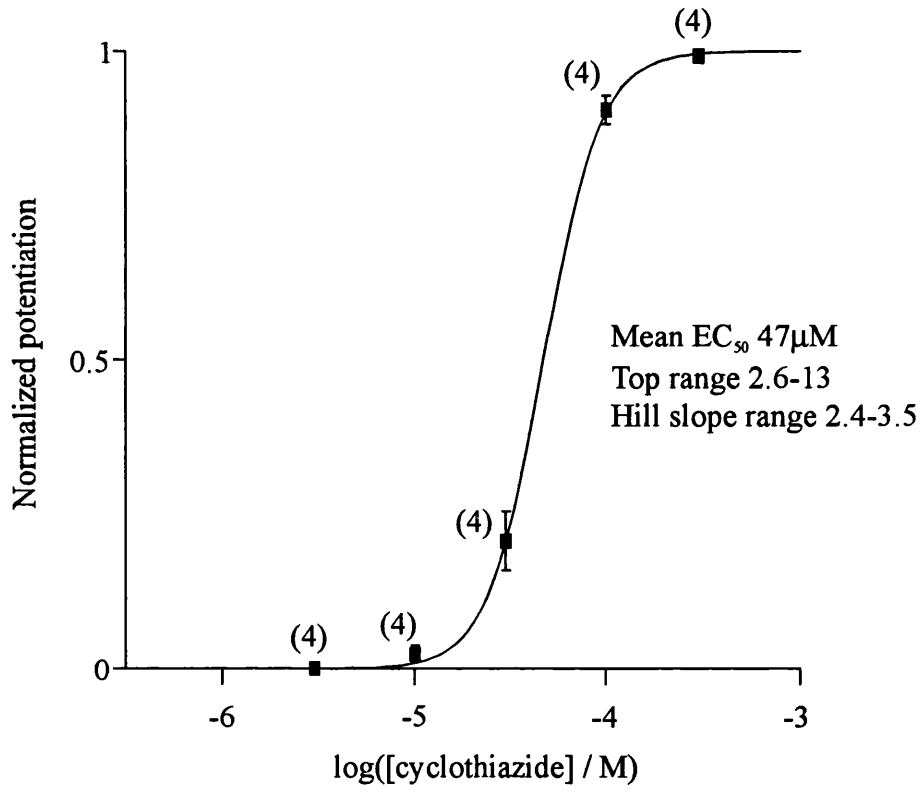
Pressure-application of 10μM AMPA
Normalized potentiation
1
0.5
0
(4)
(4)
(4)
(4)
(4)
Mean EC50 47μM
Top range 2.6-13
Hill slope range 2.4-3.5
-6
-5
-4
-3
log([cyclothiazide] / M)

B

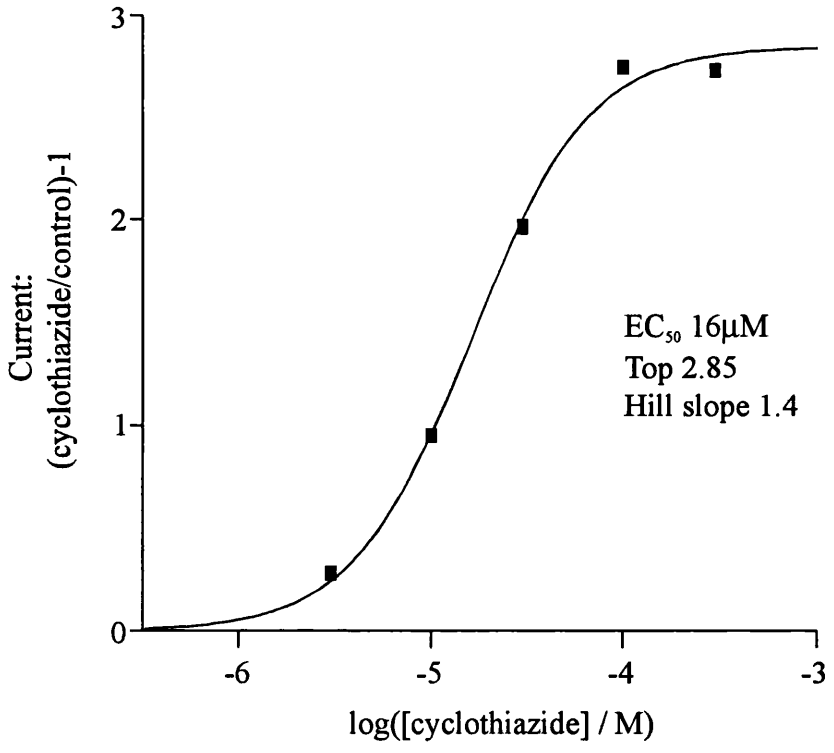
Stepper-application of 10μM kainate
Current:
(cyclothiazide/control)-1
3
2
1
0
EC50 16μM
Top 2.85
Hill slope 1.4
-6
-5
-4
-3
log([cyclothiazide] / M)

3.4 Results - GYKI 53655; resolution of the kainate receptor

3.4.1 GYKI 53655 - effect & dose-response curve

GYKI 53655 inhibited responses to kainate in a dose-dependent manner. The mean dose-response curve for the effect of GYKI 53655 on responses to 100μM kainate is given in figure 3.4.1. The IC_{50} for GYKI was 1.2μM and slope -0.89. The fitted curve indicates that a residual current remained in the presence of maximal concentrations of GYKI 53655, the residual accounting for 6.1% of the control current amplitude. With the slopes of the fitted relationships constrained to -1, values of 7.8 $\pm$ 2.3% (n=5) and 1.12 $\pm$ 0.06μM (n=5) were obtained for residual current amplitude and IC_{50} respectively.

Figure 3.4.1 shows an example of the effect of 100μM GYKI 53655 on the response to pressure-application of 100μM kainate. Dose-response data indicated that 100μM GYKI 53655 reduced current amplitude to approximately 8% of control.

In addition to inhibiting current amplitude, GYKI 53655 influenced the kinetics of the response, current to kainate in the presence of GYKI 53655 decreasing in the continued presence of kainate (n=7). Mean current amplitude at the end of agonist application (pseudo steady-state) was 70% of peak current amplitude. Since 2,3-benzodiazepines are not thought to display use-dependence (Donevan & Rogawski, 1993) it seemed likely that this may result from desensitization such as one would expect to observe were kainate acting at a kainate receptor. Whilst the kinetics of decay were slower than typically observed for kainate-induced kainate receptor desensitization, this may be a result of the relatively slow method of agonist application.

3.4.2 Kinetics of stepper-application of kainate

To resolve the issue of the kinetics of desensitization to kainate, kainate was applied to cells by stepper-application. In instances where a rapid application of agonist was achieved, pronounced desensitization to low concentrations of kainate (10μM) could be observed in the absence of GYKI 53655.

In the example shown in figure 3.4.2, the decay was fit with a single

Figure 3.4.1 Effect of GYKI 53655 & dose-response relationship

Upper panel: mean dose-response relationship for the inhibition of responses to 100μM kainate by GYKI 53655. Responses were recorded from cells clamped to -70mV using dSEVC. Kainate was applied by stepper-application, GYKI 53655 by bath-application. Data were taken only from cells where the response to kainate was sufficently rapid such that the steady-state current amplitude could be measured prior to dilution of GYKI 53655 (which was not included in the test solution). Dilution of GYKI 53655 was visible as an increase in current amplitude with time which began shortly after steady-state current amplitude was obtained. For any given cell current amplitudes under different conditions were measured at the same interval after agonist application. Note that in preliminary experiments dose-response data were generated by pressure-application of agonist, but this provided variable results (cf. discussion of dose-response data for cyclothiazide, section 3.6.1.)

Data for each cell were normalised by expression of current amplitude as a percentage of control and a curve fitted (constrained to a maximum of 100%). The curve shown was constrained to the mean EC_{50} and Hill slope values (calculated from the values for individual cells) and to a maximum of 100%.

Mean IC_{50} and Hill slopes were 1.2 $\pm$ 0.08μM (n=5) and -0.89 $\pm$ 0.06 respectively. Extrapolation of the curves for individual cells gave a current amplitude at a maximum concentration of GYKI 53655 (I_{min}) of 6.1 $\pm$ 1.6% of control (range 2.2-11.6%). Current amplitude at 100μM GYKI 53655 was 8.3 $\pm$ 2.2% of control.

Lower panel: an example of the effect of 100μM GYKI 53655 on responses to pressure-application of 100μM kainate, recorded from a cell clamped to -70mV by cSEVC. GYKI was both bath- and pressure-applied. In addition to reducing current amplitude GYKI 53655 altered the kinetics of the response to kainate. Note that in the example given cSEVC was employed hence the degree of inhibition may have been underestimated.

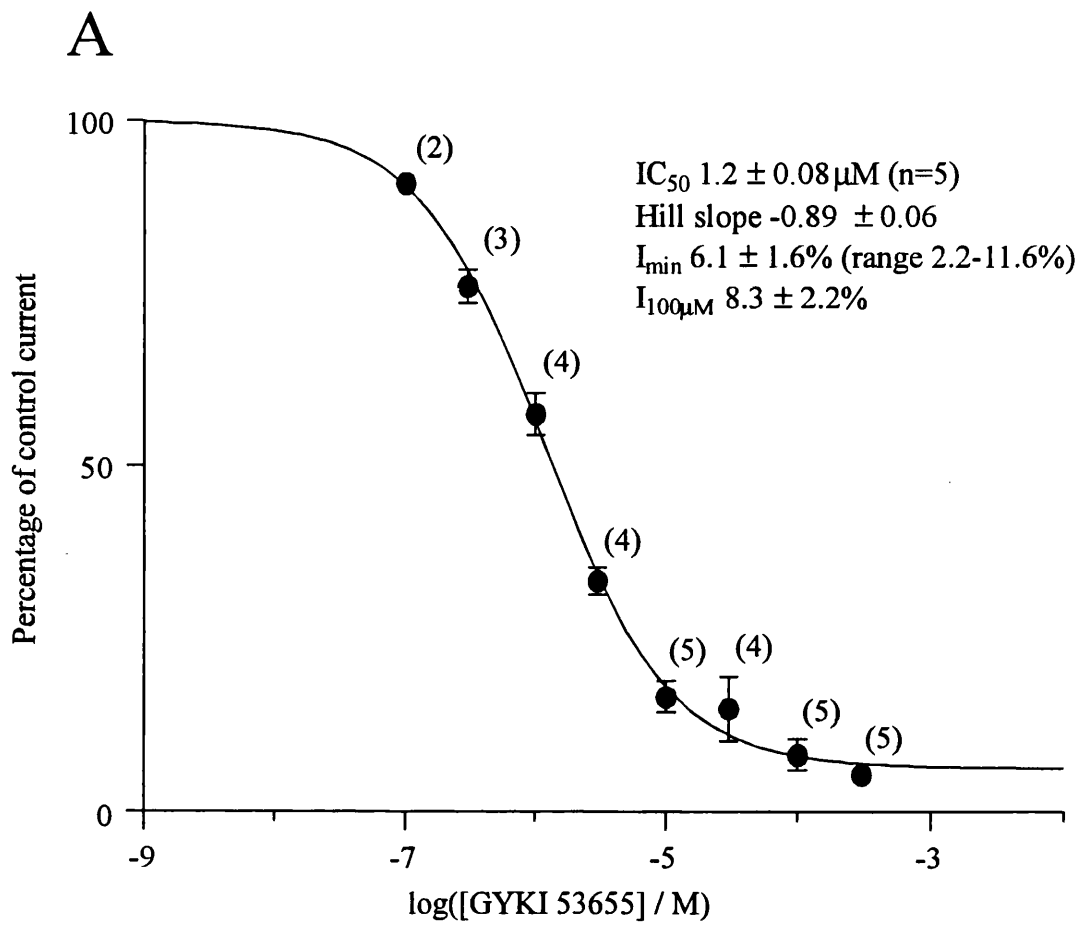
A
100
50
0
Percentage of control current
(2)
(3)
(4)
(4)
(5)
(4)
(5)
(5)
IC50 1.2 ± 0.08 µM (n=5)
Hill slope -0.89 ± 0.06
Imin 6.1 ± 1.6% (range 2.2-11.6%)
I100µM 8.3 ± 2.2%
-9
-7
-5
-3
log([GYKI 53655] / M)

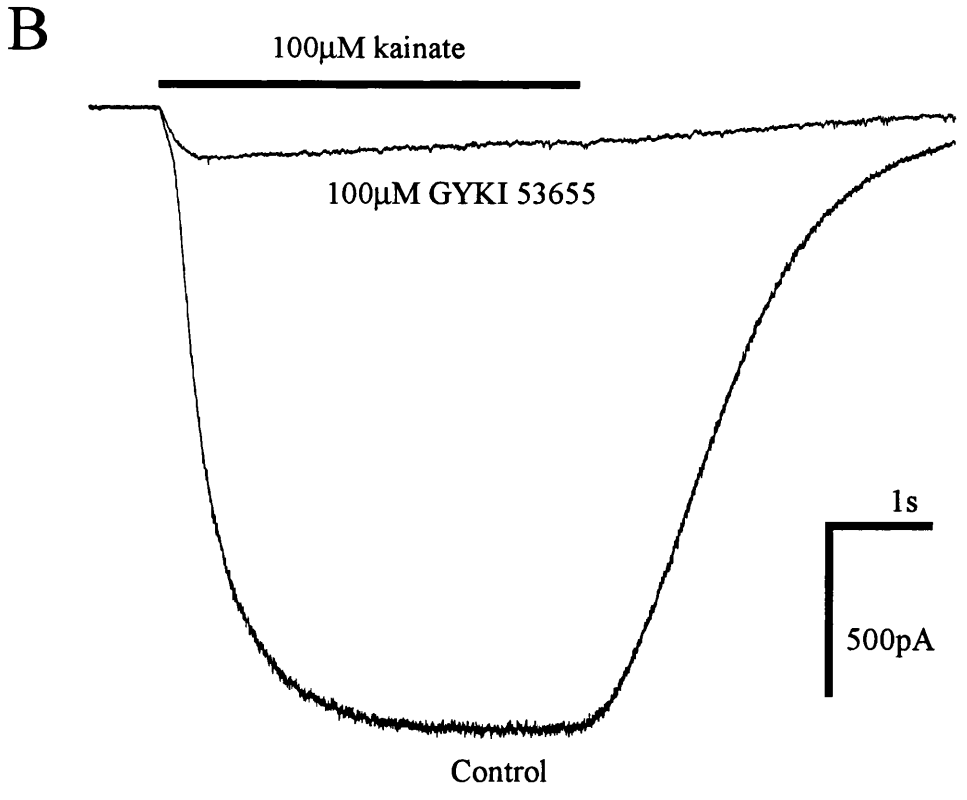
B
100µM kainate
100µM GYKI 53655
1s
500pA
Control

Figure 3.4.2 Kinetics of stepper-application of kainate

Responses to stepper-application of 10μM kainate were rapidly rising and showed pronounced desensitization. In the example given 10-90% rise time was 167ms and the decaying phase was fit with a single exponential imposed on a sloping baseline. The time constant of decay was 613ms, similar to values reported in the literature for desensitization of kainate receptors to kainate.

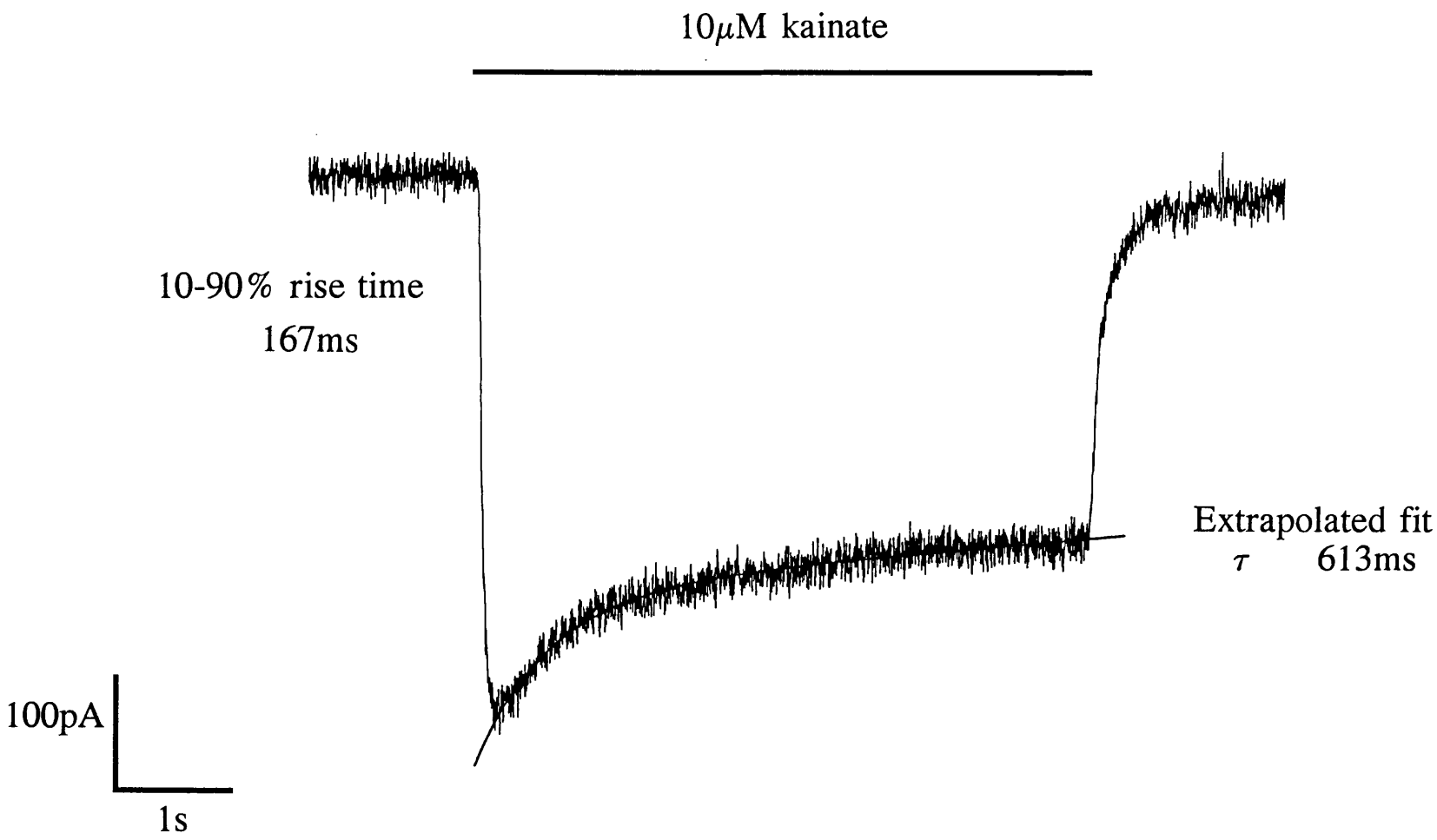
10μM kainate
10-90% rise time
167ms
Extrapolated fit
τ 613ms
100pA
1s

exponential imposed on a slightly sloping baseline. The time constant of decay (613ms) is similar to those given by Huettner (1990, $\tau \sim 400$ms) and Wong & Mayer (1993, $\tau \sim 700$ms). In both these publications the authors fitted desensitization to kainate with second order exponentials, the fast component being of the order of 40-60ms. A similarly rapid component could be present in basal forebrain neurones, but may not be resolved since stepper-application did not offer sufficiently rapid application of agonist.

3.4.3 Effects of cyclothiazide & of ConA on residual response

The receptor underlying the residual response to kainate in the presence of GYKI 53655 was investigated using cyclothiazide and ConA. Cyclothiazide had little effect on responses to kainate: of the 5 cells to which cyclothiazide was applied only one displayed potentiation (approximately 2-fold). ConA was applied to 4 cells, in all of which it reduced desensitization of the response. Mean peak:pseudo steady-state current ratio after ConA treatment was 1. ConA potentiated the pseudo steady-state current two-fold (mean value). The effect of ConA was irreversible for the length of time for which recordings were continued after removal of kainate from the bath (approximately 7 minutes).

These effects of cyclothiazide and of ConA on the residual current in the presence of GYKI 53655 underpin the assertion that basal forebrain neurones express a kainate receptor population in addition to the functionally more significant (under these recording conditions) AMPA receptor population.

These results are illustrated in figure 3.4.3.

Figure 3.4.3 Effects of cyclothiazide & of ConA on residual response
Upper panel: example of the failure of 100μM cyclothiazide to potentiate responses in the presence of GYKI 53655. Responses from a cell clamped to -70mV by cSEVC were elicited by pressure application of 100μM kainate. 100μM GYKI 53655 and cyclothiazide were applied by both bath- and pressure-application. A response in the presence of cyclothiazide is overlaid on a control response, both in the presence of GYKI 53655.

Lower panel: three traces overlaid, one control, one after 5 minutes in the presence of 0.3mg/ml ConA and one 5 minutes after removal of ConA from the bath. ConA clearly potentiates the response to kainate. In this instance, the steady-state current is potentiated approximately two-fold. Potentiation was found to be irreversible for at least 5 minutes after removal of ConA from the bath.

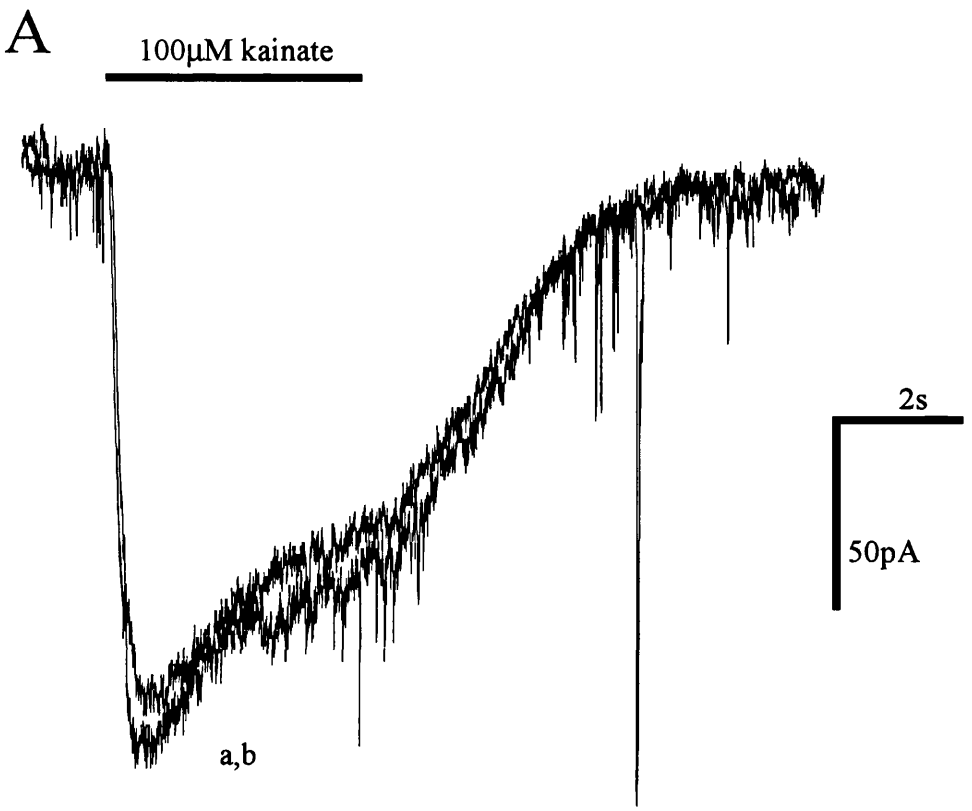

a control
b 100μM cyclothiazide

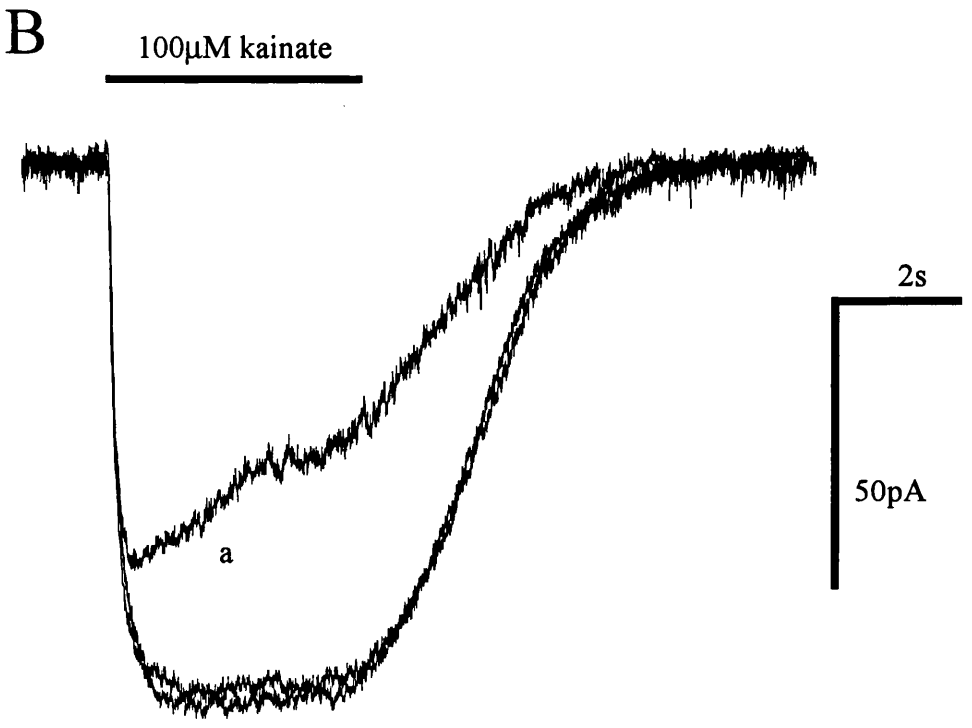

a control
b 0.3mg/ml ConA
c wash

3.5 Conclusions

1. The above data suggest that basal forebrain neurones express ionotropic glutamate receptors of all three classes; NMDA, AMPA and kainate receptors. There was no indication that these neurones might express functional metabotropic glutamate receptors.

2. A number of lines of evidence suggest that the bulk of the non-NMDA receptor-mediated current in basal forebrain neurones is mediated by AMPA- rather than kainate-type receptors. The principle evidence consists of agonist dose-response data, the effects of modulators (cyclothiazide and concanavalin A) and antagonist pharmacology (sensitivity to GYKI 53655).

3.6 Discussion

3.6.1 Effects of cyclothiazide

Cyclothiazide is known to more strongly inhibit desensitization of flip than of flop splice variants of recombinant AMPA receptors, sensitivity being determined by a single amino acid residue. Even in the presence of cyclothiazide desensitization of flop receptors to AMPA is typically quite pronounced and desensitization to kainate may also be observed. In contrast, flip receptors do not display any desensitization to kainate in the presence of cyclothiazide and desensitization to AMPA is greatly reduced or completely absent. Flip isoforms are dominant when co-expressed with flop isoforms (Partin, Patneau & Mayer, 1994; Partin, Bowie & Mayer, 1995).

With regard to basal forebrain neurones, responses to kainate show no desensitization in cyclothiazide and responses to AMPA show relatively mild desensitization in cyclothiazide (see sections 3.3.1 & 3.3.2). These data suggest that basal forebrain neurones may express AMPA receptors containing subunit(s) of flip splice variant(s).

This may also explain the observation that the degree of potentiation by cyclothiazide of brief applications of AMPA depended upon the duration of pressure-application (see section 3.3.3) since cyclothiazide is also known to shift the agonist dose-response curve at AMPA receptors of the flip splice variant. A leftward shift has been observed for homomerically and heteromerically expressed receptors containing a flip splice variant (Partin, Patneau & Mayer, 1994) and for receptors expressed by hippocampal neurones (Patneau, Vyklicky & Mayer, 1993). Thus the characteristics of the dose-response curve may be dependent on the concentration of agonist applied.

It is also possible that this dependence of potentiation on duration of pressure-application results from a failure of cyclothiazide to significantly increase the rate of rise of the response. It is evident from the traces given in figure 3.3.1 that 50-100ms is only a small fraction of the time taken to reach steady-state response amplitude, ie. the response at 50-100ms is still rapidly rising. Were cyclothiazide to only slightly increase the initial rate of rise of the response to AMPA, then responses to brief pressure-applications of agonist would show little potentiation. More prolonged applications of agonist would be less subject to this effect as the rate of rise of the control response decreases with time.

The slope of the dose-response relationship presented above is unexpectedly steep. Published data on both native (Patneau, Vyklicky & Mayer, 1993) and recombinant (Partin, Patneau & Mayer, 1994) AMPA receptors suggests that the Hill slope should be in the region of 1.2-1.4. The Hill slope for the cyclothiazide dose-response relationship generated with stepper-application of kainate was 1.4, a figure more consistent with published values.

The degree of potentiation by cyclothiazide of responses to stepper-application of kainate is also more consistent with published values for the effect of cyclothiazide on kainate-elicited responses at AMPA receptors and with potentiation of peak current responses to AMPA. The effects of cyclothiazide on peak and steady-state currents have been compared in hippocampal neurones. Whilst potentiation of peak and steady-state currents differed approximately 100-fold, the EC_{50} values were very similar (Yamada &

Tang, 1993).

The calculated maximum potentiation by cyclothiazide of responses to kainate was slightly less than published values. This is expected since control responses to kainate probably consisted of both AMPA and kainate receptor-mediated components.

It must also be noted that cyclothiazide acts as a channel blocker at both AMPA and kainate receptors. This is likely to influence dose-response data generated by both methods. No account of this effect was taken into consideration.

In summary, these dose-response data for cyclothiazide are very approximate, but seem consistent with published data. In basal forebrain neurones cyclothiazide potentiates AMPA receptor-mediated responses with an EC_{50} of slightly less than 50μM. 100μM cyclothiazide produced a slightly sub-maximal potentiation.

3.6.2 Evidence for expression of a kainate receptor

Inhibition of kainate-elicited current by GYKI 53655 is strong evidence that this current is mediated by an AMPA receptor. That a small residual current remains even in high concentrations of GYKI and that this residual shows desensitizing kinetics suggest that a kainate receptor-mediated component is also present.

Some uncertainty must shadow this conclusion given the relative amplitudes of AMPA and kainate receptor-mediated responses. The residual component may simply be a small proportion AMPA receptor-mediated current that would be blocked by higher concentrations of GYKI 53655. Unfortunately 300μM is the limit of solubility of GYKI 53655. Kainate receptor activity may also be inhibited by very high concentrations of GYKI 53655.

The lack of effect of cyclothiazide and potentiation by ConA of the residual response are therefore significant since they clearly demonstrate that the residual response is pharmacologically distinct from the non-NMDA receptor-mediated response in the absence of GYKI 53655. The pharmacology

of the residual current is similar to that of a kainate receptor rather than an AMPA receptor.

Unfortunately there is also some doubt as to the reliability of this data since 2,3-benzodiazepines and cyclothiazide interact at some AMPA receptors (Zorumski, Yamada, Price & Olney, 1993; Desai, Burnett, Ornstein & Schoepp, 1995; Johansen, Chaudhary & Verdoorn, 1995; Kessler, Arai, Quan & Lynch, 1996; Partin & Mayer, 1996).

This interaction has been examined in greatest detail by Johansen, Chaudhary & Verdoorn (1995) who concluded that GYKI 52466 does not reverse inhibition of desensitization by cyclothiazide or shift the dose-response curve for cyclothiazide. This is consistent with all other publications in which this issue was addressed, there being no published account of a 2,3-benzodiazepine modulating the effect of cyclothiazide.

Johansen, Chaudhary & Verdoorn (1995) also examined the effect of cyclothiazide on the potency of GYKI 52466 (an issue over which the data from different laboratories appeared to conflict) and found that cyclothiazide decreases the potency of GYKI 52466 at some, but not all, AMPA receptors. The authors reported that cyclothiazide caused a parallel rightward shift of the GYKI 52466 dose-response curve for all the heteromerically expressed receptors that were studied, all of which contained GluR2 and either GluR1 or GluR4 (both flip and flop splice variants). In contrast no significant effect of cyclothiazide on the GYKI dose-response curve was observed for homomerically expressed GluR1 or GluR4 (flip splice variants). Thus the differences between data from different laboratories is probably attributable to different subunit expression. An interesting possibility arising from this data is that this interaction may only occur where the GluR2 subunit is expressed, ie. this interaction may only occur at AMPA receptors with low divalent ion permeabilities.

If such an interaction between cyclothiazide and GYKI 53655 were to occur at AMPA receptors expressed by basal forebrain neurones, then in the presence of GYKI 53655 one would expect to observe an increase in current amplitude upon application of cyclothiazide as a result of relief of inhibition by

GYKI 53655. Thus it seems unlikely that such an interaction occurs at basal forebrain AMPA receptors, raising the possibility that basal forebrain neurones express divalent ion permeable AMPA receptors.

The degree of potentiation by ConA is slightly less than expected by comparison with the literature. For example, Partin, Patneau, Winters, Mayer & Buonanno (1993) reported a 150-fold increase in current amplitude to kainate upon ConA treatment of oocytes expressing GluR6. Potentiation is less marked at native GluR5 receptors: both Huettner (1990) and Wong & Mayer (1993) reported doubling of the apparent peak current amplitude to kainate in DRG neurones. Since ConA almost eliminates desensitization at these receptors, the effect on the steady-state current amplitudes would be greater. Wong & Mayer (1993) reported approximately 60% desensitization to kainate under control conditions (slightly more than observed for basal forebrain neurones) and approximately 3-fold potentiation of the pseudo steady-state response by ConA. Thus responses in basal forebrain neurones (in the presence of 100μM GYKI 53655) are potentiated only slightly less than reported for other native kainate receptors. This may reflect some remaining AMPA receptor-mediated current in 100μM GYKI 53655.

ConA also largely eliminated desensitization to kainate in basal forebrain neurones, as in DRG neurones. Wong & Mayer (1993) also noted that on DRG neurones the effects of ConA were not reversible within 20 minutes. The effects of ConA on GluR6 (expressed in oocytes) were also maintained for at least 10 minutes in contrast with the effects at GluR1, which were largely reversed after only 3 minutes (Partin, Patneau, Winters, Mayer & Buonanno, 1993). The lack of reversal of ConA effects at basal forebrain neurones is again more consistent with the presence of a kainate than an AMPA receptor.

Thus it seems very likely that basal forebrain neurones express kainate receptors as well as AMPA receptors, but that kainate receptor-mediated responses are not evident unless AMPA receptor-mediated responses are inhibited. A similar situation in a subset of cultured hippocampal neurones was reported by Paternain, Morales & Lerma (1995). The masking of kainate receptors is likely to be particularly pronounced at high agonist concentrations

since kainate receptors generally have a lower EC_{50} for kainate than have AMPA receptors (see Hollmann & Heinemann, 1994).

One might expect to observe desensitizing, ConA-sensitive responses to kainate in the absence of GYKI 53655 upon application of low concentrations of kainate. ConA sensitivity was difficult to assess (see section 3.3.2), but desensitization was observed upon stepper-application of 10μM kainate (which should produce an AMPA receptor-mediated response of approximately 5% of maximum).

3.6.3 Functional significance of the kainate receptor

Though kainate receptors have been widely studied following cloning and expression, the functional roles of kainate receptors *in vivo* are unknown, there being very few examples of functional kainate receptors in native neurones. The subset of DRG neurones which give rise to primary afferent C-fibres express functional kainate receptors (Huettner, 1990). The function of these receptors is unknown but is probably presynaptic. Within the CNS, only one example of a putative functional kainate receptor-mediated response has been reported. Chittajallu, Vignes, Dev, Barnes, Collingridge & Henley (1996) observed both pre- and postsynaptic actions of kainate, most likely mediated by a kainate receptor. The pre-synaptic actions included a sustained, repeatable depression of the amplitude of NMDA receptor-mediated excitory postsynaptic currents recorded from hippocampal CA1 neurones upon low-frequency stimulation of the Schaffer collateral-commissural pathway.

With regard to basal forebrain neurones, if the kainate receptor is only responsible for such a small proportion of non-NMDA receptor-mediated current, it may have little functional significance, glutamate being no more potent at kainate than at AMPA receptors (see Hollmann & Heinemann, 1994). Alternatively it is possible that the small current observed upon kainate receptor stimulation results from the activation of extrasomatic kainate receptors, the current amplitude being diminished by the cable properties of the cell. The distribution of kainate receptors could be examined immunocytochemically.

3.6.4 Space-clamp considerations

There can be no doubt that the distal processes of the basal forebrain neurones used for these experiments were not clamped to the somatic potential. This is an inevitable result of using a somatically located pipette to voltage-clamp cells with processes.

What proportion of a cell was effectively voltage-clamped by a somatic electrode is very difficult to estimate. Cable theory provides a starting point for such considerations. That the decays of capacitance transients recorded at the soma were generally best fit with a second order exponential suggests that the cable properties of the cell do not correspond to those of a single compartment model. Unfortunately, this biexponential decay provides no further information. The mean capacitance for basal forebrain neurones in culture was 60pF, corresponding to a sphere of 22μm radius (assuming a specific capacitance of 1μF/cm^2). This suggests that electrical access was gained to some portion of the proximal processes, but does not provide a more quantitative description. In fact, clamp of proximal processes is likely to be good since cells were simply held at -70mV, cable properties influencing DC clamp far less than AC clamp (Brown & Johnston, 1983).

Though space-clamp was not quantitatively characterised, it is unlikely that poor space-clamp significantly influenced the data presented above. Responses to agonists applied by puffer-, stepper- and bath-application were indistinguishable except for kinetic differences. Since these methods are not equally focal they would be expected to activate distally located receptors to different degrees and so reveal space-clamp errors. In addition, few significant pharmacological or kinetic differences were noted between responses recorded from cultured and acute cells or between whole-cell and outside-out patch recordings.

3.6.5 Comparison with published data

Similar data to that presented above has been published from two laboratories. Kumamoto & Murata (1995a) reported both NMDA and non-NMDA receptor-mediated responses from cultured foetal rat cholinergic septal neurones. Agonist

kinetics and potency were very similar to those presented above. In addition, the effect of CNQX on currents elicited by kainate was examined using Schild analysis. Responses to NMDA were also recorded and found to be sensitive to glycine, AP5, spermine and magnesium and zinc ions. Jasek & Griffith (1995) have reported (in abstract form) similar responses from acutely dissociated young and adult rat basal forebrain neurones mediated by both NMDA and non-NMDA receptors.

Neither accounts address the issue of whether non-NMDA receptor-mediated responses result from the activation of AMPA or of kainate receptors. Hence the data presented above are consistent with and extend the published data, adding information regarding the sensitivity of non-NMDA receptors to cyclothiazide, ConA and GYKI 53655. These extra data reveal the prominence of the AMPA receptor population and the small functional response mediated by the kainate receptor population.

Calcium permeability of the AMPA receptor

4.1 Introduction

Influx of calcium through postsynaptic receptors is thought to be an important step in some forms of synaptic plasticity such as long-term potentiation (Nicoll, Kauer & Malenka, 1988; Nicoll & Malenka, 1995) and may under certain circumstances contribute to neuronal degeneration (Choi, 1987; Choi, 1988). At glutamatergic synapses the NMDA receptor is often cited as an important route for postsynaptic calcium influx. In contrast non-NMDA receptors are rarely considered in this context, probably because in the majority of preparations studied non-NMDA receptors have been found to have low permeabilities to divalent cations. Where non-NMDA receptors have higher divalent cation permeabilities they may fulfil similar roles in processes such as synaptic potentiation (Gu, Albuquerque, Lee & MacDermott, 1996).

The Q/R site is the major determinant of calcium permeability for native AMPA receptors. This site also dictates the I-V characteristics of native receptors. These two phenomena are thus inseparable in native AMPA receptors, provided that I-V relationships are recorded in the presence of intracellular spermine.

The shape of the I-V relationship is therefore a reliable indicator with which to distinguish between AMPA receptors with relatively high and low permeabilities to calcium, though does not offer quantitative information regarding the permeability of a receptor to divalent ions. Relative ion permeabilities are commonly measured using constant field theory to interpret the effects of changes in extracellular solutions on the reversal potentials of I-V relationships.

Aims

(1) To investigate the shape of the I-V relationships of AMPA receptors expressed by basal forebrain neurones in dissociated culture. It should be possible to gain an estimate of the proportion of neurones expressing AMPA receptors with relatively high calcium permeabilities (from the

shape of the I-V relationship) using approximately physiological solutions (eg. potassium-based intracellular solution).

(2) To quantitatively determine the calcium:sodium ion permeability coefficient ratios for a number of basal forebrain neurones using constant field theory to calculate permeability coefficient ratios from at least two reversal potential measurements from the same cell made in extracellular solutions containing different monovalent and calcium ion activities.

4.2 Results - Excised outside-out patch approach

In order to generate I-V relationships, two features are essential: (i) accurate space-clamp, and (ii) good voltage control. These conditions could not be obtained using whole-cell recording.

One potential solution was to use outside-out patches. Unfortunately this proved impractical since whilst cell-attached patches with very tight seals were frequently obtained and the seal remained intact after 'breakthrough' to whole-cell mode, patch excision generally damaged the seal beyond an acceptable level. In addition, on the limited number of occasions where stable outside-out patches were obtained, imposition of the voltage ramp protocol necessary to generate I-V data invariably resulted in unacceptable deterioration of the seal. Therefore no I-V data was derived from outside-out patches.

Despite providing no I-V data, responses to glutamate were recorded from a few outside-out patches. These responses were at least qualitatively similar to whole-cell currents in that (i) both NMDA and non-NMDA receptors were present, and (ii) non-NMDA receptor-mediated current amplitudes were greatly increased by cyclothiazide. An example of currents recorded from one patch is given in figure 4.2.1.

Figure 4.2.1 Responses in outside-out patch

Responses to glutamate from a single outside-out patch excised from the soma of a cultured neurone. Intracellular and extracellular solutions and pipette resistance were identical to those used for whole-cell recording. Holding potential -70 mV. Agonists were applied by bath-application. Traces were filtered at 1kHz (12-pole Bessel filter) and acquired at 10kHz.

Upper panel: 100μM glutamate increased current noise and produced an inward current of 1.6pA. No desensitization was evident over 50s. In the continued presence of glutamate, application of 1mM $MgCl_2$ reduced current amplitude to 0.5pA, presumably by inhibition of NMDA receptors.

Lower panels: Part of the above trace is reproduced at a different scale (left) for comparison with the magnesium-insensitive current in the presence of 100μM cyclothiazide (current amplitude 29pA).

The presence of both NMDA and non-NMDA responses and marked potentiation of the latter by cyclothiazide is consistent with whole-cell recordings.

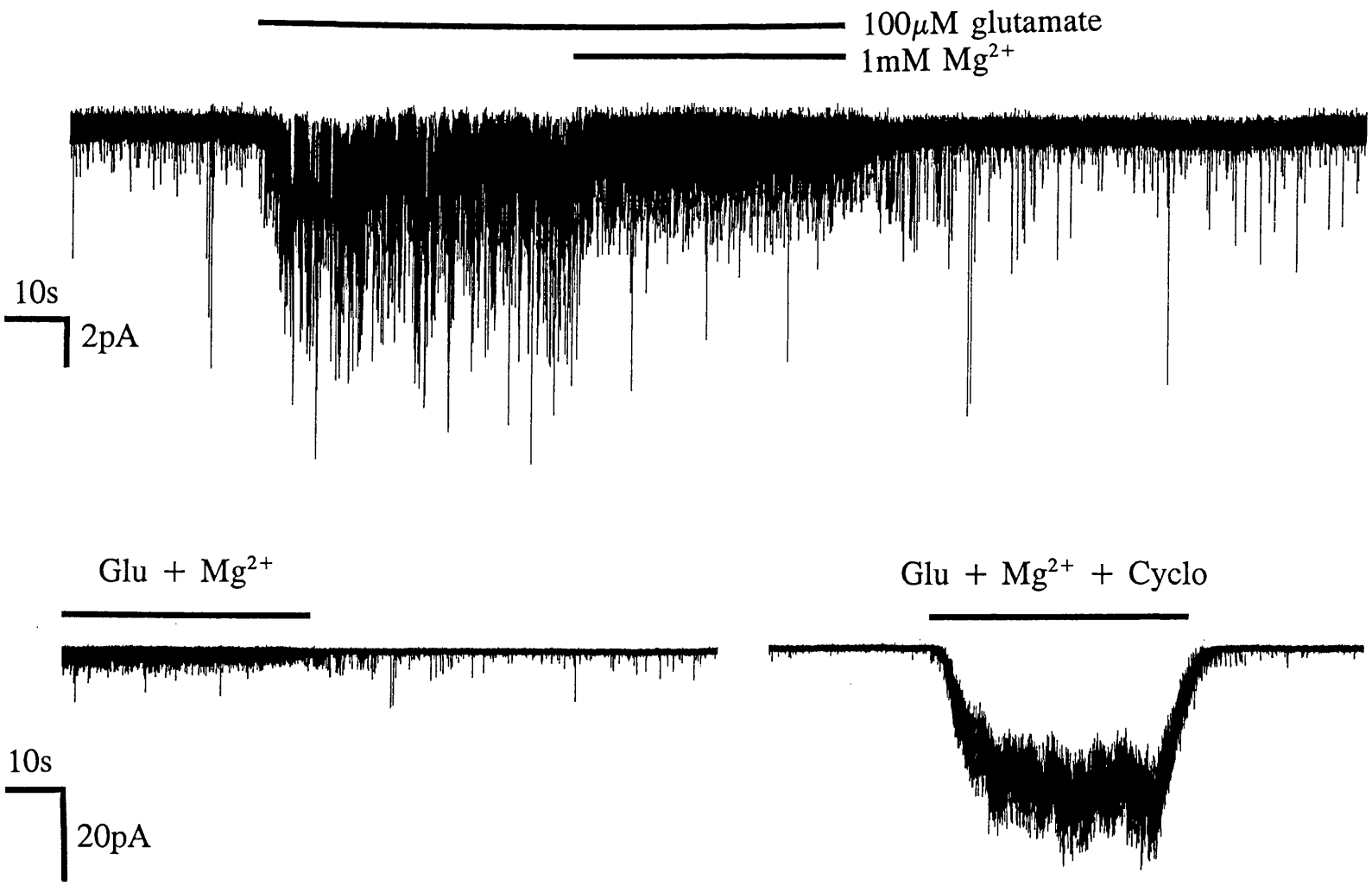
100μM glutamate
1mM Mg2+
10s
2pA
Glu + Mg2+
Glu + Mg2+ + Cyclo
10s
20pA

4.3 Results - nucleated patches

The nucleated patch method provides an alternative way of pulling what is essentially a giant outside-out patch. Nucleated patches were readily obtained from magnocellular basal forebrain neurones. The success rate was very high providing that the cultures were healthy. The seal often remained intact for prolonged periods despite repeated imposition of large voltage excursions. The fact that a significant proportion of patches remained stable for recording periods of at least 40 minutes enabled the production of I-V relationships.

Current densities in nucleated patches were lower than those from whole cell recordings. After 30-31 DIV nucleated patch current densities upon application of 1mM kainate ranged from zero to 108pA/pF (median 14pA/pF; n=13).

4.3.1 Voltage protocol and example of currents

The voltage protocol imposed on nucleated patches essentially consisted of an ascending ramp followed by a descending ramp, as illustrated in the uppermost panel of figure 4.3.1. This permitted resolution of any hysteresis which occurred in the current traces.

Examples of the corresponding current traces are shown in the central panel of the figure. Minimal hysteresis is visible in this example both under control conditions and in the presence of kainate. This was typical of traces recorded a minimum of several minutes after patch excision: hysteresis was clearly visible immediately after patch excision. This hysteresis was almost certainly attributable to calcium current inactivation since (i) the difference between ascending and descending limbs of the current trace corresponded to a loss of inward current with an activation range similar to that of the calcium current, (ii) this hysteresis was lost over the course of a few minutes, probably through calcium current rundown (note that neither ATP nor GTP was present in the intracellular solution). Since the calcium current was not entirely lost in every patch and the effect of non-NMDA receptor activation on the calcium current was unknown, the descending limb of the current response was used in the generation of I-V relationships as this exhibited less calcium current

Figure 4.3.1 Voltage protocol and example of currents

The voltage protocol used to generate I-V relationships is shown in the uppermost panel.

Corresponding current traces under control conditions and in the presence of 1mM kainate are superimposed in the central panel. Each trace is the averaged result of ten successive applications of the above voltage protocol.

The bottom panel gives the kainate-sensitive current, calculated by subtraction of the two traces shown in the central panel. Inset is the kainate-sensitive current plotted against command voltage (descending limb).

All traces were recorded from the same cell.

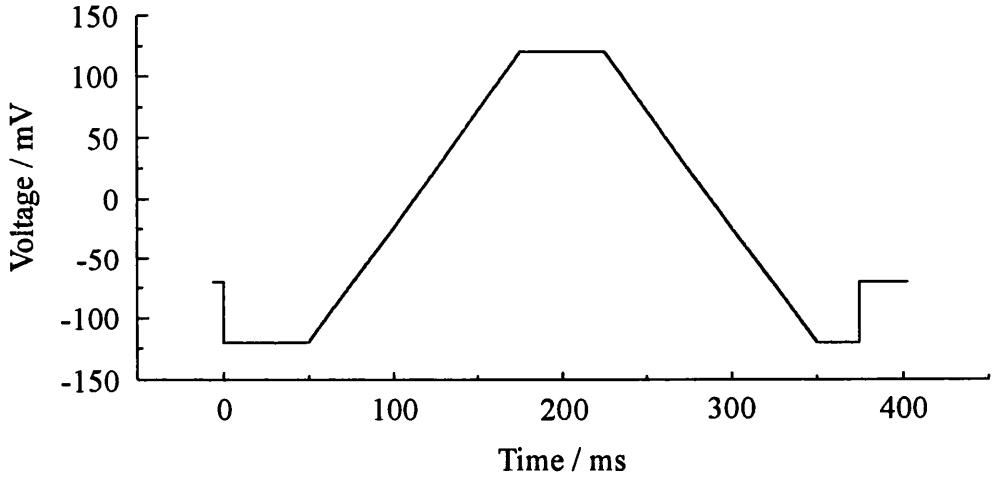
150
100
50
0
-50
-100
-150
Voltage / mV
0
100
200
300
400
Time / ms

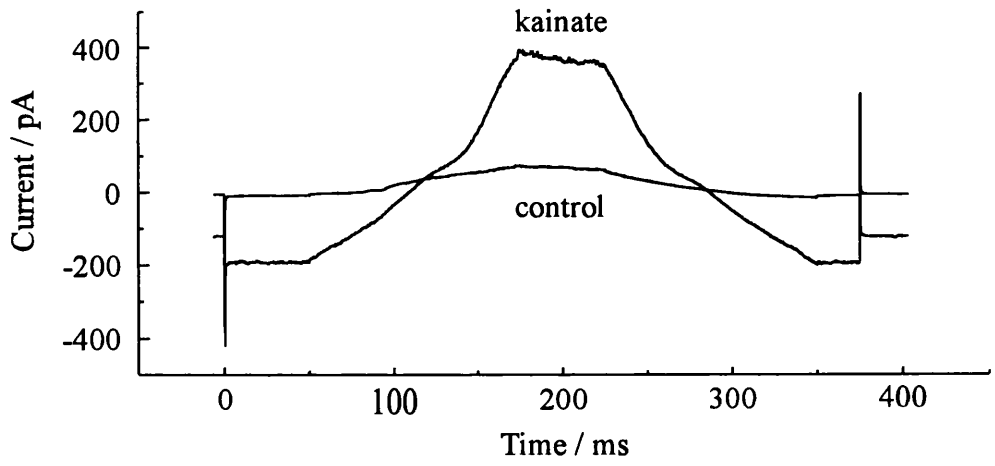
kainate
control
400
200
0
-200
-400
Current / pA
0
100
200
300
400
Time / ms

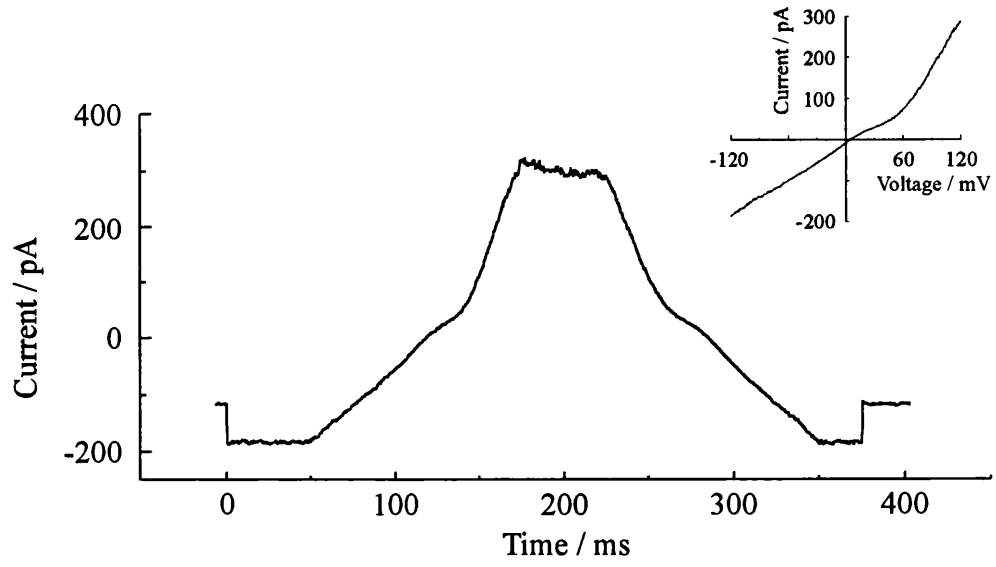
Current / pA
300
200
100
-120
60
120
Voltage / mV
-200
400
200
0
-200
Current / pA
0
100
200
300
400
Time / ms

contamination than the ascending limb.

The subtracted current response, ie. the kainate-sensitive current, is presented in the bottom panel. Mild double rectification is visible in both ascending and descending limbs of the protocol. Inset is the resulting I-V relationship for the descending limb.

Figure 4.3.2 *Control current 'rundown'*

One important criterion for accepting for analysis the data from a given cell was that, over the full voltage range, current amplitude after removal of kainate should equal that before application of kainate, ie. there must be no change in the 'leak' current during the period over which data was acquired. In practice, current amplitude at positive potentials did not stabilise for some time (see figure 4.3.2). This problem was circumvented by simply waiting until this current 'rundown' had ceased, typically 15-20 minutes or more after patch excision.

The cause of this rundown is not clear, but it may result from the loss of a potassium current, either by dialysis of the patch or through a slowly equilibrating block by TEA.

4.3.3 Rundown is kainate-insensitive

This rundown phenomenon was not the result of application of kainate, nor was it influenced by kainate (n=4). This is illustrated in figure 4.3.3. Note that the apparent increase with time of kainate-elicited current amplitude was not observed in other neurones.

4.3.4 Examples of I-V relationships from nucleated patches

I-V relationships were generated from 11 nucleated patches (with 30μM intracellular spermine). Of these, 4 were linear or mildly outwardly rectifying, 2 showed mild double rectification and the remaining 5 displayed pronounced double rectification. Two examples are given in figure 4.3.4; one with mild outward rectification and one with clear double rectification.

Rectification is commonly quantified by calculation of a rectification

Figure 4.3.2 Control current 'rundown'

Traces illustrating the change in control current with time in a nucleated patch recording. All traces are from the same patch.

The uppermost panel shows the command voltage protocol. This protocol was repeated at 30 second intervals and the resulting series of current traces are overlayed in the central panel. Current traces were filtered at 1kHz prior to display.

The bottom panel shows a plot of current amplitude against time for current amplitude at -120mV and at +120mV. Each point is derived from a single trace and represents the mean current flowing during the first epoch at -120mV or during the epoch at +120mV. Current at -120mV was stable throughout recording, indicating that the seal remained intact. In contrast, current at +120mV decreased with time and is fitted with a first order exponential decay of time constant 7.7 minutes (solid line).

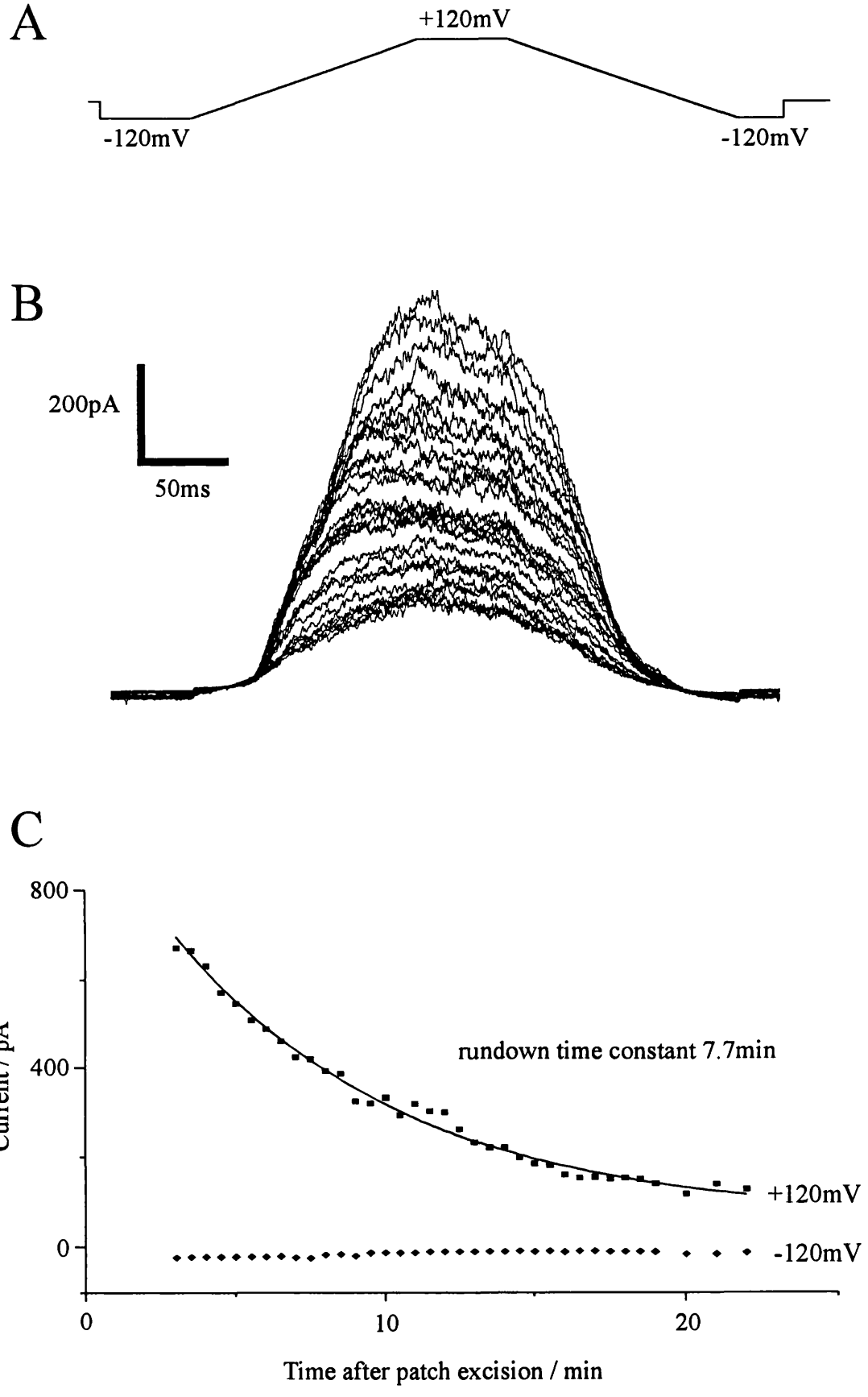
A
+120mV
-120mV
-120mV
B
200pA
50ms
C
800
400
0
Current / pA
rundown time constant 7.7min
+120mV
-120mV
0
10
20
Time after patch excision / min

Figure 4.3.3 Rundown is kainate-insensitive

Currents at -120mV and at +120mV are plotted against time after patch excision for a single nucleated patch, in the same manner as in figure 4.2.2. 1mM kainate was bath-applied three times. In each instance kainate increased inward and outward current amplitudes at negative and positive voltages respectively. After removal of kainate current amplitudes returned to the predicted control levels allowing for rundown of leak currents. Leak current rundown was fitted with a single exponential decay of time constant 15 minutes (dashed line).

In this example kainate-elicited current at +120mV increased as the leak current amplitude decreased. This effect was not observed in other patches (n=4).

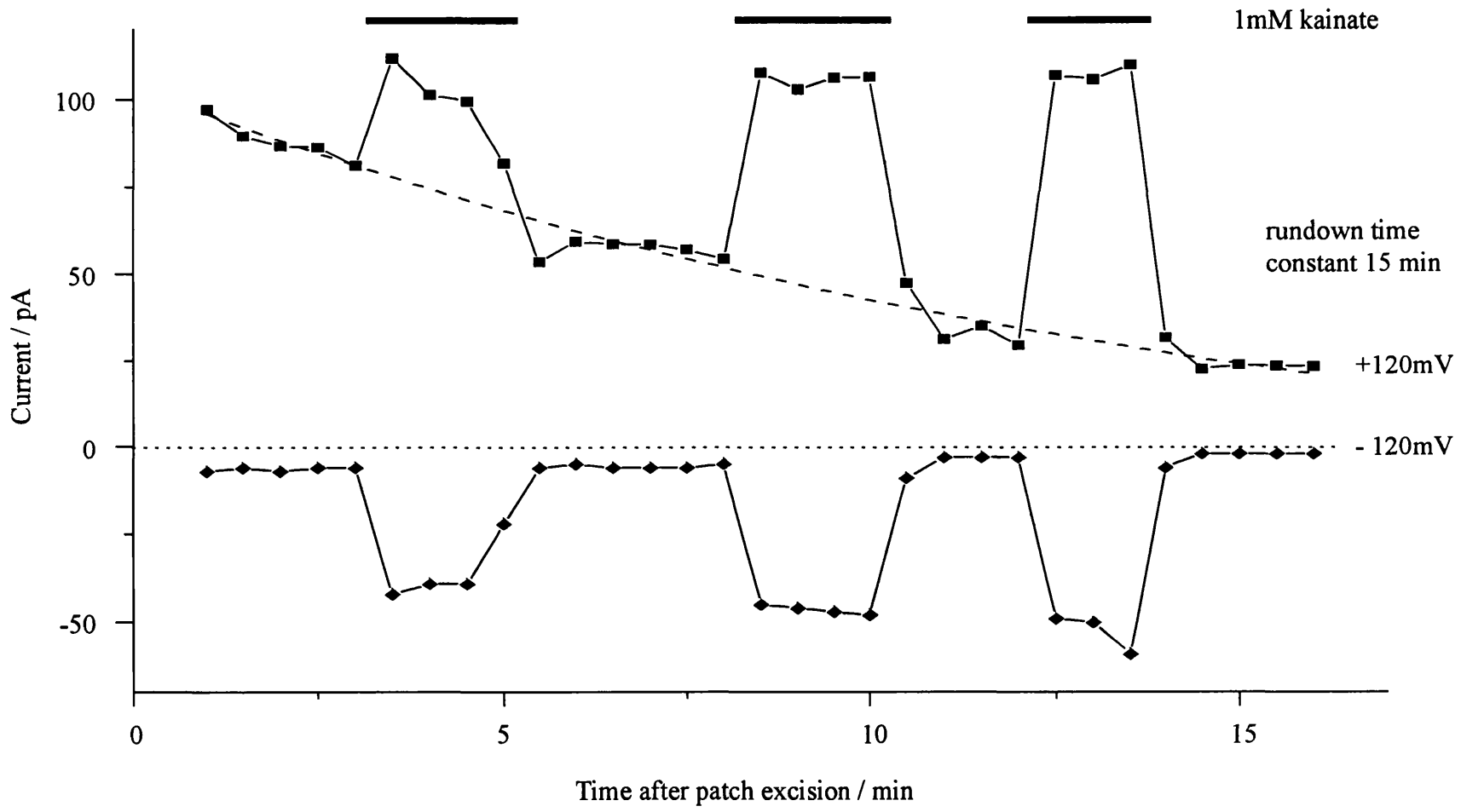
1mM kainate
100
50
0
-50
Current / pA
rundown time
constant 15 min
+120mV
- 120mV
0
5
10
15
Time after patch excision / min

Figure 4.3.4 Examples of I-V relationships from nucleated patches

I-V relationships in nucleated patches displayed a range of degrees of double rectification. The left-hand panel shows an example of a mildly outwardly rectifying relationship, with a rectification index of 1.19. On the right is an example of a doubly rectifying relationship with a rectification index of 0.28.

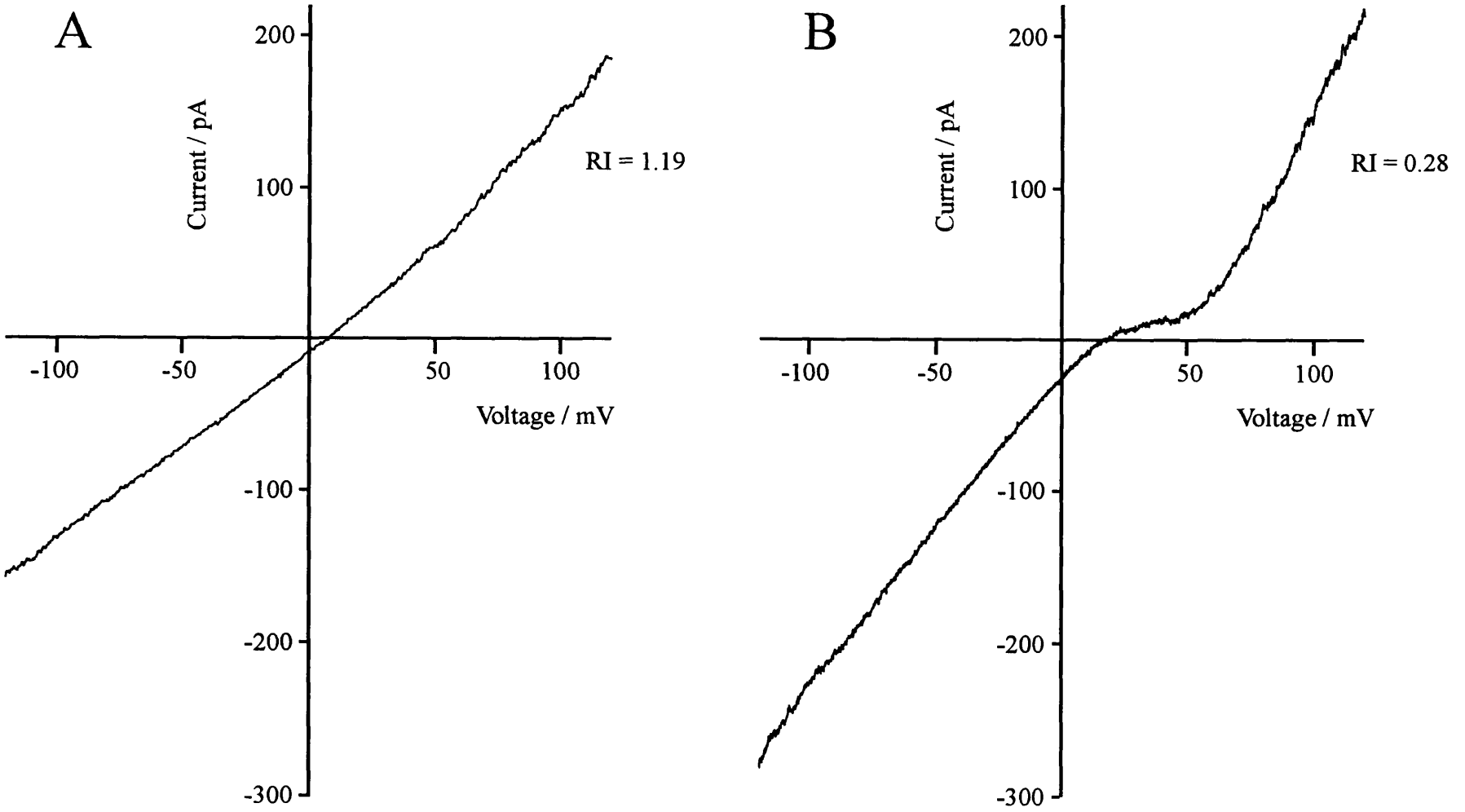
A
200
100
-100
-200
-300
-100
-50
50
100
Current / pA
Voltage / mV
RI = 1.19
B
200
100
-100
-200
-300
-100
-50
50
100
Current / pA
Voltage / mV
RI = 0.28

index (RI); essentially a ratio of current amplitudes. Rectification index values for AMPA receptor-mediated currents in basal forebrain neurones were calculated as follows:

$$RI = (I_{+40}/(40-E_{REV}))/(I_{-60}/(-60-E_{REV}))$$

Where I_{+40} and I_{-60} denote current amplitudes at +40 and -60mV respectively. Calculated values ranged from 0.28 to 1.19 (n=8). The examples given in figure 4.3.4 represent either extreme of this range.

These data suggest that basal forebrain neurones express AMPA receptors with various subunit compositions, the majority of basal forebrain neurones expressing calcium permeable AMPA receptors. The range of degrees of rectification presumably reflects the expression either of a mixture of calcium permeable and impermeable receptors in varying proportions or of receptors of different calcium permeabilities in different cells.

4.4 Results - acutely dissociated cells

4.4.1 Effects of intracellular CsF & BAPTA

The I-V relationships described above suggest that many basal forebrain neurones express calcium permeable AMPA receptors, but provide neither direct nor quantitative evidence. Divalent:monovalent cation permeability coefficient ratios of non-NMDA receptors are commonly determined using constant field theory. This requires determination of reversal potentials for the receptor-mediated current in various solutions of known composition. In practice this was not feasible using the nucleated patch method detailed above since the patches did not survive for the full length of the experiment. Acutely dissociated cells were found to be more robust in this respect.

The solutions for these experiments were designed such that the intracellular side of the membrane was exposed only to a known concentration of caesium, no other metal ions being present. This permitted simplification of the constant field equations used to calculate divalent:monovalent cation permeability coefficient ratios. Calcium buffering was initially provided by 5mM EGTA (no added calcium). This proved insufficient to prevent calcium current rundown in the elevated extracellular calcium concentrations used for

Figure 4.4.1 Effects of intracellular CsF & BAPTA

Calcium current in acutely dissociated basal forebrain neurones is sensitive to intracellular calcium concentration. Each panel consists of overlaid traces from a sequence of ramp I-V relationships generated by repetition of the voltage protocol at 20 second intervals. Current is plotted against attained voltage.

The upper left-hand panel shows pronounced calcium current rundown under control conditions. Intracellular calcium buffering was provided by 5mM EGTA. The cell was superfused with Na^+/Ca^{2+}-extracellular (see section 2.6) containing 50mM calcium.

Shown in the upper right-hand panel is a similar recording from another cell in which intracellular calcium buffering had been increased with 20mM BAPTA. Calcium current is clearly stable even in the very high calcium concentration (100mM; Ca^{2+}-extracellular).

Calcium current rundown was observed in this same cell upon application of 1mM kainate (lower left-hand panel).

Rundown was prevented by inclusion of 30mM BAPTA in the intracellular solution. Calcium current was also significantly inhibited by the inclusion of 30mM caesium fluoride (intracellular). Under these conditions calcium current was minimal, but was stable for prolonged periods even in the presence of 1mM kainate (lower right-hand panel).

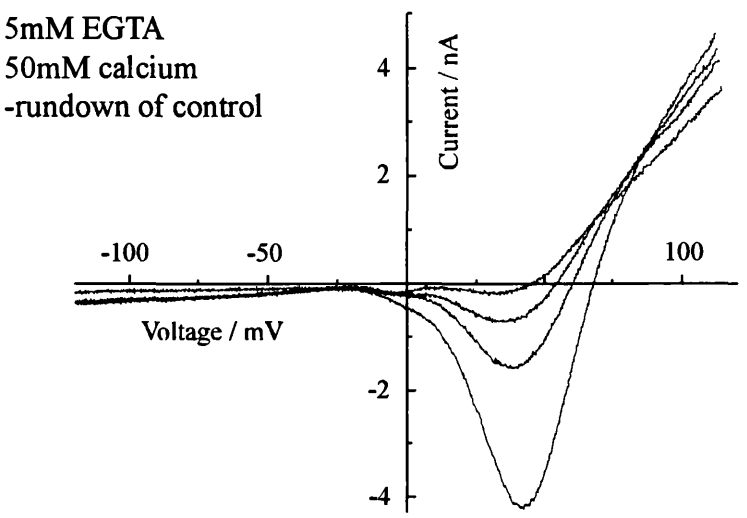
5mM EGTA
50mM calcium
-rundown of control
Current / nA
Voltage / mV
4
2
-2
-4
-100
-50
100

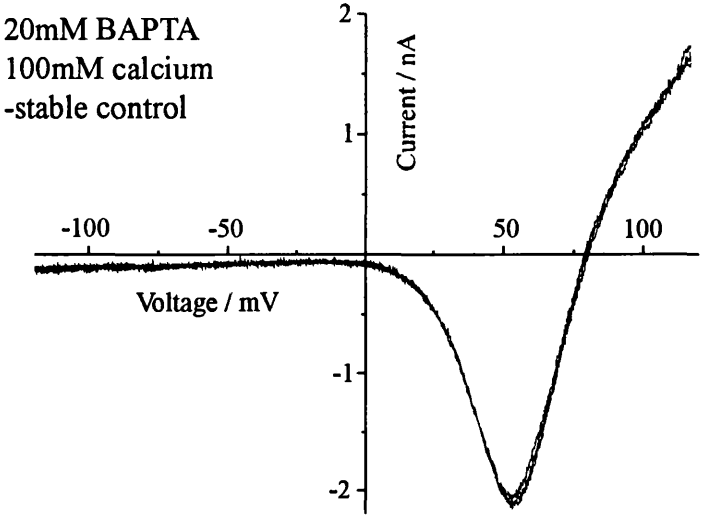
20mM BAPTA
100mM calcium
-stable control
Current / nA
Voltage / mV
2
1
-1
-2
-100
-50
50
100

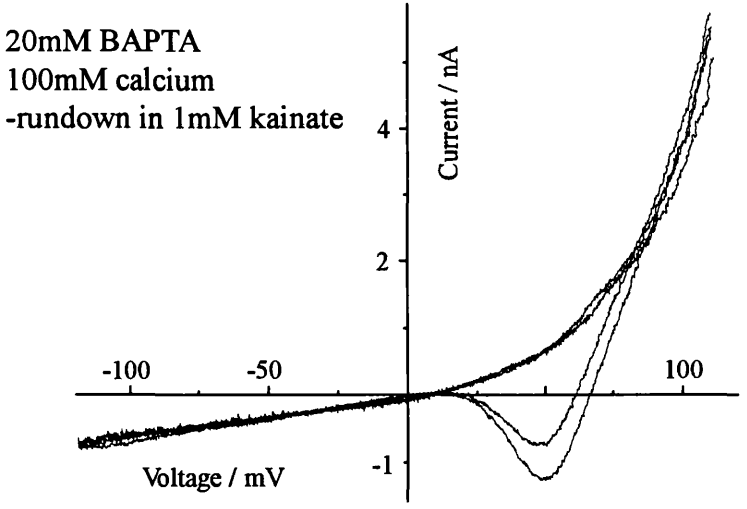
20mM BAPTA
100mM calcium
-rundown in 1mM kainate
Current / nA
Voltage / mV
4
2
-1
-100
-50
100

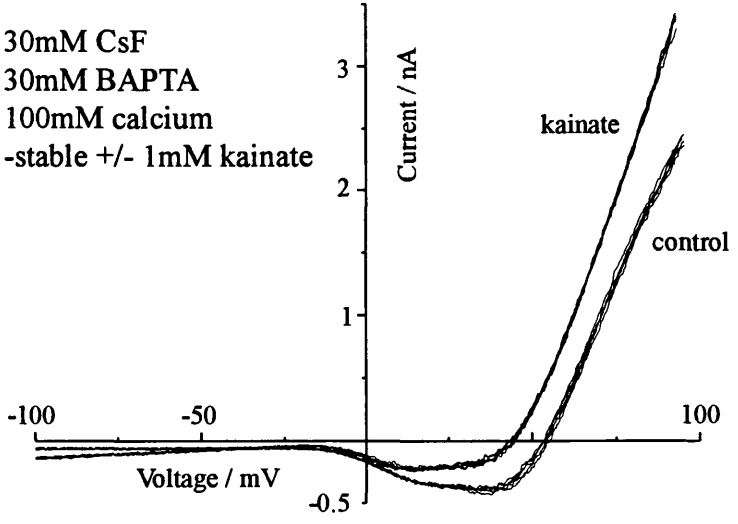
30mM CsF
30mM BAPTA
100mM calcium
-stable +/- 1mM kainate
Current / nA
Voltage / mV
kainate
control
3
2
1
-0.5
-100
-50
100

these experiments. Typical rundown in an extracellular calcium concentration of 50mM is illustrated in figure 4.4.1 (upper left-hand panel). Rundown was pronounced, suggesting that intracellular calcium levels were rising significantly during recording. Under such conditions, outward current through non-NMDA receptors could be carried by both caesium and calcium ions, invalidating the simplifying assumptions used in the constant field calculations. Hence it was imperative that this rise in intracellular calcium concentration should be prevented.

When calcium buffering was increased by using 20mM BAPTA (intracellular) the calcium current was stable under control conditions in extracellular calcium concentrations of up to 100mM (figure 4.4.1, upper right-hand panel). However, in the presence of kainate the calcium current amplitude frequently decreased with time, suggesting that the intracellular calcium concentration was still rising significantly (figure 4.4.1, lower left-hand panel). Whilst this proved interesting since it suggested that calcium may enter through the non-NMDA receptor, this situation was clearly not satisfactory. Calcium current rundown in the presence of kainate was prevented by raising the intracellular BAPTA concentration to 30mM.

Unfortunately maintenance of the calcium current provided its own problems, since the calcium current activation range was in the region in which the kainate-sensitive current was expected to reverse. This was unsatisfactory as any slight change in the calcium current amplitude during recording could significantly alter the measured reversal potential. This effect could be a major source of error given the amplitude of the calcium current and its very steep voltage-dependence. In addition, the calcium current activation curve shifts with extracellular calcium concentration as a result of charge screening. Thus the effect of the calcium current may be different in different extracellular solutions. Finally, the possibility remained that kainate may alter calcium current amplitude via a kainate receptor (Chittajallu, Vignes, Dev, Barnes, Collingridge & Henley, 1996). Calcium current amplitude was therefore reduced by incorporation of 30mM fluoride in the intracellular solution. (Fluoride ions are thought to inhibit calcium currents by activation of G-proteins, G-

protein-mediated modulation of the calcium current often being inhibitory). The combined effects of 30mM BAPTA and 30mM caesium fluoride are illustrated in figure 4.4.1 (lower left-hand panel).

4.4.2 I-V relationship hysteresis

I-V relationships from acutely dissociated cells were generated from -100 to +100mV. Hysteresis was examined by comparing ascending and descending ramps as for nucleated patches. Hysteresis was more pronounced than with nucleated patches since calcium current amplitude was maintained in acutely dissociated cells (see above). The result was that the reversal potential of the kainate-sensitive current was frequently within the potential range in which the calcium current was active. Given the uncertainties that this caused with regard to reversal potential measurements (see above) the descending rather than ascending ramps were used. The difference is clearly visible in figure 4.4.2 and is more pronounced at elevated extracellular calcium concentrations principally because the calcium current amplitude is greater.

The use of the descending limb of the protocol for analysis did not entirely circumvent the effects of the calcium current. As is clearly visible in the uppermost right-hand panel of figure 4.4.2, the reversal potential was often very close to potentials at which the calcium current was active. In view of this, the reversal potentials measured in Na^+- and Na^+/Ca^{2+}-extracellular are likely to be considerably more reliable than those in Ca^{2+}-extracellular, where the calcium current was most pronounced. Relative permeabilities were therefore calculated using reversal potential measurements for the two sodium-containing solutions. Whilst this required the assumption that the calcium activity in Na^+-extracellular was negligible, it is likely that this approximation will influence the calculated permeability less than would errors in reversal potential measurement.

As a result of these problems, reversal potentials were measured from the intersection of these ramps (rather than subtracting the control from the trace in kainate and measuring the reversal potential from this trace). Thus potential problems caused by calcium current 'contamination' were apparent.

Figure 4.4.2 I-V relationship hysteresis

This figure illustrates I-V hysteresis as a result of calcium current activity under a variety of conditions. Each of the six panels shows two curves, one derived in the absence of kainate (dotted line) and one in the presence of 1mM kainate (solid line). Traces are presented for all three extracellular solutions; Ca^{2+}-extracellular in the upper panels, Na^{+}/Ca^{2+}-extracellular in the central panels and Na^{+}-extracellular in the lower panels. For each solution current traces corresponding to both ascending and descending limbs of the voltage protocol are presented, ascending ramp on the left and descending ramp on the right. All traces are from the same cell.

Calcium current is invariably visible on the ascending limb, but is substantially reduced on the equivalent descending limb. Calcium current is also more pronounced in elevated calcium concentration. The peak of the calcium current is also shifted towards more positive voltages in elevated calcium concentrations.

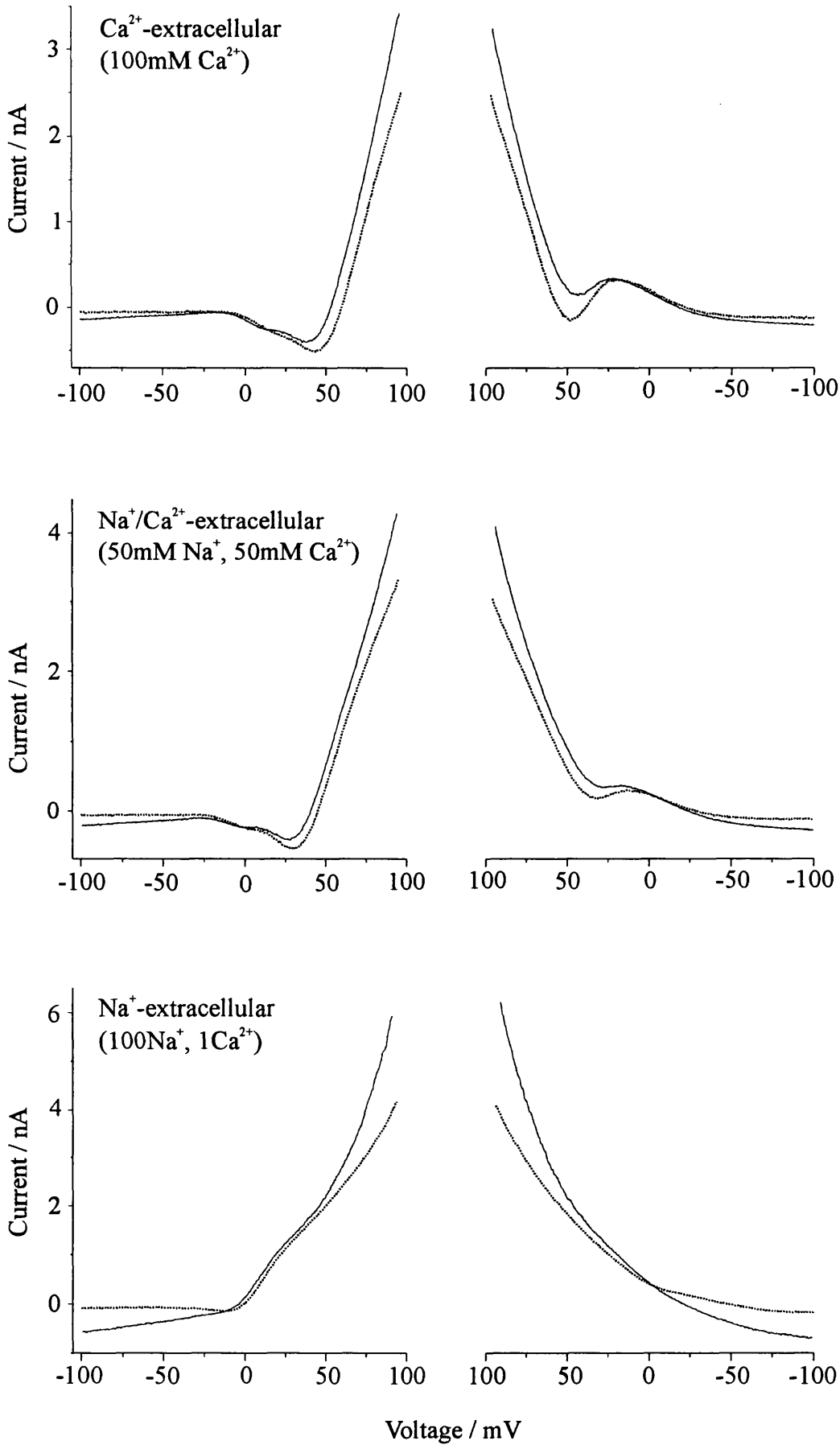
Ca2+-extracellular
(100mM Ca2+)
Na+/Ca2+-extracellular
(50mM Na+, 50mM Ca2+)
Na+-extracellular
(100Na+, 1Ca2+)
Current / nA
Voltage / mV
-100
-50
0
50
100

4.4.3 Relative permeability measurements & distribution

Relative permeabilities were calculated for 15 acutely dissociated neurones using constant field theory (see appendix 7.4). P_{Na}/P_{Cs} values were tightly grouped, describing a range of 0.87-1.53. Values for P_{Ca}/P_{Cs} were more widely scattered; range 0.33-3.32. The resulting P_{Ca}/P_{Na} range was 0.26-3.6, median 1.27. The scatter for each of these ratios is displayed in figure 4.4.3.

4.4.4 Kainate-induced currents

Of the 15 cells from which reversal potential measurements were made, 11 showed mild to pronounced rectification in Na^+-extracellular. Two examples are shown in figure 4.4.4. These two traces show kainate-induced currents in the two extremes of the range of calcium permeabilities (P_{Ca}/P_{Cs} = 3.6 & 0.26). Notably, double rectification is very strong in the cell with P_{Ca}/P_{Cs} = 3.6, but weak in the cell with P_{Ca}/P_{Cs} = 0.26.

Whilst this figure might suggest that the degree of rectification was strongly related to calcium permeability, no correlation was apparent from the plot of relative calcium permeability against rectification index (RI) shown in the lower panel. There are two possible explanations for this lack of correlation. Firstly, 15 cells may be insufficient to distinguish any trend given the inevitable variation between cells. Secondly, the calculated RI may not discriminate sufficiently between doubly rectifying and near-linear relationships. RI values have been used by various authors with some success, for instance Kamboj, Swanson & Cull-Candy (1995) found that non-NMDA receptor calcium permeability correlated with RI (calculated using the formula given in section 4.3.4) in the presence of intracellular spermine. However, the doubly-rectifying I-V relationships recorded by these authors from expressed receptors rectify such that little current flows from approximately zero mV to beyond +40mV. This is commonly observed with expressed receptors. In basal forebrain neurones current amplitude in this voltage range is often significant (see for example the upper trace of figure 4.4.4) and traces show strong outward rectification at approximately +40mV to +50mV. Thus current amplitude at +40mV is significant, resulting in quite subtle differences between

Figure 4.4.3 Relative permeabilities - distribution

The range of P_{Na}/P_{Cs} was considerably less than the ranges of P_{Ca}/P_{Cs} and of P_{Ca}/P_{Na}. The scatter for each of these three quantities is presented. Each point represents a ratio for one cell. The median value for P_{Ca}/P_{Cs} is marked. Note that data for all 15 cells are represented, but in some instances data points for two cells are very close together such that they are effectively overlaid.

The reversal potential measurements from which these permeability ratios were calculated are given below. Reversal potentials are given for each extracellular solution. Note that reversal potentials in Ca^{2+}-extracellular are not available for all neurones.

Cell	Reversal potentials			Permeability ratios		
	Ca^{2+}-extr.	Na^+/Ca^{2+}-extr.	Na^+-extr.	P_{Na}/P_{Cs}	P_{Ca}/P_{Cs}	P_{Ca}/P_{Na}
1	-3	-8	+1.5	1.00	0.93	0.93
2	+25	+2	+6	1.53	0.93	0.61
3	-4	+1	+2.5	1.04	1.50	1.44
4	+1	+2	+1	0.98	2.42	2.50
5	+1.5	+2	+3.5	1.08	1.59	1.47
6	---	+2.5	+9.5	1.36	1.26	0.92
7	---	+0.5	-0.5	0.92	1.58	1.71
8	---	-4	+4	1.10	0.81	0.74
9	---	-5.5	-1.5	0.89	0.83	0.93
10	---	0	-1	0.91	1.54	1.70
11	---	+5.5	-1.5	0.89	2.49	2.80
12	---	-4	+11	1.45	0.38	0.26
13	---	-14	-2	0.87	0.33	0.38
14	---	+7	-0.5	0.92	3.32	3.60
15	---	+0.5	+3.5	1.08	1.37	1.27

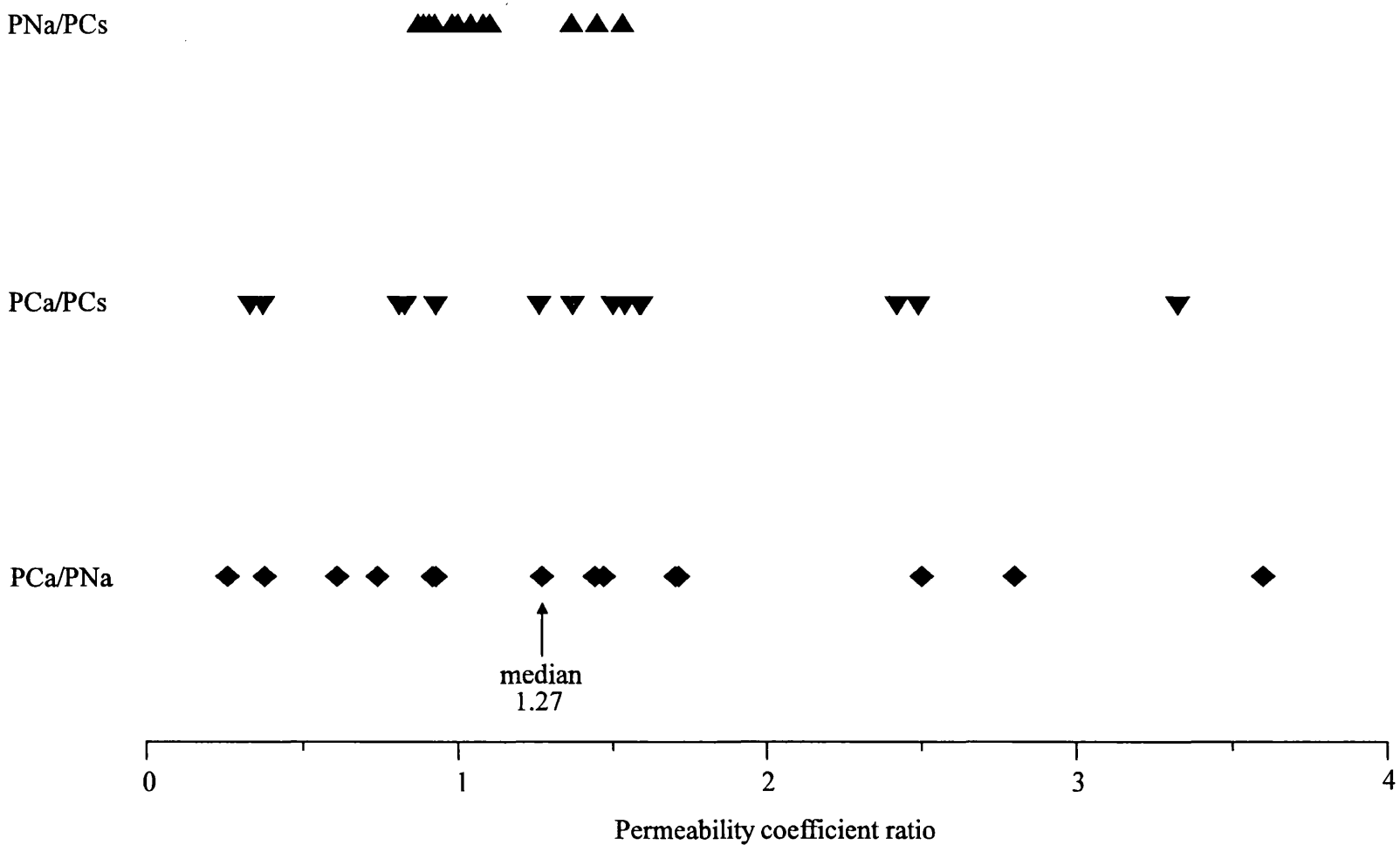
PNa/PCs
PCa/PCs
PCa/PNa
median
1.27
0
1
2
3
4
Permeability coefficient ratio

Figure 4.4.4 Kainate-induced currents

Two examples of kainate-induced currents in Na^+-extracellular, showing that double rectification is more pronounced at high P_{Ca}/P_{Na} (upper panel) than at low P_{Ca}/P_{Na} (central panel).

The lower panel shows a plot of P_{Ca}/P_{Na} against rectification index (currents measured at -60 and +40mV; see section 4.3.4).

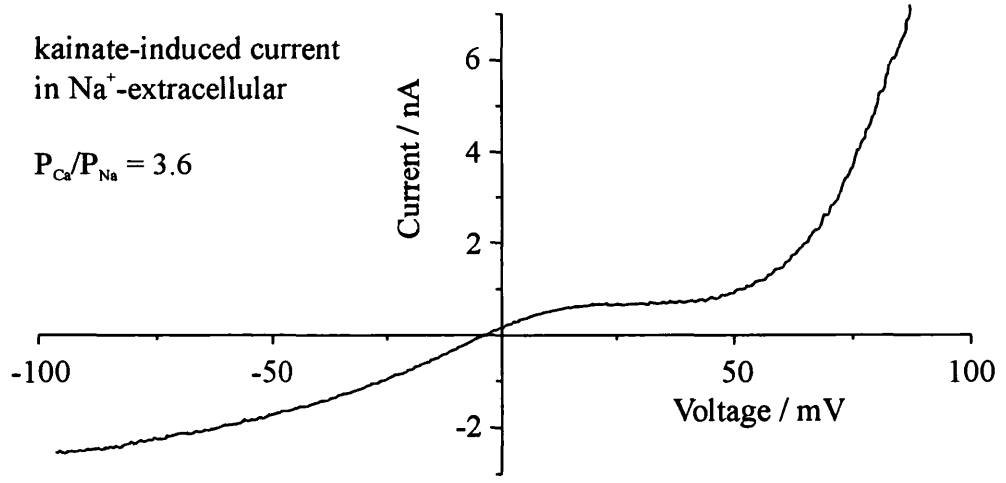
kainate-induced current
in Na+-extracellular
PCa/PNa = 3.6
Current / nA
6
4
2
-2
-100
-50
50
100
Voltage / mV

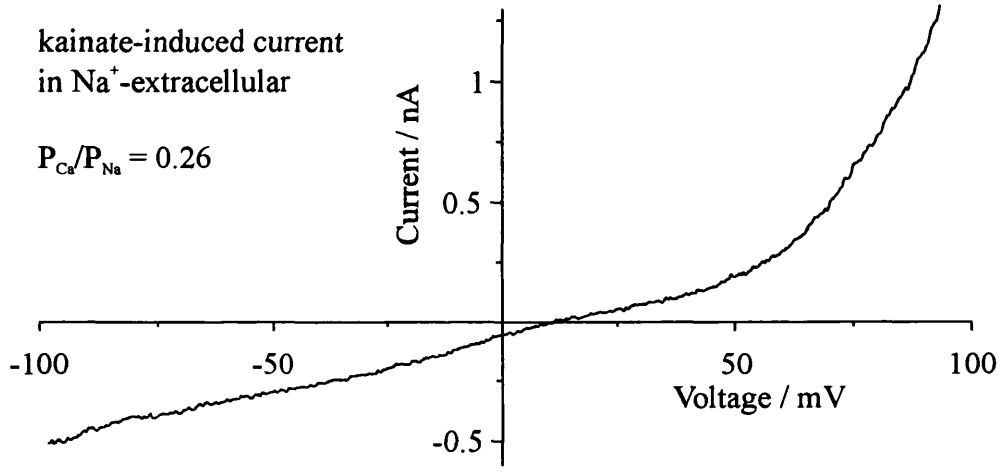
kainate-induced current
in Na+-extracellular
PCa/PNa = 0.26
Current / nA
1
0.5
-0.5
-100
-50
50
100
Voltage / mV

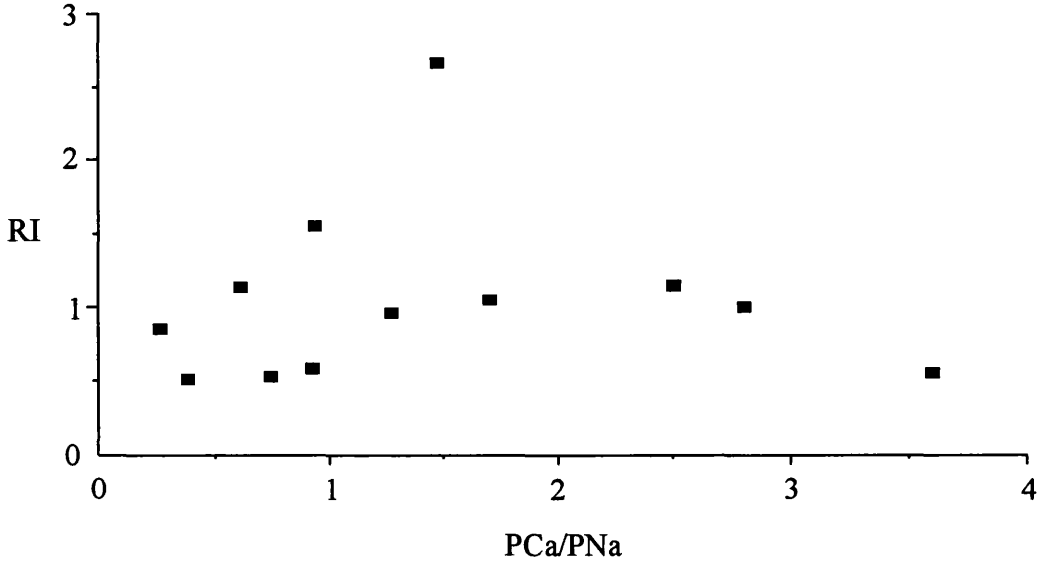
RI
3
2
1
0
0
1
2
3
4
PCa/PNa

RI values for the two traces displayed in figure 4.4.4 even though pronounced rectification is apparent upon inspection of one trace. An alternative method of quantitating the degree of rectification may thus be more useful.

4.4.5 Effects of elevated extracellular calcium

In addition to shifting the reversal potential, elevated extracellular calcium also reduced current amplitude at both positive and negative potentials and obscured/reduced double rectification. These effects were observed in all 15 cells regardless of relative calcium permeability. An example is given in figure 4.4.5.

The effects of extracellular calcium could not be quantified under these conditions as the sodium ion activities of the two extracellular solutions were different. The effect of extracellular calcium on current amplitude at -70mV was therefore examined separately. Elevation of extracellular calcium concentration from 1 to 10mM reduced current amplitude by 37±2% (n=3).

4.4.6 Concentration-dependence of block by cadmium

Cadmium and cobalt also reduced current amplitude. The dose-dependence of the effect of extracellular cadmium was examined in cells clamped to -70mV. The resulting dose-response relationship is given in figure 4.4.6. The fitted curve yields an IC_{50} of 44μM and a slope of -0.67. Cadmium inhibited a maximum of 87% of the current (calculated by extrapolation of the fitted curve). Whilst the effects of cadmium on kainate-elicited currents were found to be reversible, application of high concentrations of cadmium led to deterioration of the recording.

The dose-dependence of the effect of cobalt was not examined, though it was less effective than similar concentrations of cadmium. Cobalt block was observed in the sub- to low-millimolar range.

Figure 4.4.5 Effects of elevated extracellular calcium

Two traces (overlaid) showing kainate-induced currents in Na^+- and in Na^+/Ca^{2+}-extracellular solutions. Both traces are from the same cell, with $P_{Ca}/P_{Cs} = 0.92$.

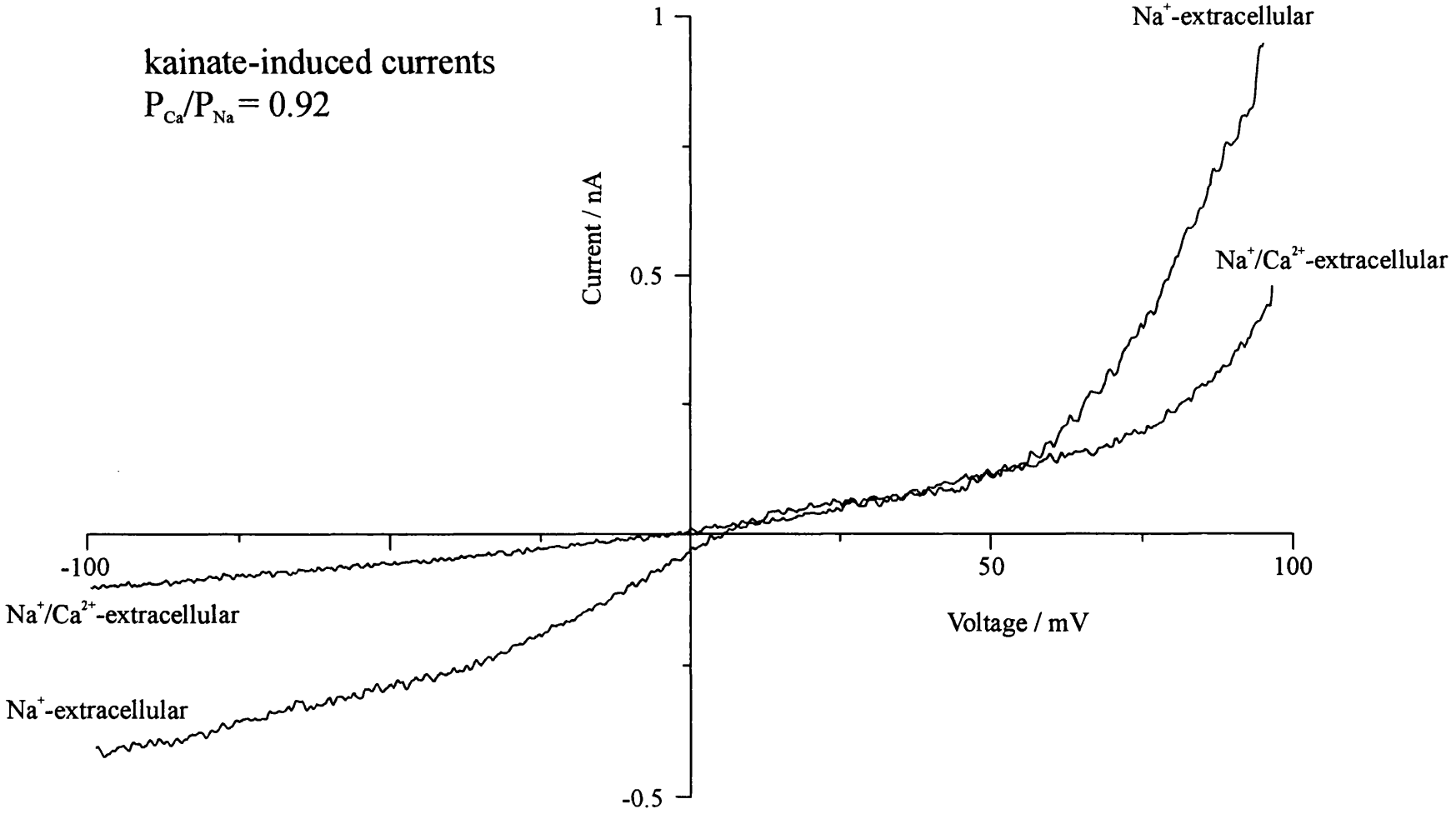
kainate-induced currents
$P_{Ca}/P_{Na} = 0.92$
1
0.5
-0.5
Current / nA
-100
50
100
Voltage / mV
Na^+-extracellular
Na^+/Ca^{2+}-extracellular
Na^+/Ca^{2+}-extracellular
Na^+-extracellular

Figure 4.4.6 Concentration-dependence of block by cadmium

Block of current to 300μM kainate was examined in acutely dissociated neurones voltage-clamped to -70mV by dSEVC. Intracellular and extracellular solutions were as described in section 2.2.4. Both kainate and cadmium (chloride salt) were bath-applied. No correction was made for the effect of cadmium on holding current in the absence of kainate, the effect being negligible at -70mV.

Block by cadmium was found to be fully reversible, but exposure to high concentrations invariably led to deterioration of the recording. Therefore each dish of cells was discarded after a single exposure to $\geq$100μM cadmium. This precluded generation of a full dose-response curve for a single cell, hence different concentrations were applied to different cells and the effect of cadmium was measured as the percentage reduction in current amplitude. Data from numerous cells were pooled to generate a mean ($\pm$SEM) inhibition for each concentration and the curve fitted to this mean data.

The fitted curve gave the following values:

IC_{50}	44μM
Slope	-0.67
Maximum inhibition	87%

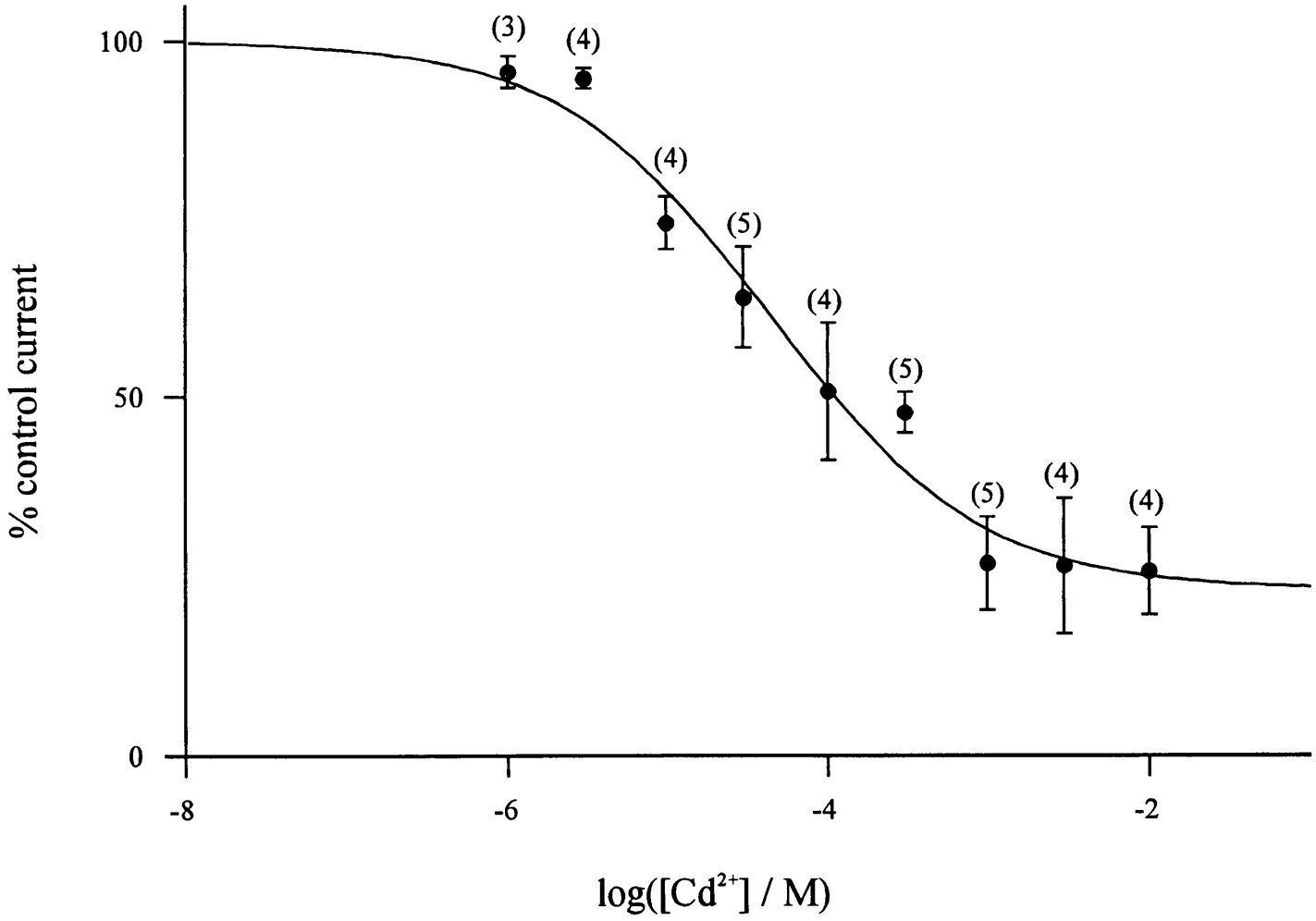
100
50
0
% control current
(3)
(4)
(4)
(5)
(4)
(5)
(5)
(4)
(4)
-8
-6
-4
-2
log([Cd2+] / M)

4.4.7 Voltage-sensitivity of block by cadmium

The effect of cadmium was found to be voltage-dependent. Of 7 cells studied, 5 exhibited block which decreased with voltage from -100mV towards zero. Minimum block was observed at 0 to +50mV, block increasing with voltage from +50 to +100mV. All these 5 cells exhibited doubly-rectifying current-voltage relationships. One cell exhibited relatively mild voltage-sensitivity which increased linearly from -100 to +100mV. This cell exhibited a mildly outwardly-rectifying current-voltage relationship. 3mM cadmium had no effect on kainate-elicited current in the one remaining cell.

Plots of percentage block by cadmium against voltage are given for three cells in figure 4.4.7. The upper and central panels illustrate the effects of voltage on 2 of the 5 cells exhibiting strong voltage-dependence and doubly-rectifying current-voltage relationships (insets). The voltage-sensitivity of cadmium block in the one cell with an outwardly-rectifying current-voltage relationship is shown in the lower panel.

Note that the percentage block by 3mM cadmium is less than that given in section 4.4.6. This presumably results from the different solutions used, possibly from the presence of spermine in experiments where the voltage-sensitivity of block was examined.

Figure 4.4.7 Voltage-sensitivity of block by cadmium

Voltage-sensitivity of block of current to 300μM kainate was examined in acutely dissociated neurones voltage-clamped by dSEVC. Inter-episode holding current was -70mV. The intracellular solution was as described in section 2.6 (containing 30μM spermine). The extracellular solution was similar to that described in section 2.2.4, with the following alterations:

(i) magnesium chloride was excluded

(ii) calcium chloride concentration was reduced to 1mM

(iii) 20mM D-mannitol was added to raise the osmolarity to that of the intracellular solution

Block was examined by the application of 3mM cadmium chloride to the extracellular solution, both kainate and cadmium being bath-applied.

Responses were leak-subtracted by subtraction of I-V data generated in the absence of kainate. Since cadmium influenced leak current amplitude in a voltage-dependent manner, 3mM cadmium was applied to each cell in the absence of kainate and I-V relationships were generated under these conditions for leak-subtraction from data generated in the presence of both kainate and cadmium. Where possible I-V relationships were generated under control conditions at the end of each experiment to verify that leak currents had not changed significantly.

Voltage protocols were similar to that illustrated in figure 4.3.1: ascending and descending voltage ramps between -100 and +100mV were imposed. Descending limbs of I-V relationships were used for further analysis.

Each panel shows the percentage block by cadmium as a function of membrane potential for a single cell and inset is the corresponding I-V data. Central section of the plots are excluded since the relationships were unclear in this region, in which I-V relationships in the presence and absence of cadmium crossed. In addition, errors due to small changes in leak currents would be expected to be particularly large in this region.

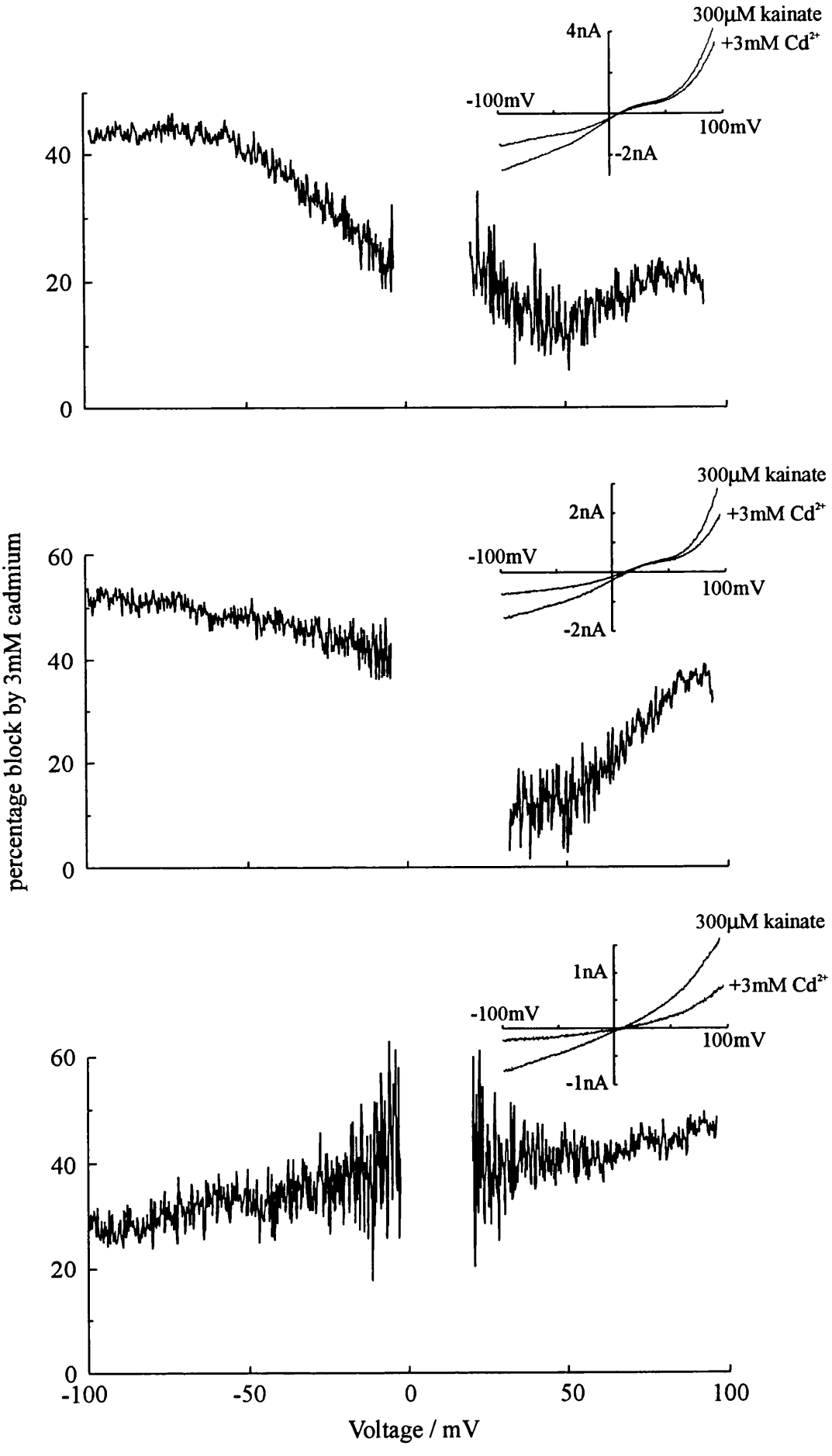
300μM kainate
+3mM Cd2+
4nA
-100mV
100mV
-2nA
40
20
0
300μM kainate
+3mM Cd2+
2nA
-100mV
100mV
-2nA
60
40
20
0
300μM kainate
+3mM Cd2+
1nA
-100mV
100mV
-1nA
60
40
20
0
-100
-50
0
50
100
Voltage / mV
percentage block by 3mM cadmium

4.5 Discussion

4.5.1 Receptor localization

Nucleated patch current densities were lower than whole-cell current densities (30pA/pF for 1mM kainate at 30-31 DIV for nucleated patches and approximately 200pA/pF for 1mM kainate at 20 DIV for whole-cell recordings).

This implies that much of the current recorded in the whole-cell configuration may have originated from receptors located on proximal processes.

Little morphological data is available regarding the distributions of synaptic inputs onto the somata and dendrites of cholinergic magnocellular basal forebrain neurones. What data there is suggests that the majority of synaptic input is onto dendrites rather than somata. The transmitter content of these inputs were not determined, but a significant proportion were classed as asymmetrical and may thus contain excitatory amino acid(s) (Ingham, Bolam, Wainer & Smith, 1985; Lemann & Saper, 1985; Bialowas & Frotscher, 1987; Dinopoulos, Parnavelas & Eckenstein, 1986; Záborszky, Cullinan & Braun, 1991). A similar situation exists in the mammalian basal forebrain (Walker, Tigges & Tigges, 1983). Thus the lower current densities observed from nucleated patch recordings is consistent with morphological data.

Given the similarities between the responses recorded in the outside-out and whole-cell configurations and the similar I-V relationships derived from nucleated patches and whole-cell recordings from acutely dissociated neurones, it seems likely that somatic and extra-somatic receptors are very similar. Somatic and extra-somatic channel characteristics have been compared only in hippocampal pyramidal neurones at present, where calcium channel types were found to be differently distributed across somata and dendrites (Christie, Eliot, Ito, Miyakawa & Johnston, 1995; Magee & Johnston, 1995) but glutamate receptors were found to be similar in patches from all regions of the neurones sampled (Spruston, Jonas & Sakmann, 1995).

4.5.2 Blocking actions of extracellular divalent ions

Two effects of elevating extracellular calcium are clearly visible in figure 4.4.5.

Firstly current amplitude is reduced at both positive and negative potentials. In the example given in figure 4.4.5, P_{Ca}/P_{Na} is approximately unity hence one might expect similar current amplitudes in the two solutions. The most likely explanation is channel block by calcium, a phenomenon observed for many channels including ionotropic receptors.

Secondly, the degree of double rectification is reduced. Block of the channel by calcium may appear to reduce double rectification by reducing slope conductance at negative potentials, as is apparent in figure 4.4.5. Whether or not calcium blocks at positive potentials is not clear since whilst current amplitude is certainly decreased, this could possibly be caused by an interaction between calcium and spermine: one could readily envisage that an elevated calcium concentration might reduce spermine access to the channel by electrostatic interactions. Thus spermine block might be shifted to more positive potentials where the driving force for spermine entry into the channel would be increased.

The voltage-sensitivity of block by calcium is likely to be similar to that of cadmium, displaying decreased block towards +50mV. Since this is the potential beyond which spermine permeation of the channel becomes apparent, this suggests that divalent ions do indeed interact with spermine. Further, in the one instance in which no block by spermine was observed, divalent ion block did not display a pronounced minimum at +50mV. It is therefore very likely that there is an interaction between spermine and extracellular divalent ions, but to what extent the voltage-sensitivity of divalent ion block is attributable to this interaction is unclear.

Block by extracellular cations has been observed for various cation-permeable ionotropic receptors, including ATP receptors (Nakazawa & Hess, 1993), nicotinic acetylcholine receptors (Zhou & Neher, 1993), NMDA receptors (Ault, Evans, Francis, Oakes & Watkins, 1980; Mayer & Westbrook, 1987a; Ascher & Nowak, 1988; Jahr & Stevens, 1993; Ruppersberg, Mosbacher, Günther, Schoepfer & Fakler, 1993) and non-NMDA receptors (Mayer, Vyklicky & Westbrook, 1989; Burnashev, Monyer, Seeburg & Sakmann, 1992; Rörig & Grantyn, 1993; Burnashev, Zhou, Neher & Sakmann,

1995).

With regard to non-NMDA receptors, block by calcium (Burnashev, Monyer, Seeburg & Sakmann, 1992; Burnashev, Zhou, Neher & Sakmann, 1995) cadmium (Mayer, Vyklicky & Westbrook, 1989; Rörig & Grantyn, 1993) and zinc (Mayer, Vyklicky & Westbrook, 1989) have been observed, though no dose-response data were presented and the voltage-sensitivities of block were not examined in detail.

Also of interest is the NMDA receptor since it is a close relative of the non-NMDA receptor in which divalent ion block is not complicated by an interaction with polyamines. A large number of extracellular cations block NMDA receptors, including magnesium, zinc, barium, calcium, manganese, nickel, cobalt and cadmium. Several of these ions produce a voltage-dependent, 'flickery' block like that observed for magnesium and some, most notably calcium, also permeate. In contrast, strontium permeates without detectable block and cadmium blocks in a voltage-independent manner. Such block results in a decreased single channel conductance and occurs at both negative and positive potentials (Mayer & Westbrook, 1987a; Ascher & Nowak, 1988; Jahr & Stevens, 1993; Ruppersberg, Mosbacher, Günther, Schoepfer & Fakler, 1993; Burnashev, Zhou, Neher & Sakmann, 1995). Ion permeability/block of the NMDA receptor is strongly influenced by the Q/R/N site, as for non-NMDA receptors (Ruppersberg, Mosbacher, Günther, Schoepfer & Fakler, 1993). In summary, with regard to divalent ion permeability and block, divalent ion-permeable non-NMDA receptors are very similar to NMDA receptors.

4.5.3 Calcium permeability measurements

The calcium permeabilities given above were calculated using constant field theory. Several potential sources of error present themselves.

Firstly it was assumed that non-NMDA receptors are essentially impermeable to anions. To date this has only been considered by Burnashev & associates (Burnashev & Sakmann, 1996; Burnashev, 1996; Burnashev, Villarroel & Sakmann, 1996) who determined that P_{Cl}/P_{Cs} was significant for homomerically expressed GluR2(R) and GluR6(R) (P_{Cl}/P_{Cs} = 0.1-0.2 and 0.7-

0.8 respectively). In contrast chloride permeabilities were insignificant for Q-form splice variants and mixed Q/R-form heteromers. Thus anion concentrations are unlikely to influence the calcium permeability values calculated for calcium-permeable receptors (Q-form splice variants) as a result of channel permeation.

Secondly the junction potential between pipette solution and cytoplasm cannot be measured, but may contribute to the observed voltage and thereby the reversal potential. In theory this error may be excluded by calculating all relative permeabilities from reversal potential shifts in individual cells rather than absolute reversal potential measurements.

In practice measurements of reversal potential shifts are unlikely to be more accurate since alterations in the compositions of intra- and extracellular solutions, particularly divalent ion concentrations, are likely to alter the membrane surface potential. This may result from interactions of ions with both the lipid bilayer and fixed charges on the channel itself (Green & Anderson, 1991). The latter effects are often dominant (see Hille, 1992, chapter 17) with the result that the effect of solution changes cannot be gauged from effects on other channels such as the shift of the calcium current peak amplitude.

The constant field approach may be modified to account for surface potential effects. Such a modification was first presented by Frankenhäuser (1960) to account for the failure of constant field theory to accurately describe the rectification of sodium current in myelinated nerve fibres. This consideration has also been successfully applied to the nicotinic acetylcholine receptor (nAChR) at the frog neuromuscular junction (Lewis, 1979) though was considered unnecessary for cardiac calcium currents (Lee & Tsien, 1984).

With regard to non-NMDA receptors, in order to allow for surface charge effects the modified constant field equation would be fitted to measured reversal potentials for a series of calcium concentrations. This was not feasible in the experiments presented above (see results sections) for two reasons, (i) cells could not be maintained in suitable condition for a sufficient length of time, and (ii) currents through voltage-gated calcium channels interfered with reversal potential measurements at elevated extracellular calcium concentrations

(see section 4.4.1, above).

Whilst several authors have studied reversal potentials for non-NMDA receptors at several extracellular calcium concentrations, none have fitted their data with the modified constant field equations of the type suggested by Frankenhäuser (1960). Despite failing to allow for surface potential effects, these data are reasonably fit by constant field theory, suggesting that surface potential effects may not greatly influence estimates of relative calcium permeabilities for non-NMDA receptors (Iino, Ozawa & Tsuzuki, 1990; Gu & Huang, 1991; Koh, Geiger, Jonas & Sakmann, 1995; Otis, Raman & Trussel, 1995; Zhang, Sucher & Lipton, 1995). This said, small differences between the experimental data and the fit could represent large differences in calculated permeabilities. In addition, it should also be noted that Ascher & Nowak (1988) have suggested that use of a similar methodology for NMDA receptors may be subject to large surface potential effects.

One assumption in the derivation of constant field equations is that ions do not interact in the channel. Block by calcium, cadmium and cobalt ions clearly contravene this principle of independence, suggesting that constant field theory is not the most appropriate model to describe ion permeation through non-NMDA receptors.

Relative permeability data derived from reversal potential shifts using constant field theory are also specific to defined conditions: the calculated values give relative permeabilities at the reversal potential and may be depend upon the intra- and extracellular solutions (particularly the extracellular calcium concentration). Extrapolation of the calculated relative permeabilities to more physiological conditions (such as -70mV and 1mM extracellular calcium) requires two assumptions, that relative calcium permeabilities are independent of both voltage and extracellular calcium concentration.

Measurement of relative calcium permeabilities under more physiological conditions is possible by combining electrophysiology with quantitation of calcium influx using fluorescent indicators such as fura-2. This approach has been used with recombinant non-NMDA receptors, revealing that for calcium permeable receptors fractional calcium current (essentially the

fraction of current flow carried by calcium) is sensitive to both voltage and to extracellular calcium concentration.

Constant field theory predicts that the fractional calcium current should be sensitive both to voltage and to calcium concentration, but the quantitative predictions of constant field theory were found inadequate to account for either effect (Burnashev, Zhou, Neher & Sakmann, 1995). Hence predictions of the magnitude of calcium influx resulting from non-NMDA receptor stimulation under physiological conditions are likely to be inaccurate when they rely on relative calcium permeabilities estimated with the constant field approach.

Fractional calcium currents under physiological conditions as calculated/measured by these two approaches have rarely been compared. Burnashev, Zhou, Neher & Sakmann (1995) concluded that constant field theory overestimated fractional calcium currents of both calcium-permeable and -impermeable non-NMDA receptors. Similar conclusions have been reached regarding the NMDA receptor though the two methods were considered to be 'in reasonable agreement' (Schneggenburger, 1996).

The combined fluorescence/electrophysiology approach is, of course, subject to its own potential sources of error. The principle methodological difficulties are (i) failure of fluorescence measurements to account for calcium entering through extra-somatic receptors, which may contribute to the receptor-mediated current, (ii) failure to accurately quantitate fluorescence from poorly focused regions of the cell, (iii) the influence of cell volume/viscosity changes on fluorescence measurements (see Schneggenburger, 1996) (iv) the method of calibration of the fluorescence signal (see Rogers & Dani, 1995) and (v) the effects of calcium efflux/sequestration.

Since these problems can be largely overcome this approach must be considered the preferred method for measuring relative calcium permeabilities, though the constant field approach has been and is still is in more common use and is therefore still appropriate, particularly for comparison of calcium permeabilities between cell types.

Comparison of ion permeability coefficient ratios and fractional calcium currents is difficult since the relationship between these two quantities depends

upon a number of variables, including extracellular calcium concentration and voltage. Burnashev, Zhou, Neher & Sakmann (1995) gave the following values for receptors expressed in human embryonic kidney cells with 143.5mM intracellular Cs^+, 143.5mM extracellular $Na^+ + K^+$ and 1.8mM extracellular Ca^{2+}:

Subunits expressed	Measured fractional calcium current (P_f) at -60mV	P_{Ca}/P_{Cs} (calculated from P_f values using constant field theory)
NR1-NR2A	11.0	3.10
NR1-NR2C	8.2	2.23
GluR1	3.2	0.82
GluR1/2(R)	0.54	0.14
GluR6 (V,C,R)	<0.2	<0.05
GluR6 (V,C,Q)	1.55	0.39

4.5.4 Comparison with published data

Kumamoto & Murata (1995a) took a similar approach to that presented above, examining I-V relationships for non-NMDA receptor-mediated currents from cultured foetal rat cholinergic septal neurones. I-V relationships for quisqualate, AMPA- and kainate-elicited currents were all slightly outwardly rectifying, though this may be because the authors did not include spermine in the intracellular solution. However, the authors also reported negligible calcium permeability of non-NMDA receptors and calcium permeability is thought to be independent of spermine (Kamboj, Swanson & Cull-Candy, 1995; Burnashev, 1996). Presumably either neurones from foetal rats express different non-NMDA receptor subunits than those from 13 day old animals or septal neurones

express receptors with lower divalent ion permeabilities than neurones from more caudal regions of the basal forebrain.

Calcium permeabilities of non-NMDA receptors in septal neurones has also been studied by combined fluorescence and electrophysiological methods (Schneggenburger, Zhou, Konnerth & Neher, 1993; Schneggenburger, Tempia & Konnerth, 1993). The authors studied responses in 14-20 day-old rat septal slices and found that the fractional calcium current through non-NMDA receptors was 1.2-1.4% and concluded that the cells expressed receptors with low to moderate calcium permeabilities. Whilst it is difficult to directly compare these fractional calcium current measurements with the permeability coefficient ratios given in section 4.4.3 (above) comparison with published data suggest that at both pre- and postnatal stages septal neurones may express non-NMDA receptors with lower calcium permeabilities than other cholinergic basal forebrain neurones.

No further published data is available regarding divalent ion permeabilities of non-NMDA receptors expressed by basal forebrain neurones.

Calcium Current Inhibition

5.1 Introduction

5.1.1 Modulation of I_{Ca} via glutamate receptors

Inhibition of the high voltage-activated (HVA) calcium current through metabotropic glutamate receptors has been observed in several central neurones.

In the majority of instances, trans-ACPD is an effective agonist and L-AP4 ineffective. A pertussis toxin-sensitive G-protein is also commonly involved. N- and/or L-type currents are inhibited in this manner in hippocampal neurones (Lester & Jahr, 1990; Swartz & Bean, 1992; Sahara & Westbrook, 1993) neocortical neurones (Sayer, Schwindt & Crill, 1992) sensory neurones (Hay & Kunze, 1994) and cerebellar granule cells (Chavis, Shinozaki, Bockaert & Fagni, 1994; Chavis, Fagni, Bockaert & Lansman, 1995). Facilitation of L-type current by trans-ACPD has also been observed in cerebellar granule neurones (Chavis, Fagni, Bockaert & Lansman, 1995). In contrast, L-AP4 inhibits high voltage-activated (HVA) calcium current olfactory bulb neurones, again via a pertussis toxin-sensitive G-protein (Trombley & Westbrook, 1992).

Inhibition of HVA calcium current through ionotropic glutamate receptor activation has also been reported. In CA1 and/or CA3 hippocampal pyramidal neurones NMDA receptor activation can result in inhition of N-type calcium current (Chernevskaya, Obukhov & Kristal, 1991). The mechanism of this effect is unknown, but calcium influx through NMDA receptors is not required.

Inhibition of HVA calcium current following activation of non-NMDA receptors has been observed in both CA1 hippocampal pyramidal neurones (Nistri & Cherubini, 1991) and hypothalamic neurones (Zeilhofer, Müller & Swandulla, 1993). In both instances, the effects were dependent on calcium influx since the inhibition was less/absent in cells containing higher intracellular concentrations of BAPTA. Substitution of extracellular calcium with barium reduced the percentage inhibition, leading Nistri & Cherubini (1991) to suggest that non-NMDA receptor activation favoured inactivation of HVA calcium channels. Zeilhofer, Müller & Swandulla (1993) also substituted strontium and magnesium for calcium, finding that currents were inhibited equally with

calcium or strontium as charge carrier, but that inhibition was absent in extracellular magnesium. The calmodulin antagonists were found to inhibit the effect, but G-proteins were not involved. The authors therefore suggested that calcium current inhibition occurred through calmodulin activation following calcium influx through non-NMDA receptors.

5.1.2 Calcium currents in basal forebrain neurones

The first published account of calcium currents in cholinergic magnocellular basal forebrain neurones was that of Allen, Sim and Brown (1993) who used dissociated cultures derived from 12-14 day old rat.

Peak calcium currents elicited from a holding potential of -80mV activated positive to -55mV and were maximal at 0mV. Both LVA and HVA components were consistently present.

Low voltage-activated (LVA) currents typically accounted for less than 20% of the total calcium current at 0mV and displayed voltage-sensitive activation and inactivation kinetics. LVA current activated upon depolarization to -55mV and was maximal beyond -10 to -20mV. Inactivation was rapid (time constant 16ms at -20mV) and occurred beyond about -70mV, steady state inactivation being complete negative to about -30mV.

HVA current displayed transient and sustained components. Both components inactivated positive to -70mV. The transient component was fully inactivated by 60 second pre-pulses to potentials positive to -10mV and the sustained component positive to +10mV. 100nM ω-conotoxin GVIA (ω-CgTx GVIA) inhibited a portion of the HVA current, ω-CgTx GVIA-sensitive and -insensitive currents possessing indistinguishable voltage dependencies. ω-CgTx GVIA inhibited a slightly greater portion of the transient than of the sustained component.

The sensitivities of these currents to certain divalent and trivalent ions were also studied. As anticipated, Cd^{2+} inhibited the HVA current more potently than the LVA and Ni^{2+} the LVA more potently than the HVA. Gd^{3+} and La^{3+} both inhibited a component of HVA current. 1,4-dihydropyridines (DHPs) also inhibited a component of HVA current. This component developed

relatively slowly upon step depolarization and displayed no inactivation. The LVA current was similarly sensitive to DHPs. HVA current was also sensitive to BayK 8644, which enhanced a sustained component and caused a small shift in the I-V curve towards more negative potentials.

It was concluded that T-type, L-type, N-type and at least one other type of HVA current are all present in these cells.

This work was continued in a second paper (Allen & Brown, 1993) which investigated the inhibition of the calcium current by stimulation of muscarinic receptors. Acetylcholine (ACh) at concentrations in excess of 10nM inhibited the peak HVA current to a maximum inhibition of approximately 60-65% of the current at 10μM (EC_{50} 204nM). The effect of ACh was mimicked by oxotremorine methiodide (oxo-M) with an EC_{50} of 363nM. Approximately 50% of the agonist-sensitive current was blocked by ω-CgTx GVIA. The effects of ACh and oxo-M were inhibited by pirenzepine and methoctramine with pA_2 values which suggested that the receptor sub-type involved was an M_2 receptor.

Irreversibility of agonist-induced inhibition in the presence of intracellular GTP-γ-S and prevention of agonist-induced inhibition by intracellular GDP-β-S suggested the involvement of a G-protein. Agonist-induced inhibition was also eliminated by 20-24 hour pre-incubation with pertussis toxin, but was insensitive to pre-treatment with cholera toxin.

Calcium currents and single calcium channels have also been studied in dissociated culture of guinea pig basal forebrain by Griffith, Taylor & Davis (1994). Calcium currents in magnocellular cells were recorded using 2mM Ba^{2+} as the charge carrier and were found to consist of both HVA and LVA components, whereas smaller cells contained only HVA current. DHP- and ω-CgTx GVIA-sensitive components of HVA current were present.

Single channels were studied in magnocellular cell-attached patches using 100mM Ba^{2+} as the charge carrier. A low-conductance channel was observed (7.8pS slope conductance) which possessed LVA-type activation voltage sensitivity, inactivated rapidly and was insensitive to nifedipine leading to the conclusion that this was a T-type channel.

Two other conductances were observed (25.9 & 13.9pS slope

conductances) each with HVA-type voltage activation. Only the 25.9pS conductance was present in patches sufficiently frequently to permit extensive study. Channels were DHP- and BayK 8644-sensitive, most recording being performed in the presence of BayK to maximise channel resolution. Ensemble currents showed little inactivation. Thus it was concluded that the 25.9pS conductance was probably L-type. The identity of the 13.9pS is unknown although, like the L-type channel, ensemble currents displayed little inactivation suggesting that this conductance is not N-type or R-type.

The effects of aging on calcium currents in basal forebrain neurones have been studied by Murchison and Griffith (1995, 1996) revealing minimal changes of both low and high voltage-activated currents.

5.1.3 Aims

To investigate whether or not glutamate inhibits HVA calcium current in basal forebrain neurones through either metabotropic glutamate receptors or through AMPA receptors.

5.2 Results

5.2.1 Possible inhibition of calcium current by kainate

Calcium current was frequently observed upon application ramp I-V protocols to both nucleated patches and acutely dissociated neurones. In addition to eliciting non-NMDA receptor-mediated current, in some cells kainate also appeared to inhibit the calcium current observed with ramp I-V protocols. An example is shown in figure 5.2.1.

The degree of inhibition by kainate cannot be estimated using such a protocol since the leak current amplitude is unknown and cannot be estimated by either (i) selective blockade of the calcium current since metal ions (such as cadmium) also block non-NMDA receptor-mediated current in these neurones, or (ii) linear leak subtraction since the leak current is most unlikely to be linear over such a large voltage range.

5.2.2 Kainate fails to inhibit calcium current

The effect of kainate application on the calcium current was examined in acutely dissociated cells. Calcium currents were elicited by depolarization of the neurone from -80 to zero mV and 100μM kainate was bath-applied.

Kainate increased the holding current amplitude at -80mV, but current at 0mV was unchanged (n=7). This is illustrated for a typical neurones in figure 5.2.2. Hence the current elicited by a voltage step from -80 to 0mV was decreased in kainate. This almost certainly reflects the voltage-sensitivity of non-NMDA receptor-mediated current rather than an effect of kainate on the calcium current (note: non-NMDA receptor-mediated current reverses at approximately 0mV).

Non-NMDA currents reverse at approximately, but rarely precisely 0mV. Thus any small effect of kainate on the calcium current might have been obscured by current flow through non-NMDA receptors at 0mV. However, 20-100μM GYKI 53655 inhibited current amplitude to kainate at -80mV, but had no effect on current amplitude at either -80 or 0mV under control conditions or on current amplitude at 0mV in the presence of kainate, suggesting that kainate elicited negligible current at 0mV. In addition, 100μM GYKI 53655 eliminated

Figure 5.2.1 Possible inhibition of calcium current by kainate

Calcium current appears to be inhibited by kainate in ramp I-V protocols. Two ramp I-V relationships are shown on the same axes, one recorded under control conditions and one during bath-application of 300μM kainate. Both relationships were recorded from the same acutely dissociated basal forebrain neurone using dSEVC. The voltage protocol was similar to those described before, consisting of a ramp from -100 to +100mV and back to -100mV. The curves shown are derived from the descending limb of the protocol, current being plotted against acquired voltage. Data were filtered at 300Hz and acquired at 5kHz. Intracellular solution contained potassium rather than caesium ions (as described in section 2.2.4) and extracellular solution was as described in section 2.2.4 except for partial replacement of NaCl with 25mM TEA.Cl (see also section 2.5.2). 300μM kainate was stepper-applied to the whole cell.

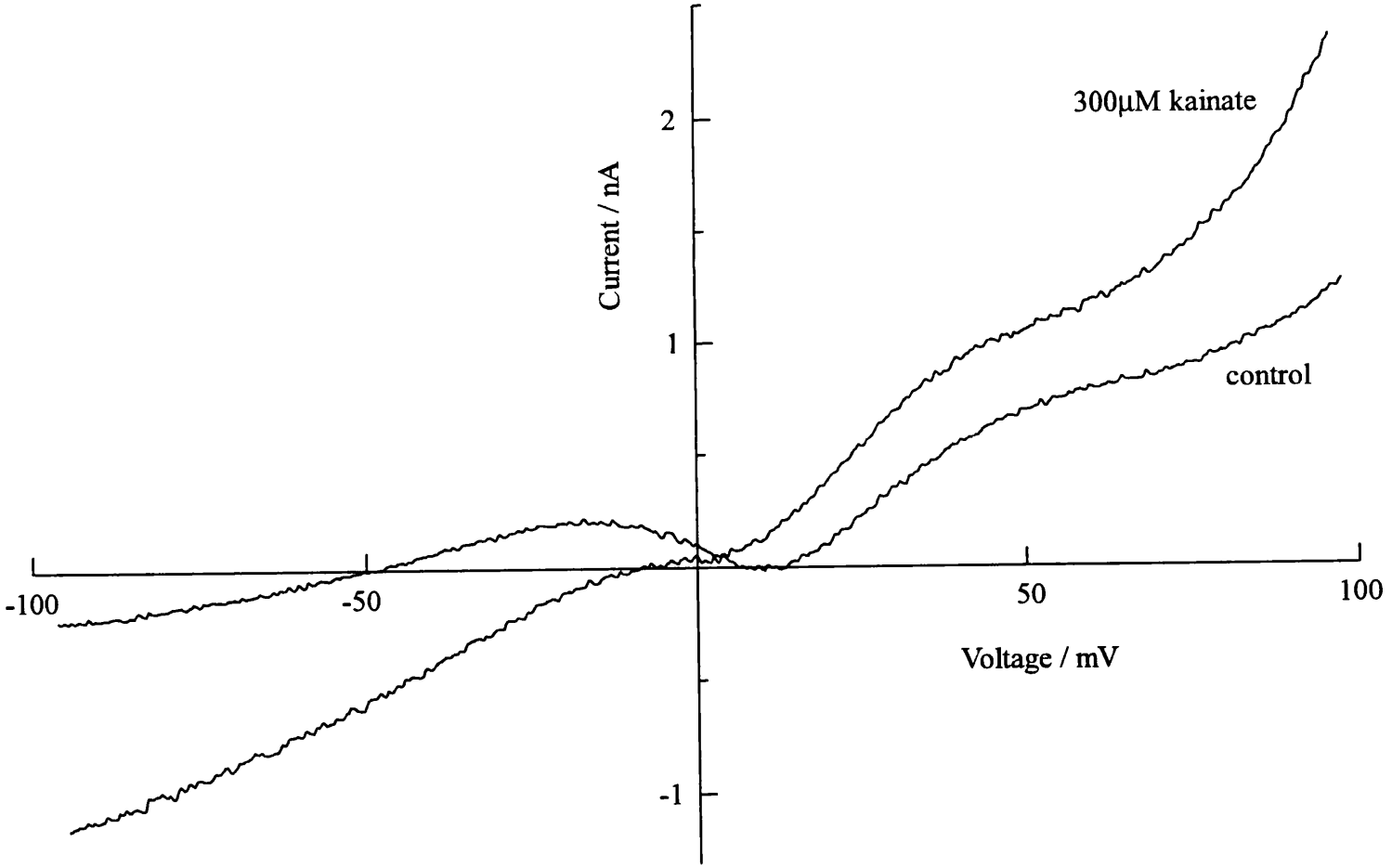
300μM kainate
control
Current / nA
2
1
-1
-100
-50
50
100
Voltage / mV

Figure 5.2.2 Kainate fails to inhibit calcium current

Upper panel (A): the effect of 100μM kainate on calcium currents recorded from acutely dissociated neurones. Neurones were voltage-clamped to -80mV by dSEVC and currents elicited at 30s intervals by 100ms voltage steps to zero mV. Data were filtered at 1kHz and acquired at 10kHz. Kainate was bath-applied. (Solutions were as described in section 2.7.) Data presented are typical traces, recorded sequentially, one under each of three conditions (control, in the presence of 100μM kainate and after removal of kainate from the bath). The same three traces are shown overlaid on the far right. Kainate clearly produced an inward current at -80mV, but failed to significantly affect current amplitude at 0mV.

Central panel (B): inhibition of calcium currents by 100μM ACh recorded from the same neurone as shown in the upper panel and presented in the same format.

Lower panel (C): tail currents recorded from a different neurone by cSEVC. Calcium currents were elicited using the same voltage protocol as in the upper and central panels, but only the section of current trace corresponding to the voltage step back from 0 to -80mV is shown. Current amplitude at 0mV is clearly inhibited by 100μM ACh, though ACh does not significantly influence tail current amplitude or kinetics.

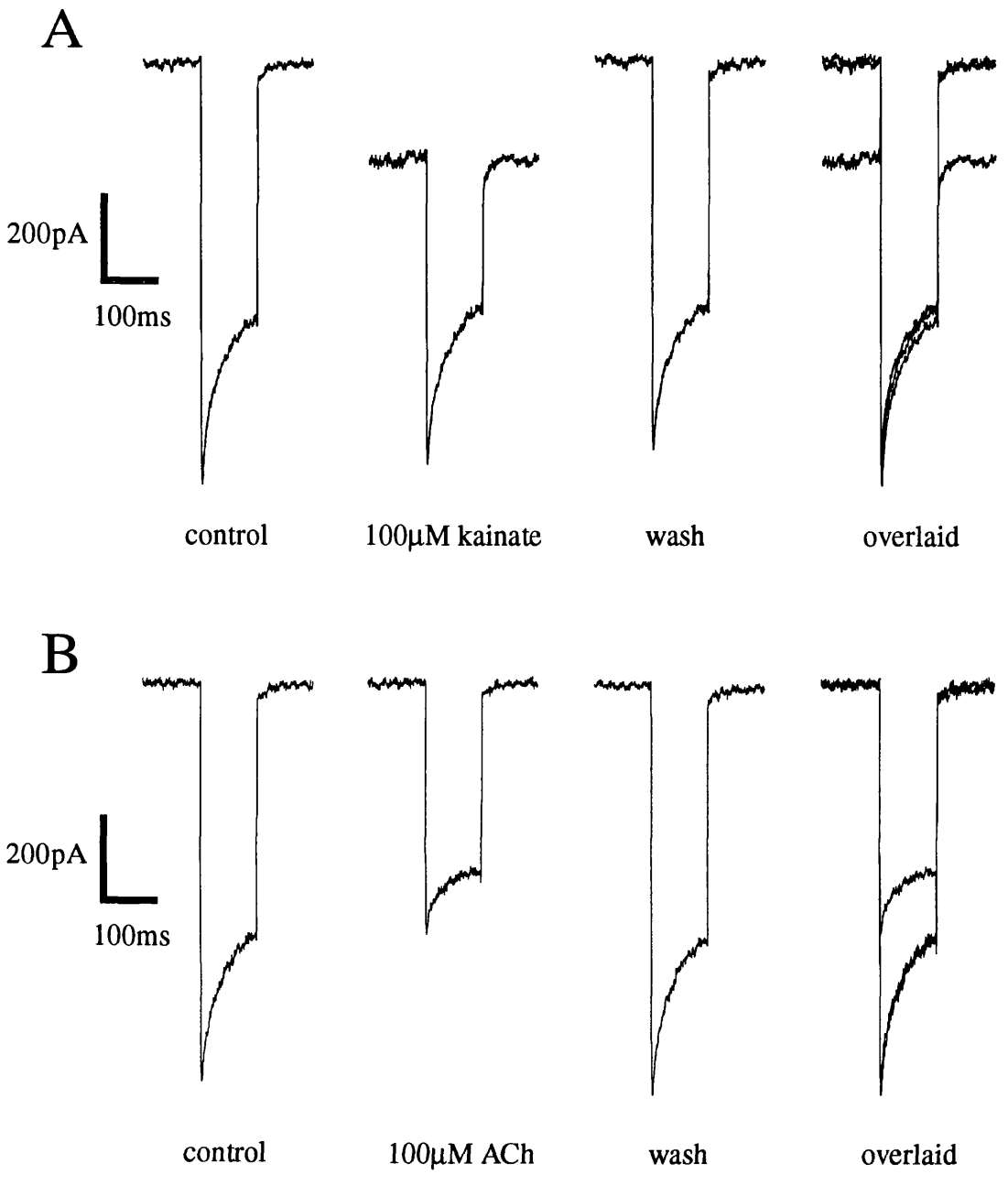
A
200pA
100ms
control
100μM kainate
wash
overlaid
B
200pA
100ms
control
100μM ACh
wash
overlaid
C
0pA
100μM ACh
Wash
Control
200pA
50ms

current to kainate at -80mV, suggesting that kainate-elicited current was AMPA receptor-mediated with no involvement of kainate receptors.

Measuring calcium current amplitude by examining tail currents (at -80mV) was considered since calcium tail current and kainate-elicited current should be additive, hence kainate-elicited current and calcium current would be easily distinguished. Unfortunately, the tail is largely due to L-type current and it is likely that other calcium current subtypes may be inhibited by kainate, hence examining the effect of kainate on calcium tail currents is not likely to reliably represent effects on calcium current elicited at depolarized voltages. This may be illustrated with ACh, which inhibits calcium current elicited by voltage steps to 0mV, but not tail currents (figure 5.2.2).

ACh was also used as a positive control, inhibiting calcium current in all 6 cells to which it was applied. The degree of inhibition by ACh was not calculated for these 6 cells since leak subtraction with cadmium was often cytotoxic. However, data were comparable with those of Allen & Brown (1993) in which 100μM ACh inhibited 35-40% of the calcium current recorded in the presence of 30mM extracellular TEA.

5.2.3 Reduced calcium buffering permits inhibition by kainate

Kainate may be able to inhibit calcium current by stimulating calcium influx through AMPA receptors, the resulting rise in intracellular free calcium ion concentration causing calcium-dependent inhibition of voltage-gated calcium channels. By this hypothesis, the failure of kainate to inhibit calcium current under these conditions may reflect insufficient elevation of the intracellular free calcium concentration.

This possibility was investigated by reducing intracellular calcium buffering, achieved by reducing the concentration of EGTA in the intracellular solution to 0.1mM. (The intracellular free calcium concentration of 30nM was maintained in this solution by appropriately reducing the quantitiy of calcium added.) Under these conditions, bath-application of 100μM kainate (for approximately 1 minute) resulted in inhibition of the calcium current (n=8; responses recorded in 1.2-5mM extracellular calcium concentrations).

Figure 5.2.3 Reduced calcium buffering permits inhibition by kainate

Effects of kainate on sequentially evoked calcium currents recorded from an acutely dissociated basal forebrain neurone. Currents were recorded under dSEVC and evoked by voltage steps from -80 to 0mV at 30 second intervals. Traces shown are representative of currents under various conditions. Data were filtered at 1kHz and acquired at 10kHz. 100μM kainate was bath-applied for 3 minutes. Extracellular solution was as described in section 2.7. Intracellular solution was basically as described in section 2.7, but with reduced calcium buffering achieved by reducing the EGTA concentration from 3mM to 0.1mM. (Free calcium concentration was maintained at 30nM by appropriately reducing the quantity of calcium chloride added to the intracellular solution.)

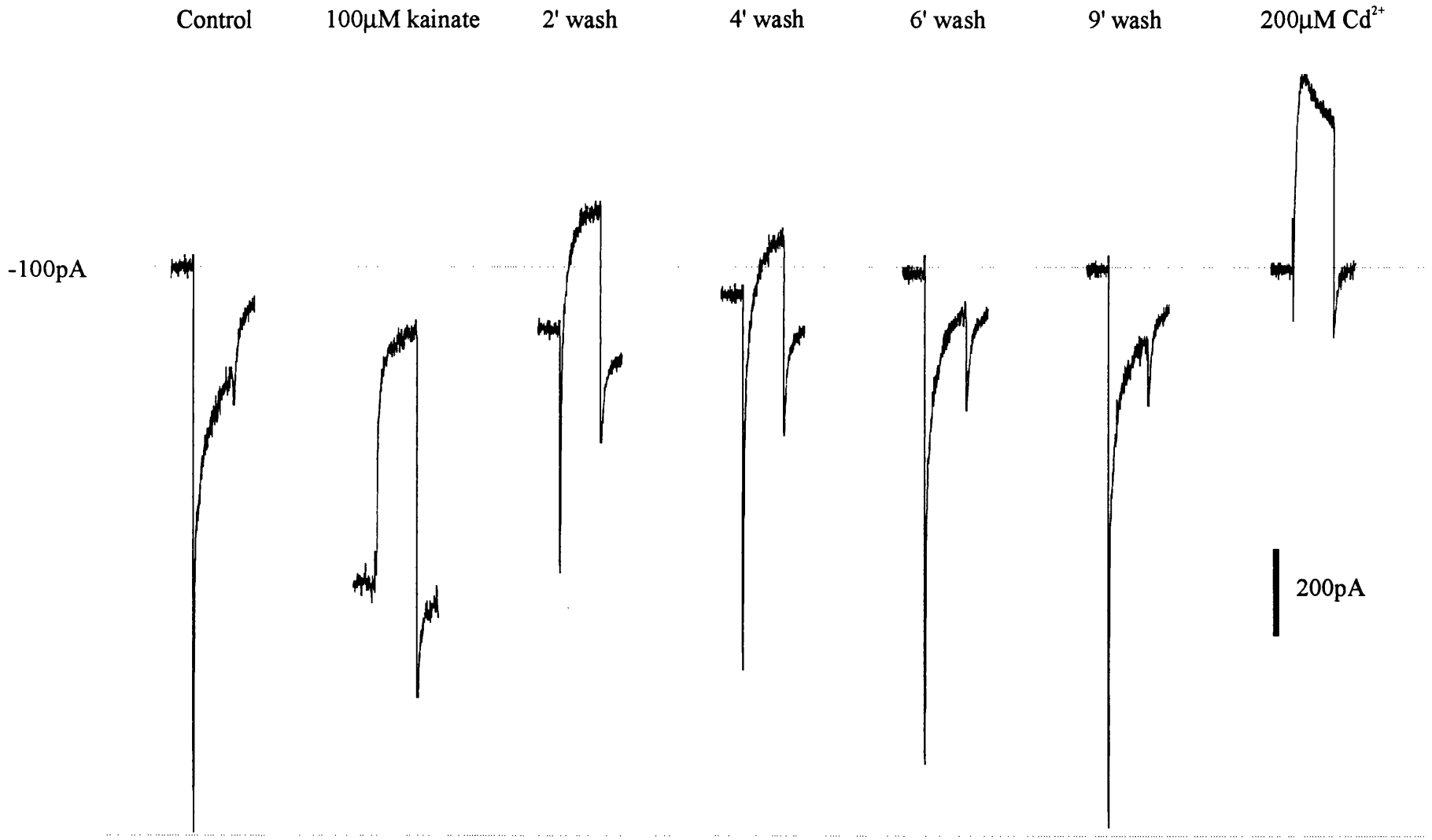
Control
100μM kainate
2' wash
4' wash
6' wash
9' wash
200μM Cd2+
-100pA
200pA

The effect of kainate was found to be reversible in 4 of these 8 cells, though repeated applications of kainate resulted in irreversible inhibition of the calcium current. Reversibility occured very slowly compared to removal of kainate from the bath: calcium current recovery upon removal of kainate from the bath typically continued for several minutes after the holding current at -80mV had decayed to zero. In addition, reversibility was never observed after kainate application in 5mM extracellular calcium, whereas at least partial reversibility was observed for 75% of responses recorded in 1.2 and 2.5mM extracellular calcium. This may reflect the greater calcium load following exposure to kainate at higher extracellular calcium concentrations.

One example is given in figure 5.2.3, showing reversible inhibition of the calcium current (extracellular calcium concentration 2.5mM). Recovery of calcium current amplitude continued for approximately ten minutes after washout of kainate from the bath. After removal of kainate from the bath, holding current at -80mV was greater than prior to kainate application. This holding current decreased with a similar timecourse to that of calcium current recovery. This probably reflects a relatively slow recovery of intracellular calcium concentratation to basal levels following kainate exposure, thus maintaining inhibition of the calcium current for some few minutes. The slow recovery of the holding current may reflect electrogenic calcium transport across the plasma membrane or stimulation of a calcium-activated current, such as a calcium-activated chloride current.

Inhibition of steady-state calcium current appears to be greater after removal of kainate. This may result from further calcium influx prior to complete removal of kainate from the bath or from contamination of current amplitude at 0mV with calcium-activated conductances and/or with non-NMDA receptor-mediated current.

5.2.4 Effects of metabotropic agonists on the calcium current

A number of agonists of various G-protein-coupled receptors were tested for effects on the calcium current in cells after 1 DIV (with 3mM EGTA in the pipette). The metabotropic glutamate receptor agonist trans-ACPD had no

effect; only adenosine and galanin had reproducible effects, both yielding slight inhibition. These data are summarised in table 5.2.4, below:

table 5.2.4

Agonist	Concentration	Number of cells in which calcium current was affected	Total number of cells exposed to agonist
trans-ACPD	30μM	0	5
Adenosine	100μM	2	17
Galanin	300nM	3	20
Baclofen	10μM & 30μM	0	9
5-HT	30μM & 100μM	0	12
Noradrenaline	100μM	0	9
Dopamine	100μM	1	8
Histamine	100μM	0	8
Sodium nitroprusside	100μM	0	6
Somatostatin	100nM	0	6
UTP	100μM	0	1
ATP	100μM	0	1
Bradykinin	100nM	0	1

5.3 Discussion

5.3.1 Calcium rise - relevance to physiological function

The above data show that AMPA receptor stimulation is capable of inhibiting calcium entry through voltage-gated calcium channels (VGCCs). In these experiments, calcium current inhibition was achieved only upon prolonged application of agonist with very low levels of intracellular calcium buffering. It therefore seems pertinent to ask whether or not this effect is of physiological relevance.

The answer to this question rests largely on the likely site of non-NMDA receptors and the method of agonist application *in vivo*. Synaptic input onto somatic receptors may be unlikely to induce calcium current inhibition, since the consequent calcium rise may be too slight. Somatic non-NMDA receptors may be more important under pathophysiological conditions where elevated extracellular glutamate concentrations may be sustained. Thus calcium entry through voltage-gated calcium channels may be reduced under pathological conditions.

In contrast, the effects of synaptic stimulation on intracellular calcium concentrations in processes may be much more pronounced, concentrations as high as 20-40μM having been observed in the dendrites of hippocampal CA1 neurones upon tetanic stimulation of Schaffer collaterals (Petrozzino, Pozzo-Miller & Connor, 1995). Thus synaptic stimulation might inhibit calcium channels in neuronal processes.

5.3.2 Physiological significance

The physiological function of this interaction between non-NMDA receptors and calcium channels is far from clear. One possibility is that pre-synaptic calcium-permeable non-NMDA receptors may promote or inhibit calcium influx into the pre-synaptic terminal thereby modulating transmitter release, possibly in a frequency dependent manner. Such a receptor might serve a similar function to pre-synaptic nicotinic receptors found at the neuromuscular junction (Bowman, Marshall, Gibb & Harborne, 1988) and at both cholinergic and non-cholinergic synapses within the CNS (McGhee, Heath, Gelber, Devay & Role, 1995).

There is however no neurone in which a pre-synaptically located AMPA receptor has been identified. In contrast, a functional pre-synaptic kainate receptor has been reported in the hippocampus. Initial enhancement followed by depression of synaptic release by this kainate receptor may result from accumulation of calcium in the terminal (Chittajallu, Vignes, Dev, Barnes, Collingridge & Henley, 1996).

5.3.3 Location of the kainate receptor

A dendritic location of the kainate receptor in basal forebrain neurones is consistent with the data presented above, there being no detectable current to kainate in acutely dissociated cells (in contrast with cultured neurones). This probably results from loss of kainate receptors during the dissociation process, such as one would expect were kainate receptors extrasomatically located.

The role of presynaptic kainate receptors in basal forebrain neurones could be examined using the 'sniffer-patch' technique to quantify acetylcholine release (Allen & Brown, 1996). Were a functional kainate receptor expressed pre-synaptically in basal forebrain neurones, one might expect exogenous application of kainate to modulate release of acetylcholine.

General Discussion

6.1 Summary of principle conclusions

(1) Cholinergic basal forebrain neurones express NMDA, AMPA and kainate receptors.

(2) AMPA receptors are responsible for the majority of somatically detected current elicited by non-NMDA receptor agonists applied either focally to the soma or to both soma and dendrites.

(3) There is some heterogeneity in the functional properties of AMPA receptors expressed by these neurones, particularly with regard to relative ion permeability coefficients. The majority of the population express AMPA receptors with a high mean calcium to sodium permeability coefficient ratio.

(4) These calcium-permeable AMPA receptors are sensitive to blockade by extracellular divalent ions including calcium, cadmium and cobalt.

6.2 Excitotoxic injury to basal forebrain neurones

A number of lesion studies have been conducted in which excitotoxic agents were used to eliminate projecting cholinergic cells within the basal forebrain with the aim being to elucidate the behavioural roles of the cholinergic projection from the basal forebrain. Excitotoxic agents were of interest for this purpose because they were considered toxic to cell bodies, but not to the axonal bundles which traverse the basal forebrain nuclei. Hardly surprisingly, excitotoxic lesions have proved rather non-specific, complicating interpretation in terms of basal forebrain function (reviewed by Dunnett, Everitt & Robbins, 1991). These studies are outlined below, being of interest because they highlight unexpected sensitivity of cholinergic basal forebrain neurones to AMPA receptor-mediated toxicity.

Dunnett, Whishaw, Jones & Bunch (1987) lesioned rat nucleus basalis using quisqualate, kainate, NMDA and ibotenate. 10 days post-lesion cortical ACh levels were assayed biochemically and coronal slices containing nucleus basalis were examined after histochemical staining for AChE. All four toxins

caused extensive damage well beyond the bounds of the nucleus basalis, but quisqualate caused noticeably less damage outside the basal forebrain than the other three agents. Quisqualate lesions also had fewer behavioral effects. These data question the validity of using excitatory amino acid agonist-induced lesions for behavioural studies of basal forebrain cholinergic neuronal function, but also suggest that cholinergic nucleus basalis neurones may be unusually sensitive to quisqualate-induced toxicity.

This sensitivity was confirmed by Page, Sirinathsinghji & Everitt (1995) who infused AMPA or ibotenate into the nucleus basalis of anaesthetized rats. The rats were decapitated 7 days post-lesion and coronal slices prepared. Cholinergic and GABAergic cells were counted after histochemical identification using labelled oligonucleotide probes for mRNAs of ChAT, GAD and preproenkephalin (a marker for GABAergic neurones). Using sufficient AMPA to lesion the vast majority of ChAT mRNA-containing neurones and sufficient ibotenate to lesion a lesser proportion, it was clear that ibotenate was more toxic to GABAergic nucleus basalis neurones. Both AMPA- and ibotenate-induced lesions of the nucleus basalis also killed a large proportion of pallidal GABAergic neurones, though ibotenate was more toxic to this population of neurones. Using very similar methodology Lindefors, Boatell, Mahy & Persson (1992) also demonstrated widespread damage after ibotenate lesion. These data highlight the greater sensitivity of cholinergic nucleus basalis neurones to injury by AMPA, but also clearly show that as a neurotoxin, AMPA is far from selective.

A slightly different approach to comparing the effects of different agonists was employed by Boegman, Cockhill, Jhamandas and Beninger (1992), who lesioned rat nucleus basalis using quisqualate, AMPA, ibotenate and NMDA and compared ChAT levels in the amygdala and cortex after 7 days. The two projections were similarly affected, though the cortical projection was found slightly more sensitive to all four agents. This suggests that nucleus basalis contains cells which are relatively homogeneous, at least with respect to their sensitivities to excitatory amino acids.

Quisqualate- and ibotenate-induced rat medial septal lesions were

performed by Mahy, Bendahan, Boatell, Bjelke, Tinner, Olson & Fuxe (1995). ChAT and AChE immunocytochemistry of coronal slices prepared 13 days after lesion by quisqualate resolved a loss of cholinergic cell bodies in both medial septum and the vertical limb of the diagonal band of Broca. Quisqualate lesion of the medial septum also caused the loss of AChE-positive termini from the molecular layer of the dentate gyrus and the CA1 region of the hippocampus. Ibotenate lesions failed to produce the same clear effects. In addition to reductions of cortical ChAT activity and basal forebrain NGFr-immunoreactivity, McAlonan, Dawson, Wilkinson, Robbins & Everitt (1995) noted considerable damage to non-cholinergic neurones in Nissl-stained sections following AMPA-induced lesions of rat medial septum and vertical limb of the diagonal band of Broca.

Behavioural studies following excitotoxic lesions are consistent with the post-mortem staining data both for nucleus basalis (Dunnett, Whishaw, Jones & Bunch, 1987) and for medial septum/vertical limb of the diagonal band of Broca (McAlonan, Dawson, Wilkinson, Robbins & Everitt, 1995): ibotenate-induced lesions have been found to have far more behavioural effects than either AMPA or quisqualate, probably as a result of more extensive damage to non-cholinergic neurones by ibotenate than by AMPA or quisqualate (Dunnett, Everitt & Robbins, 1991).

Interestingly, the rather extensive non-specific damage caused by AMPA- and quisqualate-induced lesions may not have as many side-effects as one might suppose. Torres, Perry, Blokland, Wilkinson, Wiley, Lappi & Dunnett (1994) developed an antibody which was a hybrid of the neurotoxin saporin and an antibody to the NGF receptor. This proved selectively toxic to cholinergic neurones when used to lesion each region of the basal forebrain and the behavioural, biochemical, histochemical and immunocytochemical effects of these lesions were similar to those resulting from AMPA- and from quisqualate-induced lesion.

The supposition, based on lesion data, that cholinergic basal forebrain neurones are particularly susceptible to non-NMDA receptor-induced injury and that this may be attributable to the types or numbers of non-NMDA receptors

expressed by these cells is supported by data on cultured basal forebrain neurones. Weiss, Yin & Choi (1994) found that murine magnocellular cholinergic medial septal neurones in dissociated culture were significantly more vulnerable to AMPA- and kainate-mediated injury than was the neuronal population of their medial septum culture as a whole. In contrast, cholinergic cells were not notably more vulnerable to NMDA receptor-mediated toxicity. Excitotoxicity was assessed after a 24-hour exposure to agonist. Overall cell injury was assessed by LDH assay and cholinergic cell damage by counting intact ChAT-positive cells. Yin, Lindsay & Weiss (1994) extended this data, considering the effect of raising extracellular calcium concentration on ChAT-positive cell loss following exposure to kainate and using the dye fura-2 to examine the effect of exposure on intracellular free calcium concentration. ChAT-positive cell loss increased with extracellular calcium concentration and this was reflected by an increase in intracellular free calcium concentration upon kainate application. In the continued presence of kainate, the intracellular free calcium concentration decayed to near baseline over 20-30 minutes, but under these conditions the free calcium concentrations within ChAT-positive cells were generally higher than those of the population as a whole.

Thus in cholinergic magnocellular basal forebrain neurones, the non-NMDA receptor, rather than the NMDA receptor, may be the principle route of calcium influx under excitotoxic conditions, the non-NMDA receptor expressed by these cells being both calcium-permeable and capable of generating a high current density. This would account for the pronounced sensitivity of basal forebrain neurones to non-NMDA receptor-mediated lesion.

Post-mortem immunocyctochemical localization of AMPA receptors in human nucleus basalis of Meynert has revealed that magnocellular cholinergic basal forebrain neurones express both GluR1, and GluR2 and/or GluR3 receptors. Expression of GluR2/3 decreases with age, such that at approximately 75 years of age negligible staining is evident for GluR2/3, though staining for GluR1 is maintained (Ikonomovic, Sheffield & Armstrong, 1995). This may underlie the pronounced degeneration of these neurones observed during senile dementia, where such a condition involves an elevation

of extracellular glutamate concentration.

6.3 Physiological roles for basal forebrain non-NMDA receptors

Ca^{2+}-permeability of AMPA receptors may also have some functional significance under non-pathological conditions. Ca^{2+} influx through NMDA receptors is responsible for NMDA-dependent long-term potentiation such as that observed at the hippocampal CA3-CA1 synapse (Nicoll & Malenka, 1995). Ca^{2+}-influx through NMDA receptors only occurs following non-NMDA receptor activation causing depolarization-induced relief of magnesium block of NMDA receptors. In contrast, Ca^{2+}-influx through Ca^{2+}-permeable non-NMDA receptors does not require such depolarization and so in a synaptic context relatively low-frequency stimulation (insufficient to relieve magnesium block of the NMDA receptor) may produce significant Ca^{2+}-influx through Ca^{2+}-permeable non-NMDA receptors. This calcium influx may influence synaptic plasticity, extending the range of stimulatory inputs which result in synaptic strengthening.

Such a scenario has been described in cultured dorsal horn neurones where kainate pre-treatment was found to increase the amplitude of excitatory postsynaptic potentials (Gu, Albuquerque, Lee & MacDermott, 1996). Unfortunately, the authors stimulated synaptic activity by exposing the cells to hyperosmotic solutions, rather than by electrical stimulation of a pre-synaptic neurone, and therefore did not examine the frequency-dependence of synaptic strengthening. Nonetheless, this demonstrates the principle of synaptic strengthening following calcium entry through Ca^{2+}-permeable AMPA receptors.

Under some circumstances Ca^{2+}-influx through non-NMDA receptors may modulate synaptic plasticity by decreasing NMDA receptor activity. This may occur where Ca^{2+} entry leads to elevation of the intracellular calcium concentration in the vicinity of NMDA receptors, leading to calcium-dependent desensitization of the NMDA receptor. Such an interaction occurs in dorsal horn neurones though no effects on synaptic activity were investigated (Kyrozis, Goldstein, Heath & MacDermott, 1995).

It is interesting to note that synaptic strengthening and NMDA receptor inhibition were both observed in the same preparation (cultured dorsal horn neurones). Non-NMDA receptors were activated by the same route in both studies, namely application of kainate. These data suggest that Ca^{2+}-permeable AMPA receptors could depress or strengthen excitatory synaptic activity, depending on the frequency or duration of stimulation. Strengthening would presumably result under conditions where NMDA receptors were not active and depression where NMDA receptor activity could contribute to synaptic responses. It is also interesting to note that synaptic depression through inhibition of the NMDA receptor by this route need not eliminate calcium influx through ionotropic glutamate receptors since this could still be obtained through Ca^{2+}-permeable non-NMDA receptors.

Like the NMDA receptor, voltage-sensitive calcium channels are also inhibited by intracellular calcium (see, for instance, Zeilhofer, Müller & Swandulla, 1993). A similar inhibitory effect of Ca^{2+}-influx through Ca^{2+}-permeable AMPA receptors might therefore be observed where AMPA receptors and voltage-sensitive calcium channels are co-localised at pre-synaptic terminals.

Inhibition of NMDA receptor-mediated excitatory post-synaptic potentials through stimulation of a pre-synaptic kainate receptor has also been observed. Chittajallu, Vignes, Dev, Barnes, Collingridge & Henley (1996) found that kainate receptor stimulation (by bath-application of kainate) depressed NMDA receptor-mediated evoked excitatory postsynaptic potentials at Schaffer collateral-commissural input onto CA1 neurones in hippocampal slices. To date this is the closest approximation to a functionally significant kainate receptor-mediated effect. The expression of a kainate receptor by basal forebrain neurones raises the possibility that a similar modulatory influence of a pre-synaptic kainate receptor may be observed at cholinergic synapses in the CNS should glutamate and ACh be co-released.

6.4 Future directions

The present work leads to several important questions:

(1) Where on the cell is the kainate receptor located? Only very small kainate receptor-mediated responses were recorded using a somatically located whole-cell electrode. It is possible that this is because the kainate receptor is expressed principally on processes; the only functional role of a kainate receptor which has been described is presynaptic inhibition of synaptic activity (Chittajallu, Vignes, Dev, Barnes, Collingridge & Henley, 1996). Immunocytochemistry offers the most appropriate approach to this type of question. Fluorescence localization of the antibody using light microscopy would be sufficient to differentiate between somatic and neuritic receptor localization.

Unfortunately basal forebrain neurones project to their targets by tortuous routes, hence slices containing basal forebrain somata, projecting processes and target regions are not easily cut. It would therefore be necessary to investigate receptor localization *in vitro*, though should kainate receptor subunits be localised to the soma or proximal processes, then it would be important to verify that the same situation exists *in vivo* by repeating the procedure using the slice preparation. This point may be illustrated by comparison with hippocampal neurones, which express somatically located kainate receptors in culture (Lerma, Paternain, Naranjo & Mellström, 1993; Paternain, Morales & Lerma, 1995) but not in the slice preparation (Jonas & Sakmann, 1992).

Similar questions may be asked of the AMPA receptor. Whilst a large somatic current is observed in culture, are the AMPA receptors present at synaptic sites also permeable to divalent ions? This question could initially be investigated using immunocytochemical techniques to determine whether or not GluR2 subunits are expressed on the distal dendrites of cultured neurones.

(2) What are the relative Ca^{2+}-permeabilities of the AMPA receptors expressed by basal forebrain neurones *in vivo*? Is the relative Ca^{2+}-

permeability of the AMPA receptor population identical throughout the cell?

A combination of electrophysiological and fluorescence methods would allow the fractional calcium current through AMPA channels to be assessed and could be applied to a slice preparation. This method could be applied to both the soma and dendrites of a cell provided agonist application was sufficiently localized (Garaschuk, Schneggenburger, Schirra, Tempia & Konnerth, 1996). Measurement of relative calcium permeability by this method is limited to the soma and proximal dendrites since it requires that a patch-clamp electrode be placed sufficiently close to the site of agonist application that this region of the cell can be voltage-clamped.

(3) What are the functional roles of the kainate receptor and the Ca^{2+}-permeable AMPA receptor in basal forebrain neurones? These questions should be answered using electrophysiological techniques and the brain slice preparation.

The most obvious functional role for the Ca^{2+}-permeable AMPA receptor is modulation of synaptic activity, possibly in a frequency-dependent manner. By focal extracellular stimulation of afferent inputs onto magnocellular basal forebrain neurones one can elicit excitatory (glutamatergic) postsynaptic potentials (Momiyama, Sim & Brown, 1996). This technique might be used to examine the effects of different stimulation paradigms. Should synaptic strengthening or depression be observed, the use of joro spider toxin to block only AMPA receptors with high Ca^{2+}-permeabilities may reveal the importance of the Ca^{2+}-permeable AMPA receptors in this process (Gu, Albuquerque, Lee & MacDermott, 1996).

Should the kainate receptors be post-synaptically located on basal forebrain neurones, one could likewise envisage them playing a role in synaptic plasticity. However, the best evidence obtained to date for a functional kainate receptor suggests a pre-synaptic location (Chittajallu, Vignes, Dev, Barnes, Collingridge & Henley, 1996). Furthermore,

Lerma, Morales, Vicente & Herreras (1997) found no effect of post-synaptic kainate receptors on synaptic transmission in hippocampal cultures (where it was possible to demonstrate immunocytochemically that the post-synaptic cell expressed kainate receptors).

Modulation of synaptic function by kainate receptors might therefore be expected to be pre-synaptic. In this context, basal forebrain kainate receptors are only likely to be functional if glutamate and acetylcholine are co-released. Cutting slices containing basal forebrain somata, projecting processes and target regions is extremely difficult, the only projection for which this is feasible being that to the amygdala (Moises, Womble, Washburn & Williams, 1995). Synaptic responses could be elicited by stimulation of magnocellular basal forebrain neurones and simultaneous recording from neurones in the amygdala. The role of the kainate receptor might be determined by inhibition of kainate receptor function using selective antagonists such as 5-nitro-6,7,8,9-tetrahydrobenzo(g)indole-2,3-dione-3-oxime (NS-102; Chittajallu, Vignes, Dev, Barnes, Collingridge & Henley, 1996).

Though less satisfactory, the roles of both kainate receptors and Ca^{2+}-permeable AMPA receptors could be examined in co-cultures of basal forebrain and target tissues (Gahwiler & Brown, 1985).

Alternatively these issues could be examined *in vitro*. The effects of Ca^{2+}-permeable AMPA receptors could be examined by exogenous application of glutamate to neuritic terminals of basal forebrain neurones. The rise in intracellular calcium concentration, which would cause neurotransmitter release, could be measured with appropriate imaging technology and a fluorescent dye, such as furaptra. The rise in intracellular calcium concentration is likely to be very high given the very high surface area:volume ratio of a small process (for instance see Petrozzino, Pozzo-Miller & Connor, 1995). The role of a kainate receptor could be examined by exogenously applying kainate to a basal forebrain neurones and quantitating acetylcholine release using a detector patch (Allen & Brown, 1996). Under these conditions AMPA receptor

activity would depolarize the release site. Thus in order to study the role of the kainate receptor, AMPA receptors must be inhibited with a selective antagonist such as GYKI 53655.

(4) By what mechanism do divalent ions block non-NMDA receptors? This question could be approached using single channel recording as used by Jahr & Stevens (1993) to investigate calcium block of the NMDA receptor. Acutely dissociated neurones offer an excellent source of divalent ion-sensitive non-NMDA receptors.

Such a study might include investigation of which other divalent ions block the channel, zinc being of particular interest since it is synaptically released (Frederickson & Danscher, 1990). Interestingly, there is some evidence that low concentrations of zinc potentiate non-NMDA receptor-mediated responses whereas high concentrations are inhibitory (Mayer, Vyklicky & Westbrook, 1989).

It must, however, be noted that a study of non-NMDA receptors at the single channel level may be difficult in view of their small single channel conductance, multiple conductance states and rapid gating.

7.1 - Abbreviations

ACh	acetylcholine
AChE	acetylcholinesterase
ALS/PD	amyotropic lateral sclerosis/Parkinsonism dementia
AP5 (APV)	D(-)-2-amino-5-phosphonopentanoic acid
ATP	adenosine 5'-triphosphate
4-AP	4-aminopyridine
AMPA	(S)-α-amino-3-hydroxy-5-methyl-4-isoxazolepropionic acid
BAPTA	1,2-bis(2-aminophenoxy)-ethane-N,N,N',N'-tetraacetic acid
ChAT	choline acetyltransferase
CNQX	6-cyano-7-nitroquinoxaline-2,3-dione
ConA	Concanavalin A
ω-CgTx GVIA	ω-conotoxin GVIA
DAT	digital audio tape
DHP	1,4-dihydropyridine
DIV	day(s) *in vitro*
DMA	direct memory access
DMEM	Dulbecco's modified Eagle's medium
DMSO	dimethyl sulphoxide
DNase	deoxyribonuclease
dSEVC	discontinuous single-electrode voltage-clamp
EGTA	ethylene glycol-bis(β-aminoethylether)N,N,N',N',-tetraacetic acid
FCS	foetal calf serum
GABA	γ-amino butyric acid
GAD	glutamic acid decarboxylase
GBSS	Gey's balanced salt solution
GDP-β-S	guanosine 5'-O-(2-thiodiphosphate)
GluR	glutamate receptor/AMPA receptor subunit
GTP	guanosine 5'-triphosphate
GTP-γ-S	guanosine 5'-O-(2-thiotriphosphate)
GYKI 52466	1-(4-aminophenyl)-4-methyl-7,8-methylenedioxy-5H-2,3-benzodiazepine
GYKI 53655	1-(4-aminophenyl)-3-methylcarbamyl-4-methyl-7,8-methylenedioxy-3,4-dihydro-5H-2,3-benzodiazepine
HBSS	Hanks' balanced salt solution
HEPES	N-(2-hydroxyethyl)piperazine-N'-(2-ethanesulfonic acid)

HDBB	horizontal limb of the diagonal band of Broca
HVA	high voltage-activated
5-HT	5-hydroxytryptamine
KA	kainate receptor subunit
L-AP4	L(+)-2-amino-4-phosphonobutyric acid
L-trans-2,4-PDC	L-trans-pyrrolidine-2,4-dicarboxylic acid
L-15	Leibovitz's L-15 medium
LVA	low voltage-activated
mGluR	metabotropic glutamate receptor/subunit
MS	medial septum
nAChR	nicotinic acetylcholine receptor
NB(M)	nucleus basalis (of Meynert)
NGF	nerve growth factor
NGFr	nerve growth factor receptor
NMDA	N-methyl-D-aspartate
NMDAR (NR)	NMDA receptor/subunit
NS-102	5-nitro-6,7,8,9-tetrahydrobenzo(g)indole-2,3-dione-3-oxime
Oxo-M	oxotremorine-M
PKA	protein kinase A
PKC	protein kinase C
SDAT	senile dementia of the Alzheimer-type
SI	substantia innominata
TMD	transmembrane domain
TEA(.Cl)	Tetraethyammonium (chloride)
trans-ACPD	(1S,3R)-1-aminocyclopentane-1,3-dicarboxylic acid
TTL	transistor-transistor logic
TTX	tetrodotoxin
UTP	uridine 5'-triphosphate
VDBB	vertical limb of the diagonal band of Broca
VGCC	voltage-gated calcium channel

7.2 - Equipment & Reagents

7.2.1 Tissue culture

Product	Source	Catalogue Number
Cell culture dishes	Gibco BRL, Life Technologies, Paisley, UK. Manufacturer: Nunclon.	153066
Deoxyribonuclease I type II-S from bovine pancreas	Sigma, Poole, UK.	4513
Dulbecco's modified Eagle's medium with L-glutamine	Gibco BRL, Life Technologies, Paisley, UK.	41965
Foetal calf serum (heat inactivated)	Gibco BRL, Life Technologies, Paisley, UK.	10108
Geys balanced salt solution	Gibco BRL, Life Technologies, Paisley, UK.	54030
D-Glucose (AnalaR)	BDH, Merck Ltd., Lutterworth, UK.	10117
L-glutamine	Gibco BRL, Life Technologies, Paisley, UK.	15039
Hanks' balanced salt solution	Gibco BRL, Life Technologies, Paisley, UK.	14170
HEPES N-(2-hydroxyethyl) piperazine-N'-(2-ethanesulfonic acid)	Gibco BRL, Life Technologies, Paisley, UK.	15630
Leibovitz's L-15 medium	Gibco BRL, Life Technologies, Paisley, UK.	11415

$MgCl_2$ (AnalaR)	BDH, Merck Ltd., Lutterworth, UK.	10149
Nerve growth factor 7S from mouse submaxillary glands	Boehringer Mannheim UK, Lewes, UK.	1014331
Poly-D-lysine hydrobromide mol. wt. >300,000	Sigma, Poole, UK.	P-7405
Sodium hydrogencarbonate	Gibco BRL, Life Technologies, Paisley, UK.	25080
Trypsin typeIX from porcine pancreas	Sigma, Poole, UK.	T-0134

7.2.2 Electrophysiology

Product	Source	Catalogue number
Air table	Wentworth Laboratories Ltd., Sunderland, UK.	
Amplifiers (i) axoclamp-2 and-2A (ii) axopatch 200A	Axon Instruments, Foster City, USA.	-----
Analysis software Microcal Origin (v3.5)	Microcal Software, Inc. Northampton, Massachusetts, USA	-----
Aquisition software (i) pCLAMP suite (ii) axotape	Axon Instruments, Foster City, USA.	-----
ATP magnesium salt from equine muscle	Sigma, Poole, UK.	A-0770

BAPTA 1,2-bis(2-aminophenoxy)-ethane-N,N,N',N'-tetraacetic acid	Sigma, Poole, UK.	A-4926
Borosilicate glass capillaries 1.5mm O.D. x 1.17mm I.D. thin wall with inner filament	Clark Electromedical Instruments, Reading, UK.	GC150TF -10
Caesium acetate 99.9%	Aldrich, Dorset, UK.	32,982-7
Caesium chloride (AnalaR)	BDH, Merck Ltd., Lutterworth, UK.	10067
Caesium fluoride	Fluka Chemicals, Gillingham, Dorset, UK.	20989
Caesium hydroxide	Aldrich Chemical Company, Gillingham, Dorset, UK.	23,204-1
Calcium chloride (AnalaR)	BDH, Merck Ltd., Lutterworth, UK.	19046
Calcium hydroxide	Fluka Chemicals, Gillingham, Dorset, UK.	21181
DAT recorders		
Sony DTC-1000ES	Modified & supplied by Applegarth electronics, Oxford, UK.	-----
DTR-1202	Biologic, Supplied by Intracell, Royston, UK.	-----
DMA board	Axon Instruments, Foster City, USA.	TL-1-125

EGTA ethylene glycol-bis(β-aminoethylether)N,N,N',N'-tetraacetic acid	Sigma, Poole, UK.	E-4378
Electrode pullers		
(i) L/M-3P-A	List-Medical-Electronic, Darmstadt, Germany.	-----
(ii) model 720	David Kopf Instruments, Tujunga, USA.	-----
Faraday cage	Constructed in-house	
D-glucose (AnalaR)	BDH, Merck Ltd., Lutterworth, UK.	10117
Fast stepper device	Constructed in-house	-----
Filter 8-pole lowpass Bessel	Constructed in-house	-----
GTP sodium salt type II-S	Sigma, Poole, UK.	G-8752
HEPES	Sigma, Poole UK.	H-3375
Magnesium chloride (AnalaR)	BDH, Merck Ltd., Lutterworth, UK.	10149
D-mannitol	Fluka Chemicals, Gillingham, Dorset, UK.	63560
Microforge	Narishige, Tokyo, Japan.	model MF-9
Micromanipulators (i) Narishige model MX-1 (ii) Narishige model WR-90	Narishige, Tokyo, Japan.	-----
Microscope Nikon TMS	Nikon, Japan.	-----

Pen recorder model 2400-S	Gould, Cleveland, USA.	-----
Peristaltic pump	Watson-Marlow, Buckinghamshire, UK.	-----
Potassium acetate (AnalaR)	BDH, Merck Ltd., Lutterworth, UK.	10350
Potassium chloride (AnalaR)	BDH, Merck Ltd., Lutterworth, UK.	101984
Pre-amplifiers	Constructed in-house	-----
Pressure application apparatus (puffer)	Constructed in-house	-----
Sodium chloride (AnalaR)	BDH, Merck Ltd., Lutterworth, UK.	10241
Sodium hydrogencarbonate (AnalaR)	BDH, Merck Ltd., Lutterworth, UK.	102474
Sylgard type 184	BDH, Merck Ltd., Lutterworth, UK. Manufacturer: Dow Corning	63416

7.3 - Ion Activities

Ion activities were calculated using equations and tabulated values from Pitzer & Mayorga (1973). Whilst the data of Pitzer & Mayorga are given for single aqueous electrolytes at room temperature, it is assumed that their application to mixed electrolytes is valid. For this assumption to be strictly valid, any effects on activity coefficients upon mixing of electrolytes must be accounted for by the change of ionic strength which results.

Pitzer & Mayorga give equations and tabulated data sufficient to take into consideration first, second and third virial coefficients, but state that the contribution from the third virial coefficient is 'usually very small and sometimes completely negligible.' Cursory inspection of the equations and tabulated values reveals this to be the case, so for the sake of simplicity the contribution from the third virial coefficient has been ignored and the corresponding terms have been excluded from the equations given below.

Pitzer & Mayorga give the following equations for the calculation of activity coefficients of salts:

$$\ln\gamma = |z_M z_X| f^\gamma + m\left(\frac{\nu_M \nu_X}{\nu}\right) B_{MX}{}^\gamma$$

$$f^\gamma = -A_\varphi \left[\frac{I^{1/2}}{1+1.2I^{1/2}} + \frac{5}{3}\ln(1+1.2I^{1/2})\right]$$

$$B_{MX}{}^\gamma = 2\beta_{MX}{}^{(0)} + \frac{\beta_{MX}{}^{(1)}}{2I}\left[1-e^{-2I^{1/2}}(1+2I^{1/2}-2I)\right]$$

$$\nu = \nu_M + \nu_X$$

where,

γ	is the activity coefficient for the salt
v_M & v_X	are the numbers of cations and anions respectively in the formula
z_M & z_X	are the charges in electronic units on cations and anions respectively
m	is the molality of the salt
A_φ	is the Debye-Hückel coefficient, which has a value of 0.392 for water at 25°C
$\beta_{MX}^{(0)}$ & $\beta_{MX}^{(1)}$	are tabulated values which together define the second virial coefficient
I	is the ionic strength of the solution, defined as: $I = (\Sigma m_i z_i^2)/2$ where m_i and z_i are the molality of and electronic charge on ion i. Note that for the purposes of this calculation all salts are considered fully dissociated.

Also note that (i) where used as a superscript, γ is a label not an exponent.

(ii) it is not intended that the subscript MX should indicate the stoichiometry of the salt to which it refers.

The numerical values of relevance to the present calculations are as follows:

Intracellular: I = 0.095

CsF	m=0.03	$\beta_{MX}^{(0)}$=0.1306	$\beta_{MX}^{(1)}$=0.2570
CsOH	m=0.065	$\beta_{MX}^{(0)}$=0.150	$\beta_{MX}^{(1)}$=0.3

Ca^{2+}-extracellular: I=0.3068

$CaCl_2$	m=0.1	$(4/3)\beta_{MX}^{(0)}$=0.4212	$(4/3)\beta_{MX}^{(1)}$=2.152
$Ca(OH)_2$	m=0.002	β_{MX} values not available	

Na^+/Ca^{2+}-extracellular: I=0.204

$CaCl_2$	m=0.05	$(4/3)\beta_{MX}^{(0)}$=0.4212	$(4/3)\beta_{MX}^{(1)}$=2.152
NaCl	m=0.05	$\beta_{MX}^{(0)}$=0.0765	$\beta_{MX}^{(1)}$=0.2664

NaOH	m=0.004	$\beta_{MX}^{(0)}$=0.0864	$\beta_{MX}^{(1)}$=0.253

Na^+-extracellular: I=0.107

$CaCl_2$	m=0.001	$(4/3)\beta_{MX}^{(0)}$=0.4212	$(4/3)\beta_{MX}^{(1)}$=2.152
NaCl	m=0.10	$\beta_{MX}^{(0)}$=0.0765	$\beta_{MX}^{(1)}$=0.2664
NaOH	m=0.004	$\beta_{MX}^{(0)}$=0.0864	$\beta_{MX}^{(1)}$=0.253

Note that $(4/3)\beta_{MX}$ values are tabulated for calcium chloride. The factor 4/3 corresponds to the term $2v_Mv_X/v$ in the equation for $\ln\gamma$.

In view of the very low concentrations of hydroxide salts in each of the extracellular solutions and the similarity of the β_{MX} values (where available) to those of the corresponding chloride salts, the concentrations of chloride and hydroxide salts of each ion were summed and the activities calculated using β_{MX} values for the chloride salts.

Calculated values of f^γ, B_{MX}^γ and γ were as follows:

Intracellular:

CsF	f^γ=-0.2637	B_{MX}^γ=0.5722	γ=0.7815
CsOH	f^γ=-0.2637	B_{MX}^γ=0.6630	γ=0.8020

Ca^{2+}-extracellular:

CaX_2	f^γ=-0.4634	$(4/3)B_{MX}^\gamma$=2.6187	γ=0.5170

Na^+/Ca^{2+}-extracellular:

$CaCl_2$	f^γ=-0.3978	$(4/3)B_{MX}^\gamma$=2.9208	γ=0.5223
NaX	f^γ=-0.3978	B_{MX}^γ=0.4103	γ=0.6868

Na^+-extracellular:

$CaCl_2$	f^γ=-0.3084	$(4/3)B_{MX}^\gamma$=3.3705	γ=0.5415
NaX	f^γ=-0.3084	B_{MX}^γ=0.4659	γ=0.7711

For the dissociation of a salt: $M_{v+}^{z+}X_{v-}^{z-} \rightleftarrows v_+M^{z+} + v_-X^{z-}$, the activity coefficients for individual ions and for the parent salt are related by the simple equation: $\gamma_\pm = (\gamma_+^{v+}.\gamma_-^{v-})^{1/v}$ where $v = v_+ + v_-$

However, the relative contributions of anions and cations to the activity of the parent salt are very difficult to determine. Calculation of activity

coefficients for individual salts from activity coefficients for the parent salts therefore requires further approximation.

At the concentrations considered here, cations and anions are thought to contribute approximately equally to the parent salt activity for the chloride salts of sodium and caesium (Bates, Staples & Robinson, 1970). Less data is available for fluoride and hydroxide salts, but the ion activity coefficients for chloride, fluoride and hydroxide ions are approximately equal at concentrations of up to 0.2N (Kielland, 1937). It does not seem unreasonable to assume that the same approximation is valid for the fluoride and hydroxide salts of sodium and caesium. Thus the anion and cation activity coefficients of these salts were each assumed to be equal to the coefficient for the parent salt.

Various methods for deriving the activity coefficient for a divalent ion from the value for the parent salt have been proposed. Several have been critically evaluated by Butler (1968), who suggested the use of the Guggenheim convention: $\gamma_{ion}=(\gamma_{salt})^2$. In addition, this equation is in relatively common use in physiological literature (see for instance Lee & Tsien, 1984; Mayer & Westbrook, 1987a; Otis, Raman & Trussell, 1995) so was used in the present calculations.

The resulting values for the ion activity coefficients and ion activities are tabulated below.

Intracellular:

γ_{Cs} for CsF =0.7815 m=30mN

γ_{Cs} for CsOH =0.8020 m=65mN

caesium ion activity = 75.58mM

Ca^{2+}-extracellular:

γ_{Ca} = 0.2673 m=102mN ion activity = 27.26mM

Na^+/Ca^{2+}-extracellular:

γ_{Ca} = 0.2728 m=40mN ion activity = 13.64mM

γ_{Na} = 0.6868 m=54mN ion activity = 37.09mM

Na^+-extracellular:

γ_{Ca} = 0.2932 m=1mN ion activity = 0.29mM

γ_{Na} = 0.7711 m=104mN ion activity = 80.19mM

These values for activity coefficients are consistent with those tabulated by various authors (Kielland, 1937; Bates, Staples & Robinson, 1970; Butler, 1968) and are very similar to the values calculated using the simpler equations given by Ammann, Bissig, Güggi, Pretsch, Simon, Borowitz & Weiss (1975).

7.4 - Constant Field Theory & Calculations

Constant field theory is commonly used to calculate relative ionic permeabilities. The theory was first developed by Goldman (1943) and Hodgkin & Katz (1949) to account for the resting membrane potential of the squid giant axon. The result is the Goldman-Hodgkin-Katz voltage equation:

$$E_m = (RT/F).\ln[(P_K[K]_o/P_K[K]_i)+(P_{Na}[Na]_o/P_{Na}[Na]_i)+(P_{Cl}[Cl]_i/P_{Cl}[Cl]_o)]$$

where E_m is the resting membrane potential or reversal potential (E_{rev})

This equation accounts only for the effects of monovalent ions and may be considered a simplified form of the expanded constant field equation (see Spangler, 1972; Piek, 1975):

$$E_{rev} = (RT/F)\ \ln\ \{[-b + \sqrt{(b^2-4ac)}]/2a\}$$

where E_{rev} is the reversal potential,
R, F and T are the gas and Faraday constants and the absolute temperature respectively.
At 25°C, RT/F = 25.693mV.

a, b and c are constants given by:

$$a = [K]_i+(P_{Cl}/P_K).[Cl]_o+(P_{Na}/P_K).[Na]_i+4(P_{Mg}/P_K).[Mg]_i+4(P_{Ca}/P_K).[Ca]_i$$

$$b = ([K]_i-[K]_o)+(P_{Cl}/P_K).([Cl]_o-[Cl]_i)+(P_{Na}/P_K).([Na]_i-[Na]_o)$$

$$= ([K]_i-[K]_o)-(P_{Cl}/P_K).([Cl]_i-[Cl]_o)+(P_{Na}/P_K).([Na]_i-[Na]_o)$$

$$c = -[K]_o-(P_{Cl}/P_K).[Cl]_i-(P_{Na}/P_K).[Na]_o-4(P_{Mg}/P_K).[Mg]_o-4(P_{Ca}/P_K).[Ca]_o$$

$[\alpha]$ denotes the ion activity, not concentration, of ion α.
Subscripts i and o refer to intracellular and extracellular activities respectively. P_i represents the permeability coefficient for ion i

Note that in this context square parentheses denote ion *activity, not* concentration. This nomenclature is unusual and could potentially lead to some confusion. However, in the expansion of the constant field equation, the letter a (commonly used to indicate ion activity) is a constant used in the standard form of a quadratic equation. Hence in this context square parentheses have been used in the literature to denote ion activity, though not normally considered the standard abbreviation.

A number of assumptions must be made in order to derive this equation. These may be summarised as follows:

(1) Ionic concentrations at the membrane surface are equal to those in the bulk solutions, ie. there are no unstirred or boundary layers.

(2) The intramembrane electric field is constant.

(3) Surface charges on both sides of the membrane are negligible.

In the present experiments, the intracellular solution contained only caesium ions and the extracellular solution only sodium and calcium ions. Under these conditions, the terms a, b and c reduce to:

$$a = [Cs]_i$$

$$b = [Cs]_i - [Na]_o.(P_{Na}/P_{Cs})$$

$$c = -[Na]_o.(P_{Na}/P_{Cs}) - 4[Ca]_o.(P_{Ca}/P_{Cs})$$

Note that in the source equations given above, permeability coefficients are given relative to that of potassium. The intracellular solution used in the experiments discussed here contained caesium instead of potassium ions. Permeabilities are therefore given relative to caesium rather than potassium.

Inserting numerical values for activities, one derives the following terms:

In Ca^{2+}-extracellular

$$a = 75.58$$

$$b = 75.58$$

$$c = -109.04(P_{Ca}/P_{Cs})$$

In Na^+/Ca^{2+}-extracellular

$a = 75.58$

$b = 75.58 - 37.09(P_{Na}/P_{Cs})$

$c = -37.09(P_{Na}/P_{Cs}) - 54.56(P_{Ca}/P_{Cs})$

In Na^+-extracellular

$a = 75.58$

$b = 75.58 - 80.19(P_{Na}/P_{Cs})$

$c = - 80.19(P_{Na}/P_{Cs}) - 1.16(P_{Ca}/P_{Cs})$

In order to derive the permeabilities of sodium and calcium relative to caesium one can take either of two approaches:

(1) (i) calculate P_{Ca}/P_{Cs} from the reversal potential in Ca^{2+}-extracellular, then, (ii) insert this value into the equations for the sodium-containing solutions to allow calculation of P_{Na}/P_{Cs} from the reversals in those solutions.

(2) (i) assume that the contribution of calcium to the reversal potential in Na^+-extracellular is negligible, which permits calculation of P_{Na}/P_{Cs} from the reversal potential in this solution, then, (ii) insert this value into the equation for Na^+/Ca^{2+}-extracellular to give P_{Ca}/P_{Cs}.

In the present work the latter approach was taken (see section 4.4.2.)

Values for P_{Ca}/P_{Na} were then calculated using the simple relation:

$P_{Ca}/P_{Na} = (P_{Ca}/P_{Cs}) / (P_{Na}/P_{Cs})$

7.5 - Currents with unusual kinetic characteristics

Currents recorded from magnocellular basal forebrain neurones sometimes displayed kinetics different from those described in sections 3.2.3 & 3.2.4. In these cells responses to bath-application of glutamate showed pronounced desensitization. In addition, upon removal of glutamate from the bath, current amplitude initially increased before returning to baseline. Similar kinetics were recorded using bath-, puffer- and stepper-applications. Examples are shown in figure 7.5.1. Similar kinetics were observed upon application of AMPA but not of kainate.

These kinetics were observed in a minority of cells, but were invariably present in either all or none of the cells in a given culture. Currents with these kinetics were observed during two periods each of several months, but never observed throughout the remaining time over which basal forebrain glutamate receptors were studied. It therefore seems likely that kinetics were determined by an ill-defined culture condition. The reasons for assuming that these kinetics were an artefact are as follows:

(i) Cultures were generally of very poor appearance with few magnocellular neurones and very large quantities of debris. In addition, cells often only weakly adhered to the culture dish.

(ii) Pipette-membrane seal resistance was generally very poor. In whole-cell configuration cells frequently possessed depolarised resting membrane potentials (approx. -40 to -50mV) and deteriorated after recording for a brief duration.

(iii) Despite many attempts, nucleated patches were never successfully pulled from these cells.

(iv) Currents recorded from these cells displayed very small steady-state amplitudes and were insensitive to cadmium and cobalt.

Data from cells with responses showing these kinetics was discarded, though the cause underlying these kinetics was investigated further. Current amplitudes were too small to reliably estimate membrane conductance changes

Figure 7.5.1

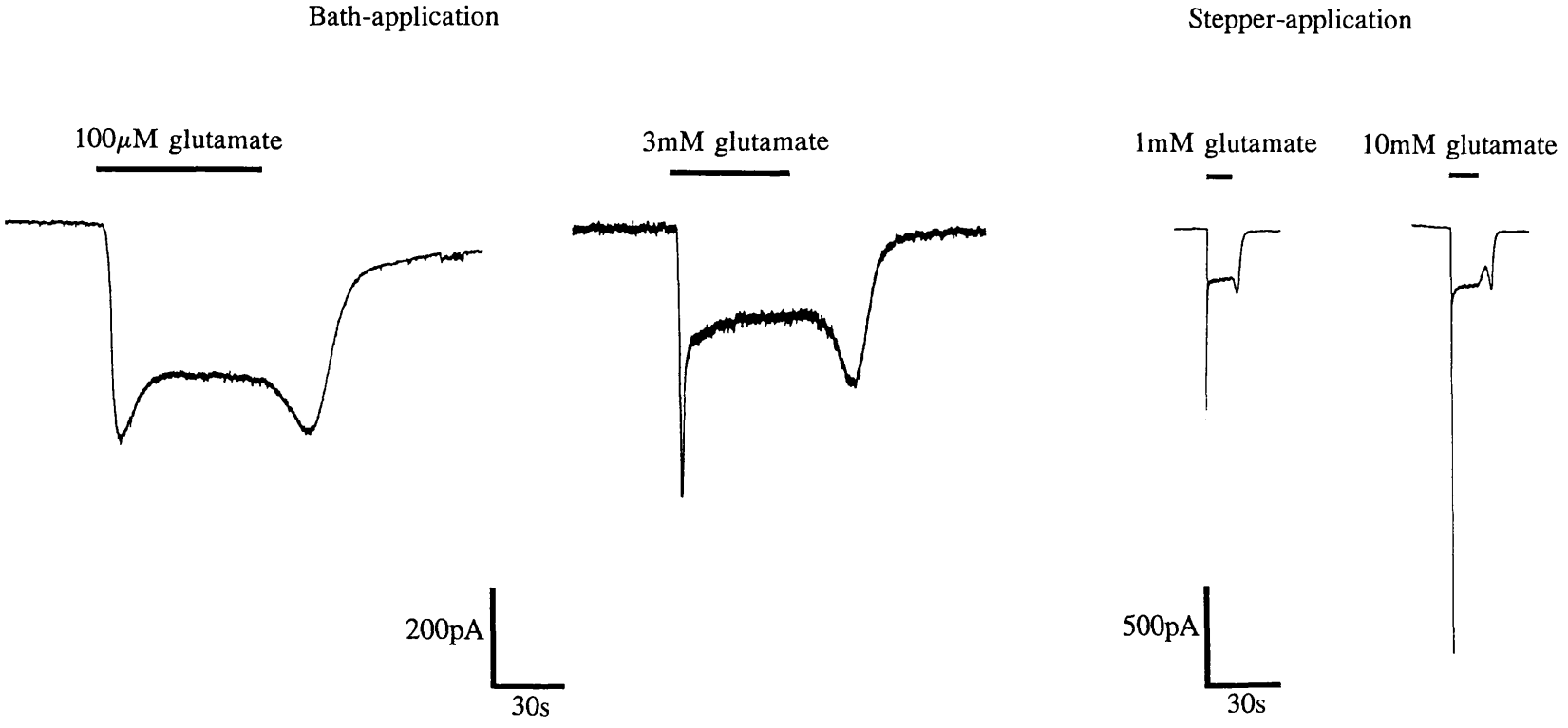
Bath-application
Stepper-application
100μM glutamate
3mM glutamate
1mM glutamate
10mM glutamate
200pA
30s
500pA
30s

during agonist applications so whether these changes in current amplitude during and after agonist application reflect increases or decreases of input resistance are unknown.

NMDA receptor activity was not responsible since all currents were recorded in the presence of 10-30μM AP5, higher concentrations having no additional effects. Reduction of the extracellular calcium concentration to 0.5mM likewise had no effect.

Possible involvement of a glutamate transporter was investigated using two approaches. The glutamate uptake inhibitor L-trans-pyrrolidine-2,4-dicarboxylic acid (L-trans-2,4-PDC) had no effect when bath-applied prior to, during and after glutamate application (300μM; n=4). This suggested that glutamate transport may not be involved, but was far from conclusive since it is possible that not all glutamate transporters are sensitive to this compound. In addition, L-trans-2,4-PDC inhibits transport of glutamate, but may not inhibit transporter-mediated anion flux which can occur independently of glutamate transport (Fairman, Vandenberg, Arriza, Kavanaugh & Amara, 1995; Wadiche, Amara & Kavanaugh, 1995; Dowd, Coyle, Rothstein, Pritchett & Robinson, 1996). In contrast D-aspartate stimulates both transport-coupled and -independent currents. Applied to basal forebrain neurones, 100μM D-aspartate generated very small inward currents (20-50pA; n=6) which were insensitive to AP5 (10-30μM; n=4) but did not influence the kinetics or amplitude of currents elicited by glutamate.

The role of metabotropic receptors was investigated using the agonists trans-ACPD and L-AP4. Neither altered responses to glutamate when used at 50 and 100μM respectively (n=4 each). In addition, replacing intracellular ATP and GTP with 1mM GDP-β-S did not influence responses to glutamate (n=3).

The mechanism underlying these kinetics therefore remains undetermined. Similar kinetics have been observed for the action of ACh at nicotinic acetylcholine receptors, where the mechanism is thought to be channel block by ACh (Maconochie & Steinbach, 1995). The response reaches a peak then declines as ACh blocks the channels. Upon removal of ACh from the bath,

current amplitude initially increases as channel block is relieved then decreases as ACh exits the agonist binding site. This mechanism is unlikely to be responsible at glutamate receptors in view of the net negative charge on the glutamate molecule.

Another possibility is that the receptor enters a desensitized state with very low agonist affinity. This hypothesis is consistent with the failure of kainate to cause this effect. In addition, these kinetics were more pronounced at higher glutamate concentrations: the effect was not observed with glutamate concentrations below approximately 30μM and the steady-state current amplitude decreased at high glutamate concentrations (even though peak current amplitude continued to rise). Dose-response curves for peak and steady-state currents to glutamate are illustrated in figure 7.5.2. This dose-dependence is consistent with a model in which the receptor enters a desensitized state at very high agonist concentrations and exits this state as the concentration of glutamate in the bath decreases upon termination of agonist application. Cyclothiazide increased steady-state relative to peak current amplitudes (n=2; data not shown) this also being consistent with such a hypothesis.

Figure 7.5.2

Peak current

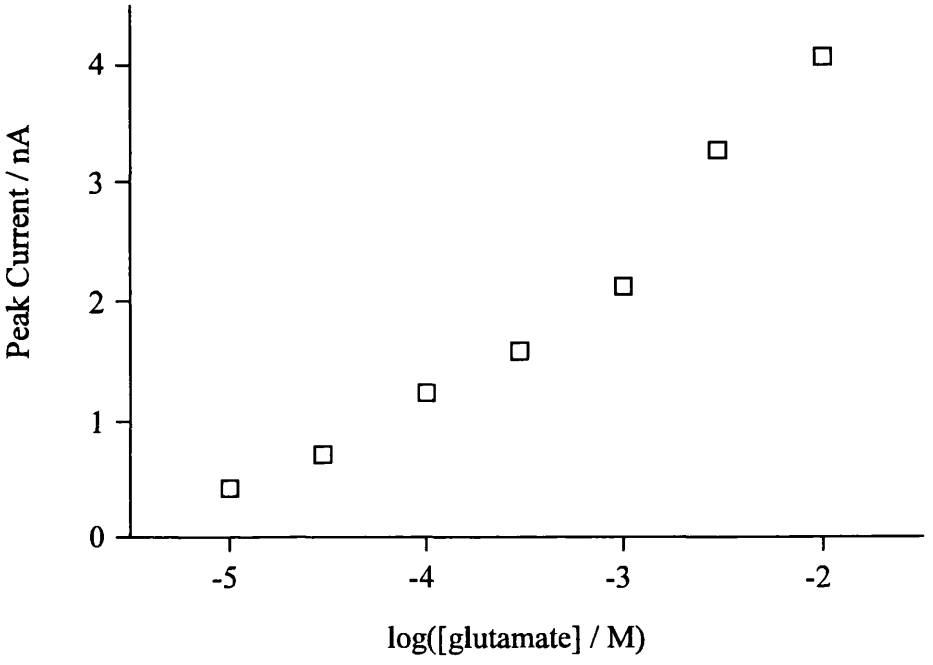

Steady-state current

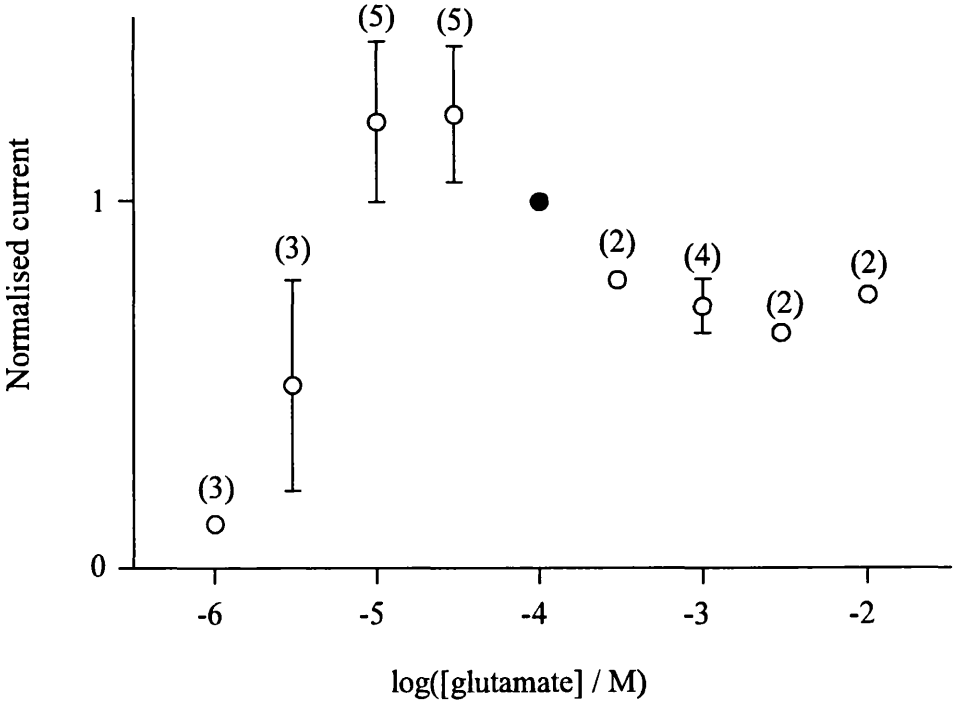

Acknowledgements

Thanks are due

to David Brown in whose laboratory the experiments were conducted,
to Eisai London Research for financial support,
to Eli Lilly for the gift of GYKI 53655
and particularly to Tim Allen and Joan Sim for teaching me the culture method and for consistent advice, interest and support

References

Allen, T.G.J. & Brown, D.A. (1993) J. Physiol. **466** 173-189. M_2 muscarinic receptor-mediated inhibition of the Ca^{2+} current in rat magnocellular cholinergic basal forebrain neurones.

Allen, T.G.J. & Brown, D.A. (1996) J. Physiol. **492.2** 453-466. Detection and modulation of acetylcholine release from neurites of rat basal forebrain cells in culture.

Allen, T.G.J., Sim, J.A. & Brown, D.A. (1993) J. Physiol. **460** 91-116. The whole-cell calcium current in acutely dissociated magnocellular cholinergic basal forebrain neurones of the rat.

Ammann, D., Bissig, R., Güggi, M., Pretsch, E., Simon, W., Borowitz, I.J. & Weiss, L. (1975) Helvetica Chimica Acta **58** 1535-1548. Preparations of neutral ionophores for alkali and alkaline earth metal cations and their applications in ion selective membrane electrodes.

Ascher, P. & Nowak, L. (1988) J. Physiol. **399** 247-266. The role of divalent cations in the N-methyl-D-aspartate responses of mouse central neurones in culture.

Ault, B., Evans, R.H., Francis, A.A., Oakes, D.J. & Watkins, J.C. (1980) J. Physiol. **307** 413-428. Selective depression of excitatory amino acid induced depolarizations by magnesium ions in isolated spinal cord preparations.

Bartus, R.T., Dean, R.L., Beer, B. & Lippa, A.S. (1982) Science **217** 408-417. The cholinergic hypothesis of geriatric memory dysfunction.

Bates, R.G., Staples, B.R. & Robinson, R.A. (1970) Analytical Chemistry **42** (8) 867-871. Ionic hydration and single ion activities in unassociated chlorides at high ionic strengths.

Bettler, B. & Mule, C. (1995) Neuropharmacology **34** (2) 123-139. AMPA and kainate receptors.

Bialowas, J. & Frotscher, M. (1987) J. Comp. Neurol. **259** 298-307. Choline acetyltransferase-immunoreactive neurons and terminals in the rat septal complex: a combined light and electron microscopic study.

Bleakman, D., Roback, J.D., Wainer, B.H., Miller, R.J. & Harrison, N.L. (1993) Brain Research **600** 257-267. Calcium homeostasis in rat septal neurons in tissue culture.

Boegman, R.J., Cockhill, J., Jhamandas, K. and Beninger, R.J. (1992) Neuroscience **51** (1) 129-135. Excitotoxic lesions of rat basal forebrain: differential effects on choline acetyltransferase in the cortex and amygdala.

Bowie, D. & Mayer, M. (1995) Neuron **15** 453-462. Inward rectification of both AMPA and kainate subtype glutamate receptors generated by polyamine-mediated ion channel block.

Bowman, W.C., Marshall, I.G., Gibb, A.J. & Harborne, A.J. (1988) TIPS **9** 16-20. Feedback control of transmitter release at the neuromuscular junction.

Brown, T.H. & Johnston, D. (1983) J. Neurophysiol. **50** (2) 464-486. Interpretation of voltage-clamp measurements in hippocampal neurons.

Burke, S.J., Yin, H. & Weiss, J.H. (1995) NeuroReport **6** 629-632. Ca^{2+} and *in vitro* kainate damage to cortical and hippocampal SMI-32(+) neurons.

Burnashev, N. (1996) Curr. Opin. Neurobiol. **6** 311-317. Calcium-permeability of glutamate-gated channels in the central nervous system.

Burnashev, N., Monyer, H., Seeburg, P.H. & Sakmann, B. (1992) Neuron **8** 189-198. Divalent ion permeability of AMPA receptor channels is dominated by the edited form of a single subunit.

Burnashev, N. & Sakmann, B. (1996) Biophys. J. **60** A78. RNA editing makes homomeric GluR6 subunit channels permeable to anions without altering the apparent size of the pore.

Burnashev, N., Schoepfer, R., Monyer, H., Ruppersberg, J.P., Günther, W., Seeburg, P.H. & Sakmann, B. (1992) Science **257** 1415-1419. Control by asparagine residues of calcium permeability and magnesium blockade in the NMDA receptor.

Burnashev, N., Villarroel, A. & Sakmann, B. (1996) J. Physiol. **496.1** 165-173. Dimensions and ion selectivity of recombinant AMPA and kainate receptor channels and their dependence on Q/R site residues.

Burnashev, N., Zhou, Z., Neher, E. & Sakmann, B. (1995) J. Physiol. **485** 403-418. Fractional calcium currents through recombinant GluR channels of the NMDA, AMPA and kainate receptor subtypes.

Butler, J.N. (1968) Biophys. J. **8** 1426-1433. The thermodynamic activity of calcium ion in sodium chloride-calcium chloride electrolytes.

Carnes, K.M., Fuller, T.A. & Price, J.L. (1990) J. Comp. Neurol. **302** 824-852. Sources of presumptive glutamatergic/aspartatergic afferents to the magnocellular basal forebrain in the rat.

Castellano, A. & López-Barneo, J. (1991) J. Gen. Physiol. **97** 303-320. Sodium and calcium currents in dispersed mammalian septal neurones.

Chavis, P., Fagni, L., Bochaert, J. & Lansman, J.B. (1995) Neuropharmacology **34** (8) 929-937. Modulation of calcium channels by metabotropic glutamate receptors in cerebellar granule cells.

Chavis, P., Shinozaki, H., Bockaert, J. & Fagni, L. (1994) J. Neurosci. **14** (11) 7067-7076. The metabotropic glutamate receptor types 2/3 inhibit L-type calcium channels via a pertussis toxin-sensitive G-protein in cultured cerebellar granule cells.

Chernevskaya, N.I., Obukhov, A.G. & Krishtal, O.A. (1991) Nature **349** 418-420. NMDA

receptor agonists selectively block N-type calcium channels in hippocampal neurons.

Chittajallu, R., Vignes, M., Dev, K.K., Barnes, J.M., Collingridge, G.L. & Henley, J.M. (1996) Nature **379** 78-81. Regulation of glutamate release by presynaptic kainate receptors in the hippocampus.

Choi, D. (1987) J. Neurosci. **7** (2) 369-379. Ionic dependence of glutamate neurotoxicity.

Choi, D. (1988) Neuron **1** 623-634. Glutamate neurotoxicity and diseases of the nervous system.

Choi, D.W. (1995) TINS **18** 58-60. Calcium: still center-stage in hypoxic-ischemic neuronal death.

Christie, B.R., Eliot, L.S., Ito, K.-I., Miyakawa, H. & Johnston, D. (1995) J. Neurophysiol. **73** 2553-2557. Different Ca^{2+} channels in soma and dendrites of hippocampal pyramidal neurons mediate spike-induced Ca^{2+} influx.

Collingridge, G.L. & Lester, R.A.J. (1989) Pharmacological Reviews **41** (2) 143-210. Excitatory amino acid receptors in the vertebrate central nervous system.

Cull-Candy, S.G. & Usowicz, M.M. (1987) Nature **325** 525-528. Multiple-conductance channels activated by excitatory amino acids in cerebellar neurons.

Curtis, D.R., Phillis, J.W. & Watkins, J.C. (1959) Nature **183** 611-612. Chemical excitation of spinal neurones.

Curtis, D.R., Phillis, J.W. & Watkins, J.C. (1960) J. Physiol. **150** 656-682. The chemical excitation of spinal neurones by certain acidic amino acids.

Davies, P. & Maloney, A.J.F. (1976) Lancet ii 1403. Selective loss of central cholinergic neurons in Alzheimer's disease.

Desai, M.A., Burnett, J.P., Ornstein, P.L. & Schoepp, D.D. (1995) Journal of Pharmacology and Experimental Therapeutics **272** (1) 38-43. Cyclothiazide acts at a site on the α-amino-3-hydroxy-methyl-4-isoxazole propionic acid receptor complex that does not recognise competitive or noncompetitive AMPA receptor antagonists.

Diamond, J.S. & Jahr, C.E. (1995) Neuron **15** 1097-1107. Asynchronous release of synaptic vesicles determines the time course of the AMPA receptor-mediated EPSC.

Dinopoulos, A., Parnavelas, J.G. & Eckenstein, F. (1986) J. Neurocytol. **15** 619-628. Morphological characterization of cholinergic neurons in the horizontal limb of the diagonal band of Broca in the basal forebrain of the rat.

Donevan, S.D. & Rogawski, M.A. (1993) Neuron **10** 51-59. GYKI 52466, a 2,3-benzodiazepine, is a highly selective, noncompetitive antagonist of AMPA/kainate receptor responses.

Donevan, S.D. & Rogawski, M.A. (1995) PNAS **92** 9298-9302. Intracellular polyamines mediate inward rectification of Ca^{2+}-permeable α-amino-3-hydroxy-5-methyl-4-isoxazolepropionic acid receptors.

Dowd, L.A., Coyle, A.J., Rothstein, J.D., Pritchett, D.B. & Robinson, M.B. (1996) Mol. Pharmacol. **49** 465-473. Comparison of Na^+-dependent glutamate transport activity in synaptosomes, C6 glioma, and *Xenopus* oocytes expressing excitatory amino acid carrier 1 (EAAC 1)

Dunnett, S.B., Whishaw, I.Q., Jones, G.H. & Bunch, S.T. (1987) Neuroscience **20** (2) 653-669. Behavioural, biochemical and histochemical effects of different neurotoxic amino acids injected into nucleus basalis magnocellularis of rats.

Dunnett, S.B., Everitt, B.J. & Robbins, T.W. (1991) TINS **14** (11) 494-501. The basal forebrain-cortical cholinergic system: interpreting the functional consequences of excitotoxic lesions.

Edmonds, B., Gibb, A.J. & Colquhoun, D. (1995) Ann. Rev. Physiol. **57** 495-519. Mechanisms of activation of glutamate receptors and the the time course of excitatory synaptic currents.

Fairman, W.A., Vandenberg, R.J., Arriza, J.L., Kavanaugh, M.P. & Amara, S.G. (1995) Nature **375** 599-603. An excitatory amino-acid transporter with properties of a ligand-gated chloride channel.

Ferrer-Montiel, A.V., Sun, W. & Montal, M. (1996) Biophys. J. **71** 749-758. A single tryptophan on M2 of glutamate receptor channels confers high permeability to divalent cations.

Frankenhäuser, B. (1960) J. Physiol. **152** 159-166. Sodium permeability in toad nerve and in squid nerve.

Frederickson, C.J. & Danscher, G. (1990) Progress in Brain Research **83** 71-84. Zinc-containing neurons in hippocampus and related CNS structures.

Gahwiler, B.H. & Brown, D.A. (1985) Nature **313** 577-579. Functional innervation of cultured hippocampal neurones by cholinergic afferents from co-cultured septal explants.

Garaschuk, O., Schneggenburger, R., Schirra, C., Tempia, F. & Konnerth, A. (1996) J. Physiol. **491.3** 757-772. Fractional calcium currents through somatic and dendritic glutamate receptor channels of rat hippocampal CA1 pyramidal neurones.

Gilbertson, T.A., Scobey, R. & Wilson, M. (1991) Science **251** 1613-1615. Permeation of calcium ions through non-NMDA glutamate channels in retinal bipolar cells.

Goldman, D.E. (1943) J. Gen. Physiol. **27** 37-60. Potential, impedance, and rectification in membranes.

Gorelova, N. & Reiner, P. (1996) J. Neurophysiol. **75** (2) 695-706. Role of the afterhyperpolarization in control of discharge properties of septal cholinergic neurons in vitro.

Green, W.N. & Anderson, O.S. (1991) Ann. Rev. Physiol. **53** 341-59. Surface charges and ion channel function.

Griffith, W.H., Taylor, L. & Davis, M.J. (1994) J. Neurophysiol. **71** (6) 2359-2376. Whole-cell and single-channel calcium currents in guinea pig basal forebrain neurons.

Gu, J.G., Albuquerque, C., Lee, C.J. & MacDermott, A.B. (1996) Nature **381** 793-796. Synaptic strengthening through activation of Ca^{2+}-permeable AMPA receptors.

Gu, Y. & Huang, L.-Y. M. (1991) Neuron **6** 777-784. Block of kainate receptor channels by Ca^{2+} in isolated spinal trigeminal neurons of rat.

Hamill, O.P., Marty, A., Neher, E., Sakmann, B. & Sigworth, F.J. (1981) Pflügers Archiv **391** 85-100. Improved patch-clamp techniques for high-resolution current recording from cells and cell-free membrane patches.

Hartmann, H., Eckert, A. & Müller, W.E. (1993) Biochem. Biophys. Res. Comm. **194** (3) 1216-1220. β-amyloid protein amplifies calcium signalling in central neurons from the adult mouse.

Hay, M. & Kunze, D.L. (1994) J. Neurophysiol. **72** (1) 421-430. Glutamate metabotropic receptor inhibition of voltage-gated calcium currents in visceral sensory neurons.

Hayashi, T. (1954) Keio Journal of Medicine **3** (4) 183-192. Effects of sodium glutamate on the nervous system.

Hille, B. (1992) Ionic channels of excitable membranes (2nd edn.) Pub.: Sinauer Associates Inc., Sunderland Massachusetts.

Hodgkin, A.L. & Katz, B. (1949) J. Physiol. **108** 37-77. The effect of sodium ions on the electrical activity of the giant axon of the squid.

Hollmann, M., Hartley, M. & Heinemann, S. (1991) Science **252** 851-853. Ca^{2+}-permeability of KA-AMPA-gated glutamate receptor channels depends on subunit composition.

Hollmann, M. & Heinemann, S. (1994) Ann. Rev. Neurosci. **17** 31-108. Cloned glutamate receptors.

Hollmann, M., O'Shea-Greenfield, A., Rogers, S.W. & Heinemann, S. (1989) Nature **342** 643-648. Cloning by functional expression of a member of the glutamate receptor family.

Honoré, T., Davies, S.N., Drejer, J., Fletcher, E.J., Jacobsen, P., Lodge, D. & Nielsen, F.E. (1988) Science **241** 701-703. Quinoxalinediones: potent competitive non-NMDA glutamate receptor antagonists.

Huettner, J.E. (1990) Neuron **5** 255-266. Glutamate receptor channels in rat DRG neurons: activation by kainate and quisqualate and blockade of desensitization by Con A.

Hume, R.I., Dingledine, R. & Heinemann, S.F. (1991) Science **253** 1028-1030. Identification of a site in glutamate receptor subunits that controls calcium permeability.

Ikonomovic, M.D., Sheffield, R. & Armstrong, D.M. (1995) Society for Neuroscience Abstracts 722.1. Selective vulnerability of neurons in the human nucleus basalis of Meynert: putative role of an age-related decrease in GluR2/3 receptor subunit immunoreactivity.

Iino, M., Ozawa, S. & Tsuzuki, K. (1990) J. Physiol. **424** 151-165. Permeation of calcium through excitatory amino acid receptor channels in cultured rat hippocampal neurones.

Ingham, C.A., Bolam, J.P., Wainer, B.H. & Smith, A.D. (1985) J. Comp. Neurol. **239** 176-192. A correlated light and electron microscopic study of identified cholinergic basal forebrain neurons that project to the cortex in rat.

Isa, T., Iino, M., Itazawa, S. & Ozawa, S. (1995) NeuroReport **6** 2045-2048. Spermine mediates inward rectification of Ca^{2+}-permeable AMPA receptor channels.

Jahr, C.E. & Stevens, C.F. (1987) Nature **325** 522-525. Glutamate activates multiple single channel conductances in hippocampal neurones.

Jahr, C.E. & Stevens, C.F. (1993) PNAS **90** 11573-11577. Calcium permeability of the N-methyl-D-aspartate receptor channel in hippocampal neurons in culture.

Jasek, M.C. & Griffith, W.H. (1995) Society for Neuroscience Abstracts 145.3. Pharmacological characterization of ionotropic glutamate receptors in basal forebrain neurons of young and aged F344 rats.

Johansen, T.H., Chaudhary, A. & Verdoorn, T.A. (1995) Mol. Pharmacol. **48** 946-955. Interactions among GYKI-52466, cyclothiazide, and aniracetam at recombinant AMPA and kainate receptors.

Jonas, P., Racca, C., Sakmann, B., Seeburg, P.H. & Monyer, H. (1994) Neuron **12** 1281-1289. Differences in Ca^{2+} permeability of AMPA-type glutamate receptor channels in neocortical neurons caused by differential GluR-B subunit expression.

Jonas, P. & Sakmann, B. (1992) J. Physiol. **455** 143-171. Glutamate receptor channels in isolated patches from CA1 and CA2 pyramidal cells of rat hippocampal slices.

Kamboj, S.K., Swanson, G.T & Cull-Candy, S.G. (1995) J. Physiol. **486** 297-304. Intracellular spermine confers rectification on rat calcium permeable AMPA and kainate receptors.

Kessler, M., Arai, A., Quan, A. & Lynch, G. (1996) Mol. Pharmacol. **49** 123-131. Effect of cyclothiazide on binding properties of AMPA-type glutamate receptors: lack of competition between cyclothiazide and GYKI 52466.

Kielland, J. (1937) Journal of the American Chemical Society **59** 1675-1678. Individual activity coefficients of ions in aqueous solutions.

Koh, D.-S., Burnashev, N. & Jonas, P. (1995) J. Physiol. **486** 305-312. Block of native Ca^{2+}-permeable AMPA receptors in rat brain by intracellular polyamines generates double rectification.

Koh, D.-S., Geiger, J.R.P., Jonas, P. & Sakmann, B. (1995) J.Physiol. **485** 383-402. Ca^{2+}-permeable AMPA and NMDA receptor channels in basket cells of rat hippocampal dentate gyrus.

Koh, J. Yang, L. & Cotman, C.W. (1990) Brain Research **533** 315-320. β-amyloid protein increases the vulnerability of cultured cortical neurons to excitotoxic damage.

Kumamoto, E. & Murata, Y. (1995a) Neuroscience **69** (2) 477-493. Excitatory amino acid-induced currents in rat septal cholinergic neurons in culture.

Kumamoto, E. & Murata, Y. (1995b) J. Neurophysiol. **74** (5) 2012-2027. Characterization of GABA current in rat septal cholinergic neurons in culture and its modulation by metal cations.

Kumamoto, E. & Murata, Y. (1996) J. Neurophysiol. **76** (1) 227-241. Glycine current in rat septal cholinergic neurons in culture: monophasic positive modulation by Zn^{2+}.

Kyrozis, A., Goldstein, P.A., Heath, M.J.S. & MacDermott, A.B. (1995) J. Physiol. **485.2** 373-381. Calcium entry through a subpopulation of AMPA receptors desensitized neighbouring NMDA receptors in rat dorsal horn neurons.

Lee, K.S. & Tsien, R.W. (1984) J. Physiol. **354** 253-272. High selectivity of calcium channels in single dialysed heart cells of the guinea pig.

Lemann, W. & Saper, C.B. (1985) Brain Research **334** 339-343. Evidence for a cortical projection to the magnocellular basal nucleus in the rat: an electron microscopic axonal transport study.

Lerma, J., Morales, M., Vicente, M.A., Herreras, O. (1997) TINS **20** (1) 9-12. Glutamate receptors of the kainate type and synaptic transmission.

Lerma, J., Paternain, A.V., Naranjo, J.R. & Mellström, B. (1993) PNAS **90** 11688-11692. Functional kainate-selective glutamate receptors in cultured hippocampal neurones.

Lester, R.A.J. & Jahr, C.E. (1990) Neuron **4** 741-749. Quisqualate receptor-mediated depression of calcium currents in hippocampal neurons.

Lewis, C.A. (1979) J. Physiol. **286** 417-445. Ion-concentration dependence of the reversal potential and the single channel conductance of ion channels at the frog neuromuscular junction.

Lindefors, N., Boatell, M.L., Mahy, N. & Persson, H. (1992) Neurosci. Lett. **135** 262-264. Widespread neuronal degeneration after ibotenic acid lesioning of cholinergic neurons in the nucleus basalis revealed by *in situ* hybridization.

Maconochie, D.J. & Steinbach, J.H. (1995) Journal of General Physiology **106** 113-147. Block by acetylcholine of mouse muscle nicitinic receptors, stably expressed in fibroblasts.

Magee, J.C. & Johnston, D. (1995) J. Physiol. **487** 67-90. Characterization of single voltage-gated Na^+ and Ca^{2+} channels in apical dendrites of rat CA1 pyramidal neurons.

Mahy, N., Bendahan, G., Boatell, M.L., Bjelke, B., Tinner, B., Olson, L. & Fuxe, K. (1995) Neuroscience **65** (1) 15-25. Differential brain area vulnerability to long-term subcortical excitotoxic lesions.

Mann, D.M.A. (1988) Neuropathological and neurochemical aspects of Alzheimer's disease. In: Psychopharmacology of the aging nervous system, Handbook of Psychopharmacology **20**, Iversen, L.L., Iversen, S.D. & Snyder, S.H. (Eds.) pp. 1-67 Pub. Plenum Press,

New York & London.

Markram, H. & Segal, M. (1990) Brain Research **513** 171-174. Electrophysiological characteristics of cholinergic and non-cholinergic neurons in the rat medial septum-diagonal band complex.

Martin, L.J., Blackstone, C.D., Levey, A.I., Huganir, R.L. & Price, D.L. (1993) J. Neurosci. **13** (5) 3349-2263. Cellular localizations of AMPA glutamate receptors within the basal forebrain magnocellular complex of rat and monkey.

Mattson, M.P. (1990) Neuron **4** 105-117. Antigenic changes similar to those seen in neurofibrillary tangles are elicited by glutamate and Ca^{2+} influx in cultured hippocampal neurons.

Mattson, M.P., Cheng, B., Davis, D., Bryant, K., Lieberburg, I. & Rydel, R.E., (1992) J. Neurosci. **12** (2) 376-389. β-amyloid peptides destabilize calcium homeostasis and render human cortical neurons vulnerable to excitotoxicity.

Mattson, M.P., Barger, S.W., Cheng, B., Lieberburg, I., Smith-Swintosky, V.L. & Rydel, R.E. (1993) TINS **16** (10) 409-414. β-amyloid precursor protein metabolites and loss of neuronal Ca^{2+} homeostasis in Alzheimer's disease.

Mayer, M.L. & Vyklicky, L. (1989) PNAS **86** 1411-1415. Concanavalin A selectively reduces desensitization of mammalian neuronal quisqualate receptors.

Mayer, M.L., Vyklicky, L. & Westbrook, G.L. (1989) J. Physiol. **415** 329-350. Modulation of excitatory amino acid receptors by group IIB metal cations in cultured mouse hippocampal neurones.

Mayer, M.L. & Westbrook, G.L. (1987a) J. Physiol. **394** 501-527. Permeation and block of N-methyl-D-aspartic acid receptor channels by divalent cations in mouse cultured central neurones.

Mayer, M.L. & Westbrook, G.L. (1987b) Progress in Neurobiology **28** 197-276. The physiology of excitatory amino acids in the vertebrate central nervous system.

McAlonan, G.M., Dawson, G.R., Wilkinson, L.O., Robbins, T.W. & Everitt, B.J. (1995) Eur. J. Neurosci. **7** 1034-1049. The effects of AMPA-induced lesions of the medial septum and vertical limb nucleus of the diagonal band of Broca on spatial delayed non-matching to sample and spatial learning in the water maze.

McBain, C.J. & Mayer, M.L. (1994) Physiological Reviews **74** (3) 723-760. N-methyl-D-aspartic acid receptor structure and function.

McGhee, D.S., Heath, M.J.S., Gelber, S., Devay, P. & Role, L.W. (1995) Science **269** 1692-1696. Nicotine enhancement of fast excitatory synaptic transmission in CNS by presynaptic receptors.

Mesulam, M.-M. (1995) Seminars in the Neurosciences **7** 297-307. The cholinergic contribution to neuromodulation in the cerebral cortex.

Moises, H.C., Womble, M.D., Washburn, M.S. & Williams, L.R. (1995) J. Neurosci. **15** (12) 8131-8142. Nerve growth factor facilitates cholinergic neurotransmission between nucleus basalis and the amygdala in rat: an electrophysiological analysis.

Momiyama, T., Sim, J.A. & Brown, D.A. (1996) J. Physiol. **495.1** 97-106. Dopamine D_1-like receptor-mediated presynaptic inhibition of excitatory transmission onto rat magnocellular basal forebrain neurones.

Monaghan, D.T., Bridges, R.J. & Cotman, C.W. (1989) Ann. Rev. Pharmacol. Toxicol. **29** 365-402. The excitatory amino acid receptors: their classes, pharmacology, and distinct properties in the function of the central nervous system.

Mosbacher, J., Schoepfer, R., Monyer, H., Burnashev, N., Seeburg, P.H. & Ruppersberg, J.P. (1994) Science **266** 1059-1062. A molecular determinant for submillisecond desensitization in glutamate receptors.

Murchison, D. & Griffith, W.H. (1995) J. Neurophysiol. **74** (2) 876-887. Low-voltage activated calcium currents increase in basal forebrain neurons from aged rats.

Murchison, D. & Griffith, W.H. (1996) J. Neurophysiol. **76** (1) 158-174. High voltage-activated calcium currents in basal forebrain neurons during aging.

Nakajima, Y., Nakajima, S., Obata, K., Carlson, C.G. & Yamaguchi, K. (1985) PNAS **82** 6325-6329. Dissociated cell culture of cholinergic neurons from nucleus basalis of Meynert and other basal forebrain nuclei.

Nakazawa, K. & Hess, P. (1993) J. Gen. Physiol. **101** 377-392. Block by calcium of ATP-activated channels in Pheochromocytoma cells.

Nicoll, R.A., Kauer, J.A. & Malenka, R.C. (1988) Neuron **1** 97-103. The current excitement in long-term potentiation.

Nicoll, R.A. & Malenka, R.C. (1995) Nature **377** 115-118. Contrasting properties of two forms of long-term potentiation in the hippocampus.

Nistri, A. & Cherubini, E. (1991) J. Physiol. **435** 465-481. Depression of a sustained calcium current by kainate in rat hippocampal neurones *in vitro*.

Ohishi, H., Shigemoto, R., Nakanishi, S. & Mizuno, N. (1933a) Neuroscience **53** (4) 1009-1118. Distribution of the messenger RNA for a metabotropic glutamate receptor, mGluR2, in the central nervous system of the rat.

Ohishi, H., Shigemoto, R., Nakanishi, S. & Mizuno, N. (1933b) J. Comp. Neurol. **335** 252-266. Distribution of the mRNA for a metabotropic glutamate receptor (mGluR3) in the rat brain: an *in situ* hybridization study.

Otis, T.S., Raman, I.M. & Trussell, L.O. (1995) J. Physiol. **482.2** 309-315. AMPA receptors with high Ca^{2+} permeability mediate synaptic transmission in the avian auditory pathway.

Ouardouz, M. & Durand, J. (1991) Neuroscience Letters **125** 5-8. GYKI 52466 antagonizes

glutamate responses but not NMDA and kainate responses in rat abducens motoneurones.

Ozawa, S., Iino, M. & Tsuzuki, K. (1991) J. Neurophysiol. **66** (1) 2-11. Two types of kainate response in cultured rat hippocampal neurons.

Page, K.J., Sirinathsinghji, D.J.S. & Everitt, B.J. (1995) Eur. J. Neurosci. **7** 1012-1021. AMPA-induced lesions of the basal forebrain differentially affect cholinergic and non-cholinergic neurons: lesion assessment using quantitative *in situ* hybridization histochemisty.

Page, K.J. & Everitt, B.J. (1995) Eur. J. Neurosci. **7** 1022-1033. The distribution of neurons coexpressing immunoreactivity to AMPA-sensitive glutamate receptor subtypes (GluR1-4) and nerve growth factor receptor in the rat basal forebrain.

Partin, K.M., Bowie, D. & Mayer, M.L. (1995) Neuron **14** 833-843. Structural determinants of allosteric regulation in alternatively spliced AMPA receptors.

Partin, K.M., Fleck, M.W. & Mayer, M.L. (1996) J. Neurosci. **16** (21) 6634-6647. AMPA receptor flip/flop mutants affecting deactivation, desensitization, and modulation by cyclothiazide, aniracetam, and thiocyanate.

Partin, K.M. & Mayer, M.L. (1996) Mol. Pharmacol. **49** 142-148. Negative allosteric modulation of wild-type and mutant AMPA receptors by GYKI 53655.

Partin, K.M., Patneau, D.K. & Mayer, M.L. (1994) Mol. Pharmacol. **46** 129-138. Cyclothiazide differentially modulates desensitization of α-amino-3-hydroxy-5-methyl-4-isoxazolepropionic acid receptor splice variants.

Partin, K.M., Patneau, D.K., Winters, C.A., Mayer, M.L. & Buonanno, A. (1993) Neuron **11** 1069-1082. Selective modulation of desensitization at AMPA versus kainate receptors by cyclothiazide and concanavalin A.

Paternain, A.V., Morales, M. & Lerma, J. (1995) Neuron **14** 185-189. Selective antagonism of AMPA receptors unmasks kainate receptor-mediated responses in hippocampal neurons.

Patneau, D.K., Vyklicky, L. & Mayer, M.L. (1993) J. Neurosci. **13** (8) 3496-3509. Hippocampal neurons exhibit cyclothiazide-sensitive rapidly desensitizing responses to kainate.

Perry, E.K., Tomlinson, B.E., Blessed, G., Bergmann, K., Gibson, P.H. & Perry, R.H. (1978) British Medical Journal **2** 1457-1459. Correlation of cholinergic abnormalities with senile plaques and mental test scores in senile dementia.

Petralia, R.S., Wang, Y.-X. & Wenthold, R.J. (1994a) J. Comp. Neurol. **349** 85-110. Histological and ultrastructural localization of the kainate receptor subunits, KA2 and GluR6/7, in the rat nervous system using selective antipeptide antibodies.

Petralia, R.S., Wang, Y.-X. & Wenthold, R.J. (1994b) J.Neurosci. **14** (10) 6102-6120. The NMDA receptor subunits NR2A and NR2B show histological and ultrastructural

localization patterns similaar to those of NR1.

Petralia, R.S., Yokotani, N. & Wenthold, R.J. (1994) J. Neurosci. **14** (2) 667-696. Light and electron microscope distribution of the NMDA receptor subunit NMDAR1 in the rat nervous system using a selective anti-peptide antibody.

Petrozzino, J.J., Pozzo-Miller, L.D. & Connor, J.A. (1995) Neuron **14** 1223-1231. Micromolar Ca^{2+} transients in dendritic spines of hippocampal pyramidal neurons in brain slice.

Piek, T. (1979) Ionic and electrical properties. In: Insect muscle, Usherwood, E.N.R., (Ed.) pp.281-336. Pub. Accademic Press, London, New York and San Francisco.

Pin, J.-P. & Duvoisin, R. (1995) Neuropharmacology **34** (1) 1-26. The metabotropic glutamate receptors: structure and functions.

Pitzer, K.S. & Mayorga, G. (1973) Journal of Physical Chemistry **77** (19) 2300-2307. Thermodynamics of electrolytes II. Activity and osmotic coefficients for strong electrolytes with one or both ions univalent.

Price, D.L. (1986) Ann. Rev. Neurosci. **9** 489-512. New perspectives on Alzheimer's disease.

Roche, K.W., O'Brien, R.J., Mammen, A.L., Bernhardt, J. & Huganir, R.L. (1996) Neuron **16** 1179-1188. Characterization of multiple phosphorylation sites on the AMPA receptor GluR1 subunit.

Roche, K.W., Tingley, W.G. & Huganir, R.L. (1994) Curr. Opin. Neurobiol. **4** 383-388. Glutamate receptor phosphorylation and synaptic plasticity.

Rogers, M. & Dani, J.A. (1995) Biophys. J. **68** 501-506. Comparison of quantitative calcium flux through NMDA, ATP, and ACh receptor channels.

Rörig, B. & Grantyn, R. (1993) Neurosci. Lett. **153** 32-36. Rat retinal ganglion cells express Ca^{2+}-permeable non-NMDA glutamate receptors during the period of histogenetic cell death.

Ruppersberg, J.P., Mosbacher, J., Günther, W., Schoepfer, R. & Fakler, B. (1993) Biochemical Pharmacology **46** (11) 1877-1885. Studying block in cloned N-methyl-D-aspartate (NMDA) receptors.

Sahara, Y. & Westbrook, G. (1993) **13** (7) 3041-3050. Modulation of calcium currents by a metabotropic glutamate receptor involves fast and slow kinetic components in cultured hippocampal neurons.

Saper, C.B. (1988) Chemical neuroanatomy of Alzheimer's disease. In: Psychopharmacology of the aging nervous system, Handbook of Psychopharmacology **20** Iversen, L.L., Iversen, S.D. & Snyder, S.H. (Eds.) pp. 131-156. Pub. Plenum Press, New York & London.

Sather, W., Dieudonné, S., MacDonald, J.F. & Ascher, P. (1992) J. Physiol. **450** 643-672. Activation and desensitization of N-methyl-D-aspartate receptors in nucleated outside-out patches from mouse neurones.

Sautière, P.-E., Sindou, P., Couratier, P., Hugon, J., Wattez, A. & Delacourte, A. (1992) Neurosci. Lett. **140** 206-210. Tau antigenic changes induced by glutamate in rat primary culture model: a biochemical approach.

Sayer, R.J., Schwindt, P.C. & Crill, W.E. (1992) J. Neurophysiol. **68** (3) 833-842. Metabotropic glutamate receptor-mediated suppression of L-type calcium current in acutely isolated neocortical neurons.

Schneggenburger, R. (1996) Biophys. J. **70** 2165-2174. Simultaneous measurement of Ca^{2+} influx and reversal potentials in recombinant N-methyl-D-aspartate receptor channels.

Schneggenburger, R., Tempia, F. & Konnerth, A. (1993) Neuropharmacology **32** (11) 1221-1228. Glutamate- and AMPA-mediated calcium influx through glutamate receptor channels in medial septal neurons.

Schneggenburger, R., Zhou, Z., Konnerth, A. & Neher, E. (1993) Neuron **11** 133-143. Fractional contribution of calcium to the cation current through glutamate receptor channels.

Seeburg, P.H. (1993) TINS **16** (9) 359-365. The molecular biology of mammalian glutamate receptor channels.

Selkoe, D.J. (1991) Neuron **6** 487-498. The molecular pathology of Alzheimer's disease.

Selkoe, D.J. (1994) Ann. Rev. Neurosci. **17** 489-517. Normal and abnormal biology of the β-amyloid precursor protein.

Shigemoto, R., Nakanishi, S. & Mizuno, N. (1992) J. Comp. Neurol. **322** 121-135. Distribution of the mRNA for a metabotropic glutamate receptor (mGluR1) in the central nervous system: an *in situ* hybridization study in adult and developing rat.

Shirasaki, T., Harata, N. & Akaike, N. (1994) J. Physiol. **475.3** 439-453. Metabotropic glutamate responses in acutely dissociated hippocampal CA1 pyramidal neurones of the rat.

Sim, J.A. (1994) J. Physiol. **480P** 33P-34P. Maintained morphology of rat magnocellular cholinergic basal forebrain neurones in culture.

Sommer, B., Burnashev, N., Verdoorn, T.A., Keinänen, K., Sakmann, B. & Seeburg, P.H. (1992) EMBO Journal **11** (4) 1651-1656. A glutamate receptor channel with high affinity for domoate and kainate.

Sommer, B., Keinänen, K., Verdoorn, T.A., Wisden, W., Burnashev, N., Herb, A., Köhler, M., Takagi, T., Sakmann, B. & Seeburg, P.H. (1990) Science **249** 1580-1585. Flip and flop: a cell-specific functional switch in glutamate-operated channels of the CNS.

Sommer, B., Köhler, M., Sprengel, R. & Seeburg, P.H. (1991) Cell **67** 11-20. RNA editing in brain controls a determinant of ion flow in glutamate-gated channels.

Spangler, S. (1975) Alabama Journal of Medical Sciences **2** (9) 218-223. Expansion of the constant field equation to include both divalent and monovalent ions.

Spruston, N., Jonas, P. & Sakmann, B. (1995) J. Physiol. **482** 325-352. Dendritic glutamate receptor channels in rat hippocampal CA3 and CA1 pyramidal neurons.

Stanfield, P.R., Nakajima, Y. & Yamaguchi, K. (1985) Nature **315** 491-501. Substance P raises neuronal membrane excitability by reducing inward rectification.

Stein, E., Cox, J.A., Seeburg, P.H. & Verdoorn, T.A. (1992) Mol. Pharmacol. **42** 864-871. Complex pharmacological properties of recombinant α-amino-3-hydroxy-5-methyl-4-isoxazole propionate receptor subtypes.

Swartz, K.J. & Bean, B.P. (1992) J. Neurosci. **12** (11) 4358-4371. Inhibition of calcium channels in rat CA3 pyramidal neurons by a metabotropic glutamate receptor.

Szatkowski, M. & Attwell, D. (1994) TINS **17** (9) 359-365. Triggering and execution of neuronal death in brain ischaemia: two phases of glutamate release by different mechanisms.

Takano, K., Stanfield, P.R., Nakajima, S. & Nakajima, Y. (1995) Neuron **14** 999-1008. Protein kinase C-mediated inhibition of an inward rectifier potassium channel by substance P in nucleus basalis neurons.

Tarnawa, I., Farkas, S., Berzsenyi, P., Pataki, A. & Andrási, F. (1989) Eur. J. Pharmacol. **167** 193-199. Electrophysiological studies with a 2,3-benzodiazepine muscle relaxant: GYKI 52466.

Torres, E.M., Perry, T.A., Blokland, A., Wilkinson, L.S., Wiley, R.G., Lappi, D.A. & Dunnett, S.B. (1994) Neuroscience **63** (1) 95-122. Behavioural, histochemical and biochemical consequences of selective immunolesions in discrete regions of the basal forebrain system.

Trombley, P.Q. & Westbrook, G.L. (1992) J. Neurosci. **12** (6) 2043-2050. L-AP4 inhibits calcium currents and synaptic transmission via a G-protein-coupled glutamate receptor.

Verdoorn, T.A, Burnashev, N., Monyer, H., Seeburg, P.H. & Sakmann, B. (1991) Science **252** 1715-1718. Structural determinants of ion flow through recombinant glutamate receptor channels.

Wadiche, J.I., Amara, S.G. & Kavanaugh, M.P. (1995) Neuron **15** 721-728. Ion fluxes associated with excitatory amino acid transport.

Wainer, B.H. & Mesulam, M.-M. (1990) Ascending cholinergic pathways in the rat brain. In: Brain Cholinergic Systems, Steriade, M. & Biesold, D. (Eds.) Pub. Oxford University Press, New York.

Walker, L.C., Tigges, M. & Tigges, J. (1983) J. Comp. Neurol. **217** 158-166. Ultrastructure of neurons in the nucleus basalis of Meynert in squirrel monkey.

Watanabe, S., Kusama-Eguchi, K., Kobayashi, H. & Igarashi, K. (1991) Journal of Biological Chemistry **266** 20803-20809. Estimation of polyamine binding to macromolecules and ATP in bovine lymphocytes and rat liver.

Watkins, J.C., Krogsgaard-Larsen, P. & Honoré, T., (1990) TIPS **11** 25-33. Structure-activity relationships in the development of excitatory amino acid receptor agonists and competitive antagonists.

Weiss, J.H., Yin, H.-Z. & Choi, D.W. (1994) Neuroscience **60** (3) 659-664. Basal forebrain cholinergic neurons are selectively vulnerable to AMPA/kainate receptor-mediated neurotoxicity.

Whitehouse, P.J., Price, D., Struble, R.G., Clark, A.W., Coyle, J.T. & DeLong, M.R. (1982) Science **215** 1237-1239. Alzheimer's disease and senile dementia: loss of neurons in the basal forebrain.

Wilding, T.J. & Huettner, J.E. (1995) Mol. Pharmacol. **47** 582-587. Differential antagonism of α-amino-3-hydroxy-5-methyl-4-isoxazolepropionic acid-preferring and kainate-preferring receptors by 2,3-benzodiazepines.

Wilding, T.J. & Huettner, J.E. (1996) Mol. Pharmacol. **49** 540-546. Antagonist pharmacology of kainate- and α-amino-3-hydroxy-5-methyl-4-isoxazolepropionic acid-preferring receptors.

Wo, Z.G. & Oswald, R.E. (1994) PNAS **91** 7154-7158. Transmembrane topology of two kainate receptor subunits revealed by N-glycosylation.

Wong, L.A. & Mayer, M.L. (1993) Mol. Pharmacol. **44** 504-510. Differential modulation by cyclothiazide and concanavalin A of desensitization at native α-amino-3-hydroxy-5-methyl-4-isoxazolepropionic acid and kainate-preferring glutamate receptors.

Yamada, K.A. & Tang, C.-M. (1993) J. Neurosci. **13** (9) 3904-3915. Benzothiadiazides inhibit rapid glutamate receptor desensitization and enhance glutamatergic synaptic currents.

Yamaguchi, K., Nakajima, Y., Nakajima, S. & Stanfield, P.R. (1990) J. Physiol. **426** 499-520. Modulation of inwardly rectifying channels by substance P in cholinergic neurones from rat brain in culture.

Yankner, B.A. (1996) Neuron **16** 921-932. Mechanisms of neuronal degeneration in Alzheimer's disease.

Yin, H.-Z., Lindsay, A.D. & Weiss, J.H. (1994) NeuroReport **5** 1477-1480. Kainate injury to cultured basal forebrain cholinergic neurons is Ca^{2+} dependent.

Záborszky, L., Cullinan, W.E. & Braun, A. (1991) Adv. Exp. Med. Biol. **295** 43-101. Afferents to basal forebrain cholinergic projection neurons: an update.

Zeilhofer, H.U., Müller, T.H. & Swandulla, D. (1993) Neuron **10** 879-887. Inhibition of high voltage-activated calcium currents by L-glutamate receptor-mediated calcium influx.

Zhang, D., Sucher, N.J. & Lipton, S.J. (1995) Neuroscience **67** 177-188. Co-expression of AMPA/kainate receptor-operated channels with high and low Ca^{2+} permeability in single rat retinal ganglion cells.

Zhou, Z. & Neher, E. (1993) Pflügers Archiv **425** 511-517. Calcium permeability of nicotinic

acetylcholine receptor channels in bovine chromaffin cells.

Zorumski, C.F. & Thio, L.L. (1992) Progress in Neurobiology **39** 295-336. Properties of vertebrate glutamate receptors: calcium mobilization and desensitization.

Zorumski, C.F., Yamada, K.A., Price, M.T. & Olney, J.W. (1993) Neuron **10** 61-67. A benzodiazepine recognition site associated with the non-NMDA glutamate receptor.